

https://dspace.org/

Microcomputed tomography analysis of the basicranial axis of emydopoid dicynodonts and an investigation of their adaptations to fossorial behaviour

Macungo, Zanildo Augusto

2021

https://hdl.handle.net/10539/33166

Downloaded from a DSpace repository. https://dspace.org/



UNIVERSITY OF THE
WITWATERSRAND,
JOHANNESBURG

MICROCOMPUTED TOMOGRAPHY ANALYSIS OF THE BASICRANIAL AXIS OF EMYDOPOID DICYNODONTS AND AN INVESTIGATION OF THEIR ADAPTATIONS TO FOSSORIAL BEHAVIOUR

Zanildo Augusto Macungo

A Dissertation submitted to the Faculty of Science, University of the Witwatersrand, in fulfilment of the requirements fo the Degree of Master of Science

ORCID Number: 0000-0002-2368-5917

Signed on 02 November 2021 in Johannesburg

Declaration

I declare that this Dissertation is my own unaided work. It is being submitted fo the Degree of Master's of Science in Palaeontology at the University of the Witwatersrand, Johannersburg. This work has not been submitted before for any degree or examination at any other University.



_____

Zanildo Augusto Macungo

02 November 2021

Abstract

Emydopoidea form one of the few clades among dicynodonts that contains fossorial species, although their basicranial adaptations to this lifestyle have been poorly studied. Various cranial and postcranial anatomical features specialized for fossoriality have been identified for a long time in cistecephalid emydopoids. Here, using X-ray micro-computed and synchrotron tomography, I provide detailed anatomical descriptions of the basicranial axis of three emydopoids, *Myosaurus*, *Kawingasaurus*, and a Malawian cistecephalid (PK-16-1), and compare them to the basal dicynodont *Pristerodon*. Notable features include the presence of divergent crests on the posterior aspect of the opisthotic and a nuchal crest on the occipital plate of various emydopoids, particularly cistecephalids, which contrasts with the relative featureless occipital plate of other dicynodonts (with the exception of *Myosaurus*). These depressions and crests increase the muscular attachment area for the atlantooccipital and may represent an adaptation to head-digging in cistecephalids, analogous to some extant fossorial taxa. *Kawingasaurus* has a highly derived basicranium, with a vast network of trabecular spaces and highly coossified basicranium, which is probably linked to the auditory system. I propose that cistecephalids, in addition to being forelimb-diggers, were likely head-diggers, and highlight some derived adaptations consistent with a quasi-obligate fossorial lifestyle. I also propose new basicranial phylogenetic characters and, reevaluate the intra- and interrelationships among emydopoids accordingly. My analysis recovers *Rastodon* as a basal emydopoid, *Thliptosaurus* as a non-kingoriid emydopoid, and *Sauroscaptor*, *Kembawacela* and the new Malawian cistecephalid PK-16-1 forming a polytomy among cistecephalids.

Acknowledgments

My deepest gratitude goes to my Supervisors Dr. Julien Benoit and Dr. Ricardo Araújo. Your help and guidance was crucial to the realization of this dissertation. Thank you so much for making me a better researcher.

I also thank Dr. Kudakwashe Jakata, Dr. Bernhard Zipfel for help to access the CT data of the Evolutionary Studies Institute; and the staff of beamline BM05 at the European Synchrotron Radiation Facility (ESRF) for providing assistance with the other CT data acquisition.

I also thank the Museu Nacional de Geologia (MNG) team for all arrangements they did to make this research a greater success. I would like to highlight my deepest gratitude for allowing me to further my studies.

Many thanks to all the ESI (Evolutionary Studies Institute) team for their tireless help, this research would never become a success without you.

To Dr. Christian Kammerer and Dr. Kenneth Angielczyk for their help with photographs of specimens of different dicynodonts, my many thanks. I also thank Dr. Vincent Fernandez for his helpful comments.

I also acknowledge the FCT and AGA KHAN grant (333206718), National Geographic Society (CP-109R-17), Centre of Excellence in Palaeoscience (CoE PAL), Palaeontological Scientific Trust (PAST) for funding.

Finally, I would like to thank and dedicate this dissertation to my family; thank you for placing your trust in me.

CONTENTS **PAGE**

Declaration ..... **i**
Abstract ..... **ii**
Acknowledgments ..... **iii**
CHAPTER I - INTRODUCTION **1**
1.1. General Introduction 1
CHAPTER II – MATERIALS AND METHODS **6**
2.1. Specimens 6
2.1.1. Emydopoidea 6
2.1.2. Eumantelliidae (Outgroup) 6
2.2. Methods 7
2.2.1. Data acquisition 7
2.2.2. Segmentation and images treatment 9
2.2.3. Phylogenetic analysis 10
CHAPTER III – RESULTS **12**
3.1. Anatomical description 1 12
3.1.1. Orbitosphenoid 12
3.1.2. Pterygoid 14
3.1.3. Parabasisphenoid 16
3.1.4. Basioccipital 18
3.1.5. Exoccipital 20
3.1.6. Supraoccipital 22
3.1.7. Prootic 24
3.1.8. Opisthotic 27
3.2. Anatomical description 2 29
3.2.1. Orbitosphenoid 29
3.2.2. Pterygoid 30
3.2.3. Epipterygoid 33
3.2.4. Parabasisphenoid 34
3.2.5. Basioccipital 36
3.2.6. Exoccipital 37
3.2.7. Supraoccipital 39
3.2.8. Prootic 41
3.2.9. Opisthotic 43

3.3. Anatomical description 3 46
3.3.1. Pterygoid 46
3.3.2. Parabasisphenoid 48
3.3.3. Basioccipital 49
3.3.4. Exoccipital 50
3.3.5. Supraoccipital 51
3.3.6. Prootic 54
3.3.7. Opisthotic 56
3.4. Anatomical description 4 57
Description 57
3.4.1. Orbitosphenoid 57
3.4.2. Pterygoid 59
3.4.3. Epipterygoid 61
3.4.4. Parabasisphenoid 62
3.4.5. Basioccipital 63
3.4.6. Exoccipital 65
3.4.7. Supraoccipital 66
3.4.8. Prootic 68
3.4.9. Opisthotic 71
CHAPTER IV - DISCUSSION **73**
4.1. Possible adaptations to fossoriality 73
4.1.1. Degree of coossification of the braincase 73
4.1.2 Cranial pneumaticity 75
4.1.3. Pineal foramen 76
4.1.4. Development of an increased area for the atlantooccipital musculature attachment 77
4.1.5. Rationale for fossorial adaptations in dicynodonts 81
4.2. Emydopoidea inter- and intrarelationships 84
4.2.1. Phylogeny results 85
CHAPTER V – CONCLUSION AND FUTURE WORKS **90**
REFERENCES **91**
CHAPTER VI – APPENDICES **118**

List of Figures

Figure 3. 1. The orbitosphenoid of *Pristerodon mackayi* (BP/1/2642) in **(A)** anterior, **(B)** dorsal and **(C)** left lateral views. obdn, the orbitosphenoid dorsal notch; ofc, olfactory cavity; obvp, orbitosphenoid medial vertical process; hpl, horizontal plate; mpw, mesethmoid posterior wall. 13

Figure 3. 2. The braincase of *Pristerodon mackayi* (BP/1/2642) in **(A)** anterior, **(B)** dorsal, **(C)** ventral, **(D)** occipital and **(E)** left lateral views. aptr, anterior pterygoid rami; co, crista oesophagea; eobg, exoccipital posterior bulge; eobt, exoccipital subvertical buttress; epi, epipterygoid; fu, pterygoid anteroposterior furrow; lvb, opisthotic lateral vertical buttress; osu, opisthotic posterior vertical sulcus; ovmp, opisthotic ventromedial process; pab, prootic anterior bulge; pad, pila antotica anterior depression; pdp, prootic dorsal process; pt dsu, pterygoid dorsal sulcus; pt ke pterygoid keel; ptll, pterygoid lateral lamina; ptmp, pterygoid median plate; pt nt, pterygoid anteroposterior notch; ptvt, pterygoid ventral trench; sap, supraoccipital anterior process; sap, supraoccipital anteriorly projected crest; sar, supraoccipital anterior recess; slr, supraoccipital lateral recess; sor, supraoccipital anterior horizontal ridges; spp, supraoccipital posterior process. 16

Figure 3. 3. The parabasisphenoid of *Pristerodon mackayi* (BP/1/2642) in **(A)** dorsal, **(B)** right lateral and **(C)** ventral views. bpdc, basisphenoidal dorsal subvertical concavity; bpt, basisphenoidal tubera; bpvsu, basisphenoidal ventral sulcus; clp, clinoid process; ds, dorsum sellae; ic, internal carotid foramina; ps, parasphenoid rostrum; psgr, parasphenoid dorsal rostrum groove; tse, tuberculum sellae; stu, sella turcica. 18

Figure 3. 4. The basioccipital of *Pristerodon mackayi* (BP/1/2642) in **(A)** posterior, **(B)** dorsal, **(C)** ventral, and **(D)** right lateral views. bocc, basioccipital condyle; bocex, basioccipital colar-

like excavation; bocf, basioccipital condyle foramina; bocr, basioccipital condyle median ridge; bomr, basioccipital median ridge; bosr, basioccipital lateral ridges; bovtr, basioccipital ventral trough; bpca, basisphenoidal sutural area; bt, basioccipital tubera; itr, intertuberal ridge; fo, fenestra ovalis; jf, jugular foramen; ve, vestibule. 20

Figure 3. 5. The exoccipital of *Pristerodon mackayi* (BP/1/2642) in **(A)** anterior and **(B)** posterior views. eoat, exoccipital anterior tuberosity; eobg, exoccipital posterior bulge; eobt, exoccipital subvertical buttress; fm, foramen magnum; jf, jugular foramen. 22

Figure 3. 6. The supraoccipital of *Pristerodon mackayi* (BP/1/2642) in **(A)** anterior, **(B)** internal, **(C)** right lateral and **(D)** posterior views. assca, attachment of the anterior semicircular canal; cca, attachment of the crus communis; flo, floccular fossa; fm, foramen magnum; pa, pila antotica; pr, prootic; ptf, posttemporal fenestra; sap, supraoccipital anteriorly projected crest; sar, supraoccipital anterior recess; slr, supraoccipital lateral recess; sor, supraoccipital anterior horizontal ridges; spp, supraoccipital posterior process. 24

Figure 3. 7. The right prootic of *Pristerodon mackayi* (BP/1/2642) in **(A)** anterior, **(B)** lateral, **(C)** posterior **(D)** ventral and **(E)** medial views. assca, attachment of the anterior semicircular canal; boa, basioccipital sutural area; bsa, parabasisphenoidal sutural area; CNV, passage of the cranial nerve five (V); fa, facial foramen; flo, floccular fossa; fo, fenestra ovalis; lscca, attachment of the lateral semicircular area; pa, pila antotica; pab, prootic anterior bulge; pad, pila antotica anterior depression; pdp, prootic dorsal process; prd, prootic lateral depression; ve, vestibule. 26

Figure 3. 8. The left opisthotic of *Pristerodon mackayi* (BP/1/2642) in **(A)** anterior, **(B)** lateral and **(C)** posterior views. afac, articulation facet concavity; eoa, exoccipital sutural area; fo, fenestra ovalis; jf, jugular foramen; lscc, attachment of the lateral semicircular canal; osu, opisthotic posterior vertical sulcus; ovmp, opisthotic ventromedial process; pra, prootic sutural

area; psb, opisthotic lateral vertical buttress; pscc, attachment of the posterior semicircular canal; ptf, posttemporal fenestra; spa, supraoccipital sutural area; vea, vestibular area. 28

Figure 3. 9. The orbitosphenoid of *Myosaurus* (BP/1/2690) in **(A)** anterior, **(B)** dorsal and **(C)** right lateral views. obacr, orbitosphenoid vertical crest; obasu, orbitosphenoid lateral sulci; obdfo, orbitosphenoid dorsal fossa; ofc, olfactory cavity; ltcr, lateral wall oblique crests. 30

Figure 3. 10. The pterygoid of *Myosaurus* (BP/1/2690) in **(A)** dorsal, **(B)** right lateral and **(C)** ventral views; pterygoid of *Myosaurus* (BP/1/2701a) in **(D)** dorsal and **(E)** right lateral views; epipterygoid of *Myosaurus* BP/1/2701a in **(F)** anterior, **(G)** lateral and **(H)** medial views. apf, pterygoid anteroposterior furrow; aptr, anterior pterygoid rami; co, crista oesophagea; epar, epipterygoid ascending ramus; epdp, epipterygoid dorsal plate; epft, epipterygoid footplate; msc, muscle scars; pt amp, pterygoid anteromedial process; pt gr, pterygoid dorsal groove; ptmp, pterygoid median plate; ptqr, pterygoid quadrate ramus. 32

Figure 3. 11. The parabasisphenoid of *Myosaurus* (BP/1/2690) in **(A)** dorsal, **(B)** left lateral and **(C)** ventral views. bpt, basisphenoidal tubera; clp, clinoid process; ds, dorsum sellae; ic, internal carotid foramina; ps, parasphenoid rostrum; psc, parasphenoidal crests; psf, parasphenoidal foramen; pss, parasphenoidal sulcus; stu, sella turcica.....35

Figure 3. 12. The basioccipital of *Myosaurus* (BP/1/2690) in **(A)** posterior, **(B)** dorsal, **(C)** ventral and **(D)** right lateral views. bocc, basioccipital condyle; bod, basioccipital ventral depression; bodcr, basioccipital condyle dorsal ridge; bomr, basioccipital median ridge; bonf, basioccipital nutritive foramina; bosr, basioccipital lateral ridges; bt, basioccipital tubera; fo, fenestra ovalis; jf, jugular foramen; vea, vestibular area. 37

Figure 3. 13. The exoccipital of *Myosaurus* (BP/1/2690) in (A) anterior, (B) posterior, (C) dorsal, (D) ventral and (E) ventromedial views. eoat, exoccipital anterior tuberosity; eoc,

exoccipital condyle; eodc, exoccipital dorsal component; eoptr, exoccipital posterior trench; eovf, exoccipital vertical furrow; fm, foramen magnum; hf, hypoglossal foramen; jf, jugular foramen; occp, occipital pit.....39

Figure 3. 14. The supraoccipital of *Myosaurus* (BP/1/2690) in **(A)** anterior, **(B)** posterior, **(C)** ventral and **(D)** dorsal views. assc, attachment of the anterior semicircular canal; flo, floccular fossa; fm, foramen magnum; psca, attachment of the posterior semicircular canal; sac, supraoccipital semicircular crests; sap, supraoccipital anteriorly projected crest; slr, supraoccipital lateral recess; smb, supraoccipital subvertical buttress; spi, supraoccipital posterior pit; svd, supraoccipital posterior vertical depressions. 40

Figure 3. 15. The prootic of *Myosaurus gracilis* (BP/1/2690) in **(A)** anterior, **(B)** left lateral, **(C)** medial **(E)** posterior and **(F)** dorsal views; **(D)** the braincase of BP/1/2690 in left lateral view. assc, attachment of the anterior semicircular canal; boc c, sutural area of the prootic and the basioccipital; CNV, passage of the cranial nerve five (V); fa, facial foramen; flo, floccular fossa; gp, gap between the prootic and the clinoid process; lscca, attachment of the lateral semicircular area; pa, pila antotica; opt c, sutural area between prootic and opisthotic; pabt, prootic anterior buttress; plf, prootic lateral flange; ppex, prootic posterior excavation; prac, pila antotica anterior crests; prmc, prootic medial crest; prpb, prootic posterior bulge; sup c, sutural area of the prootic and supraoccipital; vea, vestibular area. 43

Figure 3. 16. The left opisthotic of *Myosaurus gracilis* (BP/1/2690) in **(A)** anterior and **(B)** posterior views; left opisthotic of (BP/1/2690) in **(C)** posterior; the braincase of (BP/1/2690) in **(D)** ventral views. fo, fenestra ovalis; jf, jugular foramen; lsca, attachment of the lateral semicircular canal; lvb, opisthotic lateral vertical buttress; ob, opisthotic body; obu, opisthotic bulges; olc, opisthotic lateral crest; omc, opisthotic medial crest; opmb, opisthotic

posteromedial buttress; osu, opisthotic posterior vertical sulcus; ovmp, opisthotic ventromedial process; pr c, prootic sutural area. 45

Figure 3. 17. The ventral region of the braincase of the Malawian cistecephalid (basisphenoid, parabasisphenoid and pterygoid) in **(A)** dorsal, **(B)** right lateral and **(C)** ventral views. bod, basioccipital ventral depression; bok, basioccipital dorsal knob; bosr, basioccipital lateral ridges; bplr, basisphenoidal lateral recess; clp, clinoid process; co, crista oesophagea; ds, dorsum sellae; epi, epipterygoid; fo, fenestra ovalis; jf, jugular foramen; ic, internal carotid foramina; ps, parasphenoid rostrum; pss, parasphenoid rostrum dorsal sulcus; pt ltr, pterygoid lateral trench; pt vsc pterygoid ventral sulcus; stu, sella turcica; uz, unossified zone.....47

Figure 3. 18. The exoccipital of the Malawian cistecephalid (PK-16-1) in **(A)** anterior, **(B)** posterior and **(C)** medial views. eoat, exoccipital anterior tuberosity; eodc, exoccipital dorsal component; eoptr, exoccipital posterior trench; hf, hypoglossal foramen; jf, jugular foramen. 51

Figure 3. 19. The lateral and posterior wall of the braincase of the Malawian cistecephalid (PK-16-1). Right prootic in **(A)** anterior, **(B)** lateral, **(C)** medial, **(D)** ventral and **(E)** posterior views. Opisthotic and supraoccipital in **(F)** anterior, **(H)** posterior and **(I)** right lateral views; opisthotic in **(G)** medial view. ascc, attachment of the anterior semicircular canal; cc, attachment of the crus communis; fa, facial foramen; flo, floccular fossa; fm, foramen magnum; fo, fenestra ovalis; lscc, attachment of the lateral semicircular canal; oac, opisthotic anterior crests; oad, opisthotic anterior depression; obg, opisthotic anterior bulge; od, opisthotic posterior depression; opc, opisthotic posterior crests; opp, opisthotic posterior process; ovmp, opisthotic ventromedial process; pa, pila antotica; pbl, prootic blade-like process; plf, prootic lateral flange; pssc, attachment of the posterior semicircular canal; ptf, posttemporal fenestra;

sap, supraoccipital anteriorly projected crest; slr, supraoccipital lateral recess; vea, vestibular area. 53

Figure 3. 20. The orbitosphenoid of *Kawingasaurus fossilis* (GPIT/RE/9272) in **(A)** anterior, **(B)** dorsal and **(C)** left lateral views. dsu, orbitosphenoid dorsal sulcus; nt, lateral notch; obacr, orbitosphenoid vertical crest; obasu, orbitosphenoid lateral sulci; obpl, orbitosphenoid dorsal plate; ofc, olfactory cavity; vpw, vertical process of the orbitosphenoid wing. 59

Figure 3. 21. The ventral portion of the braincase of *Kawingasaurus fossilis* (GPIT/RE/9272): basioccipital, parabasisphenoid and pterygoid in (A) dorsal, (B) left lateral and (C) ventral views; parabasisphenoid in (D) ventral view; and basioccipital in (E) posterior view. bocf, basioccipital longitudinal furrow; bolp, basioccipital lateral process; bovr, basioccipital median ridge; bovs, basioccipital vestibular space; bpt, basisphenoidal tubera; bt, basioccipital tubera; bvex, basioccipital-basisphenoidal ventral excavation; clp, clinoid process; eoa, exoccipital sutural area; ic, internal carotid foramina; jf, jugular foramen; psgr, parasphenoidal groove; pt afo, pterygoid oval foramina; pt dl, pterygoid dorsal lamina; ptve, pterygoid ventral excavation; ptvl, pterygoid ventral lamina. 60

Figure 3. 22. The epipterygoid of the *Kawingasaurus fossilis* (GPIT/RE/9272) in **(A)** anterior and **(B)** right lateral views. epap, anteriomedial angular process of the epipterygoid; epar, ascending ramus of the epipterygoid; epft, epipterygoid footplate. 62

Figure 3. 23. The occiput region of *Kawingasaurus fossilis* (GPIT/RE/9272): exoccipital in **(A)** anterior view; supraoccipital in **(B)** anterior, **(C)** posterior, **(D)** left lateral and **(E)** medial views. ascc, attachment of the anterior semicircular canal; cc, attachment of the crus communis; eoc, exoccipital condyle; eocr, exoccipital descending crest; eodc, exoccipital dorsal component; flo, floccular fossa; fm, foramen magnum; ihb, impressions of the hindbrain; jf, jugular foramen; nc, nuchal crest; pscc, attachment of the posterior semicircular canal; ptf,

posttemporal fenestra; saex, medial excavation of the supraoccipital lateral ala; sacr, crests of the supraoccipital ala; sap, supraoccipital anterior process of the median lobe; slr, supraoccipital lateral recess; sor, supraoccipital anterior oblique ridges; vea, vestibular area. 66

Figure 3. 24. The lateral wall of the braincase of *Kawingasaurus fossilis* (GPIT/RE/9272): prootic in **(A)** anterior, **(B)** lateral, **(C)**, medial, **(D)** posterior views; opisthotic in **(E)** anterior, **(F)** medial and **(G)** posterior views. ascc, attachment of the anterior semicircular canal; fa, facial foramen; flo, floccular fossa; fo, fenestra ovalis, lscc, attachment of the lateral semicircular canal; oae, opisthotic anterior depression; od, opisthotic depression; opc, opisthotic posterior crests; pa, pila antotica; pabt, prootic anterior buttress; pade, pila antotica ellipsoidal depression; pard, pila antotica anterodorsally-directed ridges; pbg, prootic anterior bulge; pg, prootic anterior groove; plbt, prootic lateral vertical buttress; pmbt, prootic medial vertical buttress; pvfo, prootic vertical fossa; vea, vestibular area. 71

Figure 4. 1. Comparisons of the braincase between *Pristerodon* and emydopoids. *Pristerodon mackayi* (BP/1/2642) in **(A)** anterior, **(B)** left lateral, **(C)** posterior and **(D)** ventral views. *Myosaurus gracilis* (BP/1/2690) in **(E)** anterior, **(F)** left lateral, **(G)** posterior and **(H)** ventral views. The Malawian cistecephalid (PK-16-1) in **(I)** anterior, **(J)** left lateral, **(K)**, posterior and **(L)** ventral views. *Kawingasaurus fossilis* (GPIT/RE/9272) in **(M)** anterior, **(N)** left lateral, **(O)** posterior and **(P)** ventral views. 83

Figure 4. 2. Phylogenetic results simplified to highlight Emydopoidea intra- and interrelationships. Numbers at nodes represent: Symmetric Resampling values / CG values above nodes; Bremer Support values / Relative Bremer Support values below nodes. See appendices D, E and F for the complete trees. **A** – Dicynodontia; **B** – Emydopoidea; **C** –

Kistecephalia; **D** – Cistecephalidae; **E** – Endothiodontia; **F** – Kingoriidae; **G** – Emydopidae; **H** – Myosauridae.....87

CHAPTER I - INTRODUCTION

1.1.General Introduction

Emydopoid dicynodonts were typically small-bodied synapsids that lived from the late Permian to the middle Triassic in terrestrial ecosystems, being one of the few synapsid clades to survive the End-Permian mass extinction (Cluver 1974). The external cranial anatomy of emydopoid dicynodonts is well documented (e. g., Broom 1913; Haughton 1917; Cox 1959; 1972; Keyser 1965; Cluver 1974a; Cluver 1974b; Hammer and Cosgriff 1981; Cluver and King 1983; Fröbish 2007; Fröbish et al. 2010; Nasterlack et al. 2012; Angielczyk and Kammerer 2017; Kammerer et al. 2016; Kammerer 2019a; Angielczyk et al. 2019). Recently, important novel insights into the internal cranial anatomy of anomodonts is being gained thanks to non-destructive techniques such as X-ray micro-computed tomography (µCT) (e.g., Laaß 2015a; Benoit et al. 2018; Laaß and Kaestner 2017; Araújo et al. 2018). Yet, the relative abundance of some dicynodonts in the South African Karoo enabled some early detailed studies using destructive serial sectioning techniques (e.g., *Dicynodontoides* in Cox 1959; *Emydops* in Fourie 1991, 1993; *Myosaurus* in Cluver 1974b, see also Cluver 1971 for *Lystrosaurus*, see Benoit and Jasinoski 2016 for a review).

An improved understanding of the anatomy of emydopoids may help resolve some long-standing phylogenetic problems and their unique palaeobiology. For instance, the taxonomic instability of the clade is an important issue to this day with species recovered in and out of the group with varying phylogenetic reconstructions, such as *Niassodon* (Castanhinha et al. 2013; Kammerer et al. 2015; Boos et al. 2016). Other examples of phylogenetic instability comprise the basal position of Emydopidae among Emydopoidea, or the relative position of Kingoriidae and Emydopidae (Fröbish 2007; Kammerer et al. 2015; Kammerer 2019a; Angielczyk et al. 2019). Conversely, the most taxonomically stable family

among Emydopoidea is the Cistecephalidae. Cistecephalids are represented by *Cistecephalus microrhinus*, *Cistecephaloides boonstrai*, *Kawingasaurus fossilis*, *Sauroscaptor tharavati*, the Malawian cistecephalid PK-16-1, and *Kembawacela kitchingi* (Keyser 1965; Cox 1972; Cluver 1974a, 1978; Boos 2012; Kammerer et al. 2016; Angielczyk et al. 2019, Araújo et al. 2021). Cistecephalid diagnostic characters include several conspicuous anatomical features suggestive of a fossorial lifestyle (Owen 1876; Keyser 1965; Cox 1972; Cluver 1974; 1978; Nasterlack et al. 2012; Laaß 2015a; Angielczyk et al. 2019), although, to date, no cistecephalid was ever found in a burrow cast despite the increasingly rich fossil record of vertebrate burrow casts in Permian and Triassic rocks (Groenewald et al. 2001; Damiani et al. 2003; Modesto and Brink 2012; Fernandez et al. 2013; Kammerer et al. 2016, Smith et al. 2021). Characters consistent with a fossorial lifestyle observed in the forelimbs of cistecephalids, and include: enlarged forelimbs and robust humerus that served for the accommodation of large deltopectoral muscles, notably in *Kawingasaurus* (Cox 1972); prominent olecranon process of the ulna (Cox 1972; Cluver 1978), and broad manus strongly suggesting usage of claws for digging (Keyser 1965; Cox 1972; Cluver 1978). Some cranial features are also interpreted as evidence for a fossorial lifestyle, such as the relatively broad and short skull shaped like a box (Owen 1876; Keyser 1965; Cluver 1974; 1978; Nasterlack et al. 2012; Laaß 2014), highly convergent with some fossorial lizards, that may have helped compacting the tunnel walls after digging (Brock 1939; Bellairs 1949). Recent studies have highlighted other cranial features indicating fossorial lifestyle in cistecephalids, specifically in *Kawingasaurus* (Laaß and Schillinger 2015; Laaß 2014). These include the loss of the pineal foramen, the presence of an inflated vestibule and enlarged stapedial footplates that served for bone-conducting hearing and seismic sensitivity (Keyser 1965; Cluver 1978; Nasterlack et al. 2012; Laaß and Kaestner 2017). Historically, *Cistecephalus* was previously proposed to be an arboreal species (Keyser 1965) but a later description of *Kawingasaurus* (Cox 1972) illustrated that the postcranial morphology of

cistecephalids conforms more conclusively to a fossorial lifestyle (see also Angielczyk et al. 2019). Among non-emydopoid dicynodonts, fossoriality is further inferred for *Diictodon* and *Lystrosaurus* based on their postcranium, and the fact that fossils of these taxa were found in burrow casts (Smith 1987; King and Cluver 1991; Ray and Chinsamy 2003; Bordy et al. 2010; Modesto and Brink 2010; Smith et al. 2021). However, the adaptations seen in the dicynodontoid *Lystrosaurus* and pylaecephalid *Diictodon* are relatively superficial, pointing towards a different level of commitment to a fossorial lifestyle compared to cistecephalids.

Fossoriality can be classified into four different sub-categories: taxa adapted to head-digging or forelimb-digging, and facultative or obligate fossorial taxa (Gans 1978; Müller et al. 2011). Head-digging species use their snout or the chisel-shaped incisors to excavate the upper and anterior parts of the tunnel and is practiced mostly by caecilians, amphisbaenians, and mole-rats (Rose and Emry 1983; Martin and Bennett 1977; Kleinteich et al. 2012; Sherratt 2014; Maddin and Sherratt 2014; Christine 2016). Forelimb-digging refers to the use of claws mostly for excavating the bottom and lateral regions of their burrows, as in moles (Freeman 1979; Catania 2000, Navas et al. 2004; Rose et al. 2013; Rodrigues et al. 2016; Sansalone et al. 2020), rabbits (Leigh et al. 1987), and meerkats (van Staden et al. 2014). Obligate fossorial forelimb-diggers have a broad humerus, broad olecrenon process, narrow and elongate scapula, short and robust manus, enlarged and curved claws, and enlarged areas for forelimb musculature attachment, whereas facultative fossorial forelimb-diggers show some of these features to a lesser extent (Shimer 1903; Quintana et al. 2011; van Staden et al. 2014; Rodrigues et al. 2016; Walker et al. 2020). Therefore, head-digging and forelimb-digging should be regarded as a continuum, as both postcranial and cranial specializations can be seen in some taxa that employ both modes of digging methods, such as golden moles (Martin and Bennett 1977; Anderson et al. 2009), wombats and vombatiforms (Grand and Barboza 2001; Woolnough and Steele 2001; Beck et al. 2020). On the other hand, obligate fossorial taxa live

nearly the entirety of their lives subterraneously, such as naked mole-rats and moles. Facultative fossorial taxa use the burrow only for some aspects of their behavior, such as for shelter and/or breeding, and include meerkats, rabbits and hares, or warthogs (Strahan 1995; Kinlaw 2006; James and Eldridge 2007; White and Cameron 2008; van Staden 2014). Obligate fossorial taxa display the most extreme morphological adaptations. Based on Keyser (1965), Cox (1972), and Cluver (1978) descriptions of the postcranial skeleton of cistecephalids, it is clear that they share convergent morphology with extant obligate fossorial species (Bellairs and Gans 1983; Maddin and Sherratt 2014). Evidence pointing towards cistecephalids being head-diggers is not conclusive at the moment. This study provides new evidence for head-digging among cistecephalids.

Historically, only the external anatomy of the dicynodont basicranial elements (i. e., basioccipital, basisphenoid, parasphenoid, opisthotic, prootics, exoccipital, and supraoccipital) has been described (e. g., Olson 1944; Cluver 1974a; Barry 1974; Surkov and Benton 2004; Maisch and Gebauer 2005; Castanhinha et al. 2013; Kammerer et al. 2015, 2016; Boos et al. 2016; Angielczyk et al. 2017; Kammerer and Smith 2017; Olroyd et al. 2018; Kammerer 2019b; Kammerer et al. 2019; Liu 2020). These studies have only superficially demonstrated the interrelationships between the bones, their relative orientation and organisation, degree of coossification, the development of detailed anatomical sub-units, and musculature reconstruction (Cox 1959; Barry 1967; 1974; Cluver 1971; 1974a; 1974b; 1978; Sullivan 2000; Renaut 2000; Ray and Chinsamy 2003; Angielczyk et al. 2017).

Here I analyze in detail the internal anatomy of the basicranium and anterior occiput of some emydopoids, with a particular focus on characters that may relate to fossoriality. Using µCT-scanning and synchrotron techniques and segmentation, detailed anatomical descriptions of *Myosaurus*, specimen PK-16-1 (a Malawian cistecephalid), and *Kawingasaurus* are provided, that is contrasted to the basal dicynodont *Pristerodon*. Also, further palaeobiological

evidence for the fossorial adaptations at the level of the basicranium in these taxa, which seem to support a head-digging behavior for at least some of them are provided. Furthermore, I propose eleven new phylogenetic characters based on the emydopoid braincase that are integrated into the most recent phylogenetic matrix. The inclusion of the new characters and the re-evaluation of previously proposed characters implies new topological arrangements among Emydopoidea when compared with most recent analyses (Angielczyk et al. 2019; Kammerer 2019a; Kammerer and Ordoñez 2021; Liu 2021).

CHAPTER II – MATERIALS AND METHODS

2.1. Specimens

2.1.1. Emydopoidea

BP/1/2690: *Myosaurus gracilis*, Katberg Formation, *Lystrosaurus* Assemblage Zone, Karoo Basin, Induan (Early Triassic). Scanned at the ESI using *Nikon Metrology XTH* 225/320 LC. Voxel size: 0.0221 mm.

BP/1/2701a: *Myosaurus gracilis*, Katberg Formation, *Lystrosaurus* Assemblage Zone, Karoo Basin, Induan (Early Triassic). Scanned at the ESI using *Nikon Metrology XTH* 225/320 LC. Voxel size: 0.0327 mm.

PK-16-1: Malawian cistecephalid, Lower Bone Beds, Chiweta Beds, Wuchiapingian (upper Permian). Scanned at the European Synchrotron Radiation Facility using PPC-SRµCT. Voxel size: 0.02272 mm. The Malawian cistecephalid is currently being prepared to be submitted for publication (Araújo et al. 2021) and can be ascribed to the Cistecephalidae due to the presence of the following diagnostic characters: box-like skull shape, nearly flat occiput, anteriorly oriented orbits, and acute notch between the anterior margin of the orbit and snout region.

GPIT/RE/9272: *Kawingasaurus fossilis*, Usili Formation, Ruhuhu Basin, Wuchiapingian (upper Permian). Scanned at the European Synchrotron Radiation Facility using PPC- SRµCT. Voxel size: 0.02652 mm.

2.1.2. Eumantelliidae (Outgroup)

BP/1/2642: *Pristerodon mackayi*, Abrahamskraal Formation, *Cistecephalus* Assemblage Zone, Karoo Basin, Wuchiapingian (late Permian). Scanned at the ESI using *Nikon Metrology XTH* 225/320 LC. Voxel size: 0.0469 mm

2.2. Methods

2.2.1. Data acquisition

Propagation phase-contrast synchrotron X-ray micro-computed (PPC-SRμCT)

I – Malawian cistecephalid PK-16-1

PK-16-1 was scanned at the beamline BM05 of the European Synchrotron Radiation Facility (ESRF, Grenoble, France), using propagation phase contrast X-ray synchrotron micro-Computed Tomography (PPC-SRμCT). The experimental set-up comprised: filtered white beam (2 pole bending magnet 0.85 T; filtration, Cu 3 mm, Al 2mm, 8 Al rod of 5 mm in diameter and 100 mm in length place horizontally) with a total integrated detected energy of 114 keV; an indirect detector comprising a 2 mm thick LuAG scintillator, 0.5x magnification obtained with a set of Hasselblad photographic lenses (Victor Hasselblad AB, Gothenburg, Sweden) and a PCO.edge 4.2 USB3 cameralink sCMOS detector (PCO, Kelheim, Germany). The sample-detector distance was set to 4.5 m for PPC-SRμCT. In this configuration, the measured pixel size was 11.36 μm. The data acquisition comprised 6000 projections of 0.06 s each over a rotation of 360°. Each projection resulted from the accumulation of five frames of 0.012 s each. The centre of rotation was laterally shifted by 10.22 mm (900 pixels) to increase the reconstructed horizontal field of view (i.e., half-acquisition protocol Carlson et al. 2011). Forty-four acquisitions were performed, using a vertical step of 1.8 on the vertical axis, ensuring an approximate 50% vertical overlap to compensate for the vertical beam profile.

Before the tomographic reconstruction, radiographs were stitched on the vertical axis (Fernandez and Tafforeau 2018). The tomographic reconstruction of the stitched dataset was performed using the single distance phase retrieval approach of the software PyHST2 (Mirone et al. 2014; Paganin et al. 2002). The resulting 32-bit data were converted to a stack of 16-bit tiff images using the minimum and maximum values excluding 0.001% of voxels on both sides

of the 3D histogram generated by PyHST2. Additional processing of the data included: ring correction (Lyckegaard et al. 2011), normalization of artefactual grey level gradients and metallic inclusions (Cau et al. 2017), cropping of the dataset and binning 2x2x2 to reduce the size of the data.

II – *Kawingasaurus fossilis* GPIT/RE/9272

Kawingasaurus was characterised using PPC-SRμCT at the BM05 beamline of the ESRF. The beam configuration consisted of white beam filtered with 10 mm of aluminium and 3 mm of copper, resulting in a total integrated detected energy of 107 keV. Images were recorded with an indirect detector comprising a 750 μm thick LuAG scintillator; 2x magnification from a set of Hasselblad lenses; a sCMOS PCO.edge 5.5 with USB3 camera link. The detector was placed 2250 mm after the sample in the X-ray path for PPC-SRμCT and the measured pixel size in this configuration was 13.26 μm. The X-ray beam on the sample was 29.72 mm horizontally by 4.25 mm vertically. As the sample was larger than the field of view, we first, shifted the rotation axis of the sample stage by about 8 mm (i.e., half acquisition protocol, Carlson et al. 2011). This resulted in reconstructed tomograms of 45.63 mm in diameter (3441 pixels). Secondly, 20 acquisitions were undertaken, each time moving the specimen by 2.12 mm on the vertical axis, resulting in an overlap of 50% between consecutive datasets. Each acquisition consisted of 8000 projections of 40 millisecond each (the large number of projections was used to compensate for the noise of the camera as frame averaging or accumulation was not available at the time). For the white field image (i.e., image of the beam with no sample), we recorded 101 images and generated a median image; for the darkfield (i.e., recording the noise of the camera with no beam), we recorded 40 images that we averaged.

Tomographic reconstruction was done using PyHST2 (Mirone et al. 2014) using the single distance phase retrieval approach (Paganin et al. 2002). The δ/β parameter (indicating

the nature of the material for single-phase material) was set to reduce the noise while avoiding blurring. The remaining processing included: modification of the bit depth from 32 to 16 bits, using the 0.001% minimum and maximum exclusion values of the 3D histogram generated by PyHST2; ring correction (Lyckegaard et al. 2011); and cropping the volume. Finally, a 2x2x2 binning was applied to increase the signal-noise-ratio and reduce the size of the data for segmentation.

2.2.2. Segmentation and images treatment

The 3D reconstruction of the braincase was performed using Avizo 9 (FEI VSG, Hillsboro OR, USA) at the Virtual Imaging Palaeontology laboratory of the Evolutionary Studies Institute, University of the Witwatersrand (Johannesburg, South Africa). The five braincases were mostly segmented manually by using the "brush tool", but when possible, interpolation of five slices maximum was performed. The *Pristerodon* and *Myosaurus* specimens allowed the nearly complete separation of the bones as they are in optimal preservational conditions and show closed but not fused sutures. The Malawian cistecephalid PK-16-1 specimen had extensively fused bones that prohibited the clear identification of the sutures. Because *Kawingasaurus* has the most coossified braincase among dicynodonts (Cox, 1972; Laaß, 2014; Laaß and Kaestner 2017) its bones were segmented by 1) comparing their morphology and shape to those of other dicynodont such as *Niassodon* (Castanhinha et al., 2013), and 2) the sutures were identified by following the orientation and density of the trabecular spaces. This was mostly done on the basisphenoid, basioccipital, prootic, basioccipital and opisthotic. The surfaces were generated for each bone using the Unconstrained Smoothing of the Generate Surface function under Avizo. Pictures were generated using the same software. Figure plates were generated using Adobe Illustrator CC 2015 19.0.0. Measurements were made using Avizo.

2.2.3. Phylogenetic analysis

To re-evaluate Emydopoidea phylogenetic intra- and interrelationships based on the new characters here proposed, eleven new discrete morphological characters were scored (from character 180 to 190, see appendix A for a character list) using Mesquite 3.61 (build 927) 26 December 2019 version. My proposed discrete-state characters are divided into two groups, five external characters whose evaluation can be done without CT data, and six internal characters that require CT data for observation (see appendix B for discussion of these new characters). The internal characters were only scored for the segmented specimens, pending CT data for other dicynodont species for further analysis. I recoded the discrete-state character 114 to character-state 1 for *Thliptosaurus*, rather than former state 2 (Kammerer 2019), because its mandibular fenestra is not occluded as in other kingoriids. This recoding contributed to the exclusion of *Thliptosaurus* from Kingoriidae (Figure 4.1). I also recoded the discrete-state character 49 for *Rastodon procurvidens* based on the observation of a groove on the dorsal surface of the pre-parietal and parietal that hosted the pineal foramen in *Rastodon* UNIPAMPA PV317P (Boos et al. 2016), being consistent with character-state 1. Nonetheless, this recoding did not contributed to the change the position of *Rastodon*. I added the data to the recent dicynodont-focused data matrix of Kammerer and Ordoñez (2021), where I incorporated the new codings of *Turfanodon jiufengensis* and *Turfanodon bogdaensis* from Liu (2021). The final modified matrix included 119 operational taxonomic units, 190 discrete-state morphological characters, and 23 continuous morphometric characters (see appendix C for the coded matrix). I analyzed the data matrix using TNT 1.5 November 2020 version with no taxon limit for Windows (Goloboff and Catalano 2016). Morphological characters 58, 61, 79, 140, 150, 151, and 166 were ordered. The analysis used the 'FUSE' algorithm to find the most parsimonious trees, which took 16.017.364.635 cladogram rearrangements. Once the shortest tree length was hit 20 independent times using 'xmult' plus 10 cycles of tree-drifting cycles

(Goloboff 1999), the strict consensus tree was drawn by collapsing the tree using tree bisection-reconnection and respective node supports. Synapomorphies common to all four trees are shown in appendix D. Absolute and relative Bremer supports (Figure 4.2, below nodes; appendix F) were calculated for the nodes using tree bisection-reconnection by swapping the trees (Bremer 1994, Goloboff and Farris 2001). I also used resampling to assess node support, which was calculated by doing 10000 replications of symmetric resampling (Goloboff et al. 2003, Figure 4.2 above nodes; appendix E), analyzing each data set with a single random addition sequence plus tree bisection-reconnection and then collapsing the resulting tree (Goloboff and Farris, 2001). Because of the nature of the main results regarding the formation of polytomy of three cistecephalids (appendix D, E, F), the phylogenetic analysis was repeated two more times: one without the characters I proposed in this research, and the other excluding the currently underdescribed and unnamed Malawian cistecephalid from the analysis (appendix G) as this is a relatively new species.

CHAPTER III – RESULTS

3.1. Anatomical description 1

SYSTEMATIC PALAEONTOLOGY

Order THERAPSIDA Broom, 1905

Suborder ANOMODONTIA Owen, 1859

Infraorder DICYNODONTIA Owen, 1859

Superfamily PRISTERODONTOIDEA Cluver and King, 1983

Family PRISTERODONTIDAE King, 1988

Pristerodon mackayi Huxley, 1868

Specimen: BP/1/2642

In the present study *Pristerodon* is considered the outgroup taxon for comparisons with the emydopoids because it displays the more generalized anatomy for basal dicynodonts (Barry 1967; Cluver and King 1983; King and Rubidge 1993; Ray 2001; Modesto 2003; Angielczyk 2007).

3.1.1. Orbitosphenoid

The orbitosphenoid is a vertically-oriented bone located at the skull midline. The orbitosphenoid contacts the frontal and parietal dorsally and the parabasisphenoid complex ventrally. It supported the olfactory bulbs in life (Hopson 1979). Its exact anatomical constituents have been heavily debated (Olson 1938, 1944; Barry 1967; Kemp 1969; Cluver 1971), however, it is generally agreed that the orbitosphenoid consists of two dorsally projecting wings and a medial vertical crest (the mesethmoid) in non-mammalian synapsids (Araújo et al. 2017; Angielczyk et al. 2019). The orbitosphenoid of *Pristerodon* conforms to this pattern, as it displays the typical Y-shaped cross-section.

In anterior view, the wings of the orbitosphenoid are curved, which results in a slightly convex outer wall, which makes an angle of 48^{o} with the sagittal plane (Figure 3.1A). Anterodorsally, the median vertical process (obvp) projects dorsal and divides the olfactory cavity medially (ofc). The median vertical process is slender at its midheight but has expanded dorsal and ventral edges in anterior view (Figure 3.1A). At its dorsalmost part, the median vertical process forms a broad horizontal surface (hpl) that contacts the frontal anterodorsally. The articulation surface is oval in dorsal view (Figure 3.1B). The wings of the orbitosphenoid are thin anteriorly but thicken posteriorly (Figure 3.1B). In dorsal view, the wings of the orbitosphenoid form a long anteroposterior gutter that hosted the olfactory bulbs (Figure 3.1B).

In lateral view, the orbitosphenoid has a subtrapezoidal outline. The dorsal margin of the wings is horizontal in lateral view, except for a notch that excavates the wings at midlength (obdn, Figure 3.1C). The ventral margin of the mesethmoid articulates with the dorsal groove of the parasphenoid rostrum. In lateral view, the mesethmoid extends posteriorly as a wall (mpw) that supports the dorsal wings (Figure 3.1C).

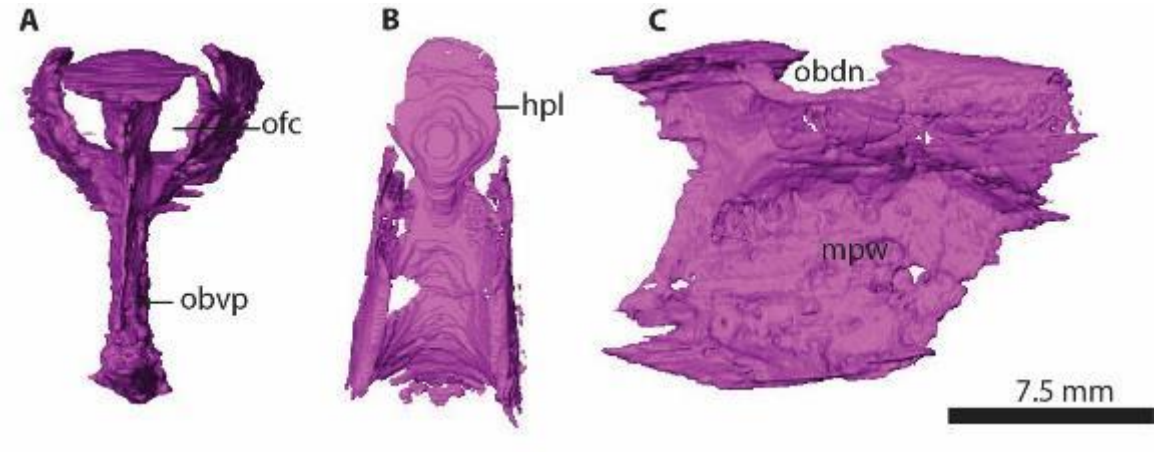


Figure 3. 1. The orbitosphenoid of *Pristerodon mackayi* (BP/1/2642) in **(A)** anterior, **(B)** dorsal and **(C)** left lateral views. obdn, the orbitosphenoid dorsal notch; ofc, olfactory cavity; obvp, orbitosphenoid medial vertical process; hpl, horizontal plate; mpw, mesethmoid posterior wall.

3.1.2. Pterygoid

In *Pristerodon* the pterygoids form an important part of the palate and display the typical dicynodont X-shaped morphology. The median plate sends divergent anterior palatal and posterior quadrate rami that form an angle of 115° between them. The median plate of the pterygoid forms an interdigitated suture with the parabasisphenoid internally, but this suture has an M-like outline in ventral view (Figure 3.2C). The pterygoid bounds the narrow and long interpterygoid vacuity just anterior to the median plate, and in this taxon, the vacuity extends forward to reach the vomer (Barry, 1967; Cluver and King, 1983). The pterygoid in BP/1/2642 is affected by cracks that hamper the description of the complete morphology of the quadrate ramus (Figure 3.2B/C).

In dorsal view, there is a small anteromedial process (pt amp, Figure 3.2B) that develops on the dorsal edge of the palatal ramus of the pterygoid in BP/1/2642, similar to that described as the anterior pterygoidal process in SAM-10153 by Cluver and King (1983). The two processes nearly touch each other at the midline and contact the vomer laterally (Cluver and King, 1983). The pterygoidal process is separated from the rest of the anterior ramus by an anteroposterior notch (pt nt, Figure 3.2B). The pterygoid median plate is overlapped dorsally by the laterally expanded basisphenoid.

In lateral view, the palatal ramus is broader anteriorly than posteriorly. This ramus presents a blunt keel (pt ke) on its anteroventral region (Figure 3.2E). The pterygoidal process gives a Y-shape to the palatal ramus in lateral view. The median plate expands laterally, forming the short and stout pterygoid lateral lamina (ptll). The pterygoid lamina is bordered by a sulcus dorsally (pt dsu, Figure 3.2E). The quadrate ramus is considerably narrower than the palatal ramus. It projects posteriorly and reaches the quadrate. A small triangular portion of the epipterygoid footplate (epi) is discernible on the left quadrate ramus (Figure 3.2E). Due to

damage, I could not determine how much of the epipterygoid was overlapping the quadrate ramus of the pterygoid.

The anterior margin of the palatal ramus is U-shaped in ventral view. Because a lamina is present laterodorsally, the pterygoid median plate is wider than the anterior ramus in *Pristerodon*. There is a trough lateral to the pterygoid lamina that tapers posteriorly and anteriorly in ventral view (ptvt, Figure 3.2C). This excavation is delimited medially by the prominent crista oesophagea (co). The two cristae oesophagea extend posteriorly and meet at the midline just anterior to the carotid foramina posteriorly in BP/1/2642. This union opens a deep and long anteroposterior furrow (fu) between the crista oesophagea (Figure 3.2C). The crista oesophagea fuse into a thin median ridge in well-preserved specimens of *Pristerodon* such as BP/1/3024, BP/1/7206 and USNM 23580. This seems different in BP/1/2642 because acid preparation has flattened this crest (Christian Kammerer, pers. comm.).

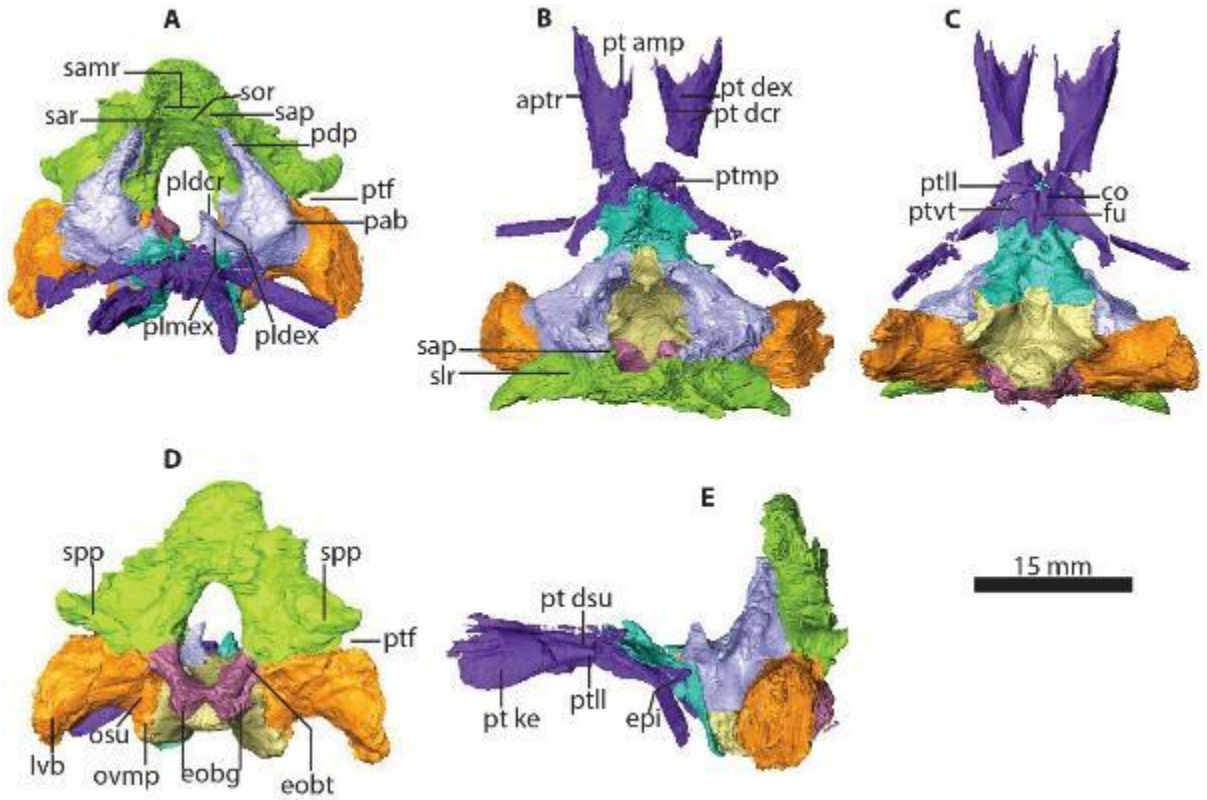


Figure 3. 2. The braincase of *Pristerodon mackayi* (BP/1/2642) in **(A)** anterior, **(B)** dorsal, **(C)** ventral, **(D)** occipital and **(E)** left lateral views. aptr, anterior pterygoid rami; co, crista oesophagea; eobg, exoccipital posterior bulge; eobt, exoccipital subvertical buttress; epi, epipterygoid; fu, pterygoid anteroposterior furrow; lvb, opisthotic lateral vertical buttress; osu, opisthotic posterior vertical sulcus; ovmp, opisthotic ventromedial process; pab, prootic anterior bulge; pad, pila antotica anterior depression; pdp, prootic dorsal process; pt dsu, pterygoid dorsal sulcus; pt ke pterygoid keel; ptll, pterygoid lateral lamina; ptmp, pterygoid median plate; pt nt, pterygoid anteroposterior notch; ptvt, pterygoid ventral trench; sap, supraoccipital anterior process; sap, supraoccipital anteriorly projected crest; sar, supraoccipital anterior recess; slr, supraoccipital lateral recess; sor, supraoccipital anterior horizontal ridges; spp, supraoccipital posterior process.

3.1.3. Parabasisphenoid

The parabasisphenoid complex forms the anterior floor of the braincase. The parabasisphenoid in BP/1/2642 is affected by minute cracks, but a small portion of the parasphenoid rostrum (ps) is present together with the basipresphenoidal region (anterior to the pituitary fossa) and its basipostsphenoid portion (posterior to the pituitary fossa). The basipostsphenoid portion in *Pristerodon* protrudes posteroventrally and overlaps the basioccipital forming the basal tubera and, is perforated by the carotid foramina as in other dicynodonts (Modesto et al. 2003; Castanhinha et al. 2013). Along its dorsal aspect the basipostsphenoid hosted the pituitary gland posterior to the sella turcica. In *Pristerodon*, the complex formed by the parasphenoid rostrum and basipresphenoid (PRB complex) is slender, tapers posteriorly, and has an anteroposterior groove (psgr) on its anterodorsal portion in dorsal view (Figure 3.3A). The posterior half of the PRB bears a tall process of triangular outline in lateral view.

In dorsal view the basipostsphenoid in *Pristerodon* flares laterally from the posterior end of the parasphenoid rostrum. It is excavated by a subvertical concavity (bpdc) which is delineated ventromedially by the tuberculum sellae (tse, 3.3A). The left and right tuberculum

sellae meet at the midline anterior to the sella turcica and continue towards the suture with the parasphenoid rostrum. The tuberculum sellae marks the anterior border of the sella turcica (stu, Figure 3.3A). The bottom of the pituitary fossa (sella turcica) is perforated by the carotid foramina (ic) and is bordered laterally by a discrete clinoid process (clp). The clinoid processes (Figure 3.3A/B) consist of thin crests that give a triangular outline to the pituitary fossa in dorsal view. Posterior to the pituitary fossa, the dorsum sellae (ds) forms a low tuberosity. The carotid foramina do not join dorsally into a single orifice. The carotid foramina in *Pristerodon* are oval with the longest diameter extending anteroposteriorly in ventral view (Figure 3.3C). The distance between the two internal carotid foramina in ventral view is narrow in *Pristerodon* (1.2 mm).

In ventral view the basipostsphenoid contacts the basioccipital posteriorly along a sigmoidal suture, and the pterygoid anteriorly along an interdigitated M-shape suture. There is an anteroposterior sulcus with a lobate shape on the posterior median end of the basipostsphenoid delimited by the basisphenoidal tubera laterally (bpvsu, Figure 3.3C). This sulcus is 3.5 mm wide and extends posteriorly onto the basioccipital as described by Ray (2001) for specimen ISIR 372. The posteroventrally projected basisphenoidal tubera (bpt) form buttress-like structures that broaden ventrally, where they form a secluded wall to the fenestra ovalis posteriorly.

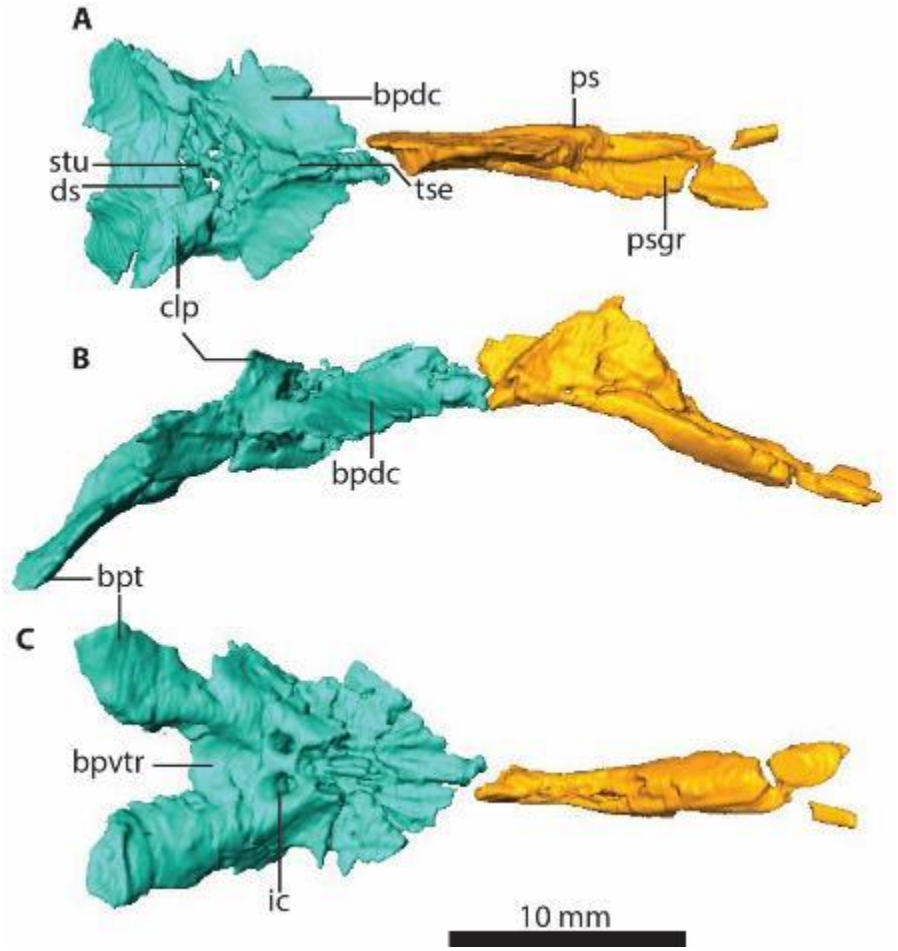


Figure 3. 3. The parabasisphenoid of *Pristerodon mackayi* (BP/1/2642) in **(A)** dorsal, **(B)** right lateral and **(C)** ventral views. bpdc, basisphenoidal dorsal subvertical concavity; bpt, basisphenoidal tubera; bpvsu, basisphenoidal ventral sulcus; clp, clinoid process; ds, dorsum sellae; ic, internal carotid foramina; ps, parasphenoid rostrum; psgr, parasphenoid dorsal rostrum groove; tse, tuberculum sellae; stu, sella turcica.

3.1.4. Basioccipital

The basioccipital in *Pristerodon* forms the posterior portion of the braincase floor, posterior to the parabasisphenoid complex. The basioccipital in *Pristerodon* is expanded mediolaterally but tapers anteriorly and posteriorly, resulting in a subhexagonal shape in both ventral and dorsal views. The basioccipital can be divided into two main anatomical subunits: the basioccipital portion of the occipital condyle posteriorly and the basioccipital tubera anterolaterally.

In posterior view the basioccipital displays an inverted U-shape with the tubera pointing ventrally. As in other dicynodonts, the basioccipital in *Pristerodon* forms the ventral lobe of the occipital condyle and extends laterally to border the vestibule (fenestra ovalis) and the jugular foramen medially. In posterior view, the basioccipital condyle is less prominent than the exoccipital condyles (Figure 3.2D), and its dorsal portion flares out laterally to form two symmetrical concavities (bocc) in which the exoccipital condyles are hosted (Figure 3.4A). The two concavities are separated by a median ridge (bocr) on the dorsal face of the basioccipital condyle. There is an occipital pit at the intersection between the basioccipital and exoccipital condyles in posterior view (Figure 3.2D).

In dorsal view the basioccipital tubera portion is outlined by two anteriorly conjoined S-like ridges (bosr) that terminate posteriorly, contacting the opisthotic and bordering the medial wall of the fenestra ovalis (fo, Figure 3.4B). These ridges meet anteriorly to form the anteroposteriorly-oriented median ridge of the basioccipital (bomr). The basioccipital median ridge is thinner than the S-ridges and is present only on the anteriormost region of the basioccipital. In dorsal view, the dorsal suture of the basioccipital condyle in *Pristerodon* is marked by a stretched M-shaped flat edge (ms) that smoothly develops ventrally to accommodate the exoccipital condyles (Figure 3.4B). The jugular foramen (jf) opens a hemicylindrical sulcus between the M-shaped suture and the S-ridge as the basioccipital forms its floor in dorsal view. In *Pristerodon*, only a very small portion of the basioccipital contributes to the jugular foramen laterally compared to the exoccipital and opisthotic.

In ventral view, the basioccipital tubera have a smoothly excavated anteroventral surface that contacts the basisphenoidal tubera. They are separated by a deeper and wider anteroposteriorly oriented midline trough (bovtr) that opens posteriorly (Figure 3.4C). This trough is interrupted posteriorly by a low and blunt transverse intertuberal ridge (itr). Previous workers (Huxley 1868; Broom 1915; Barry 1967; Cluver and King 1983 and Ray 2001),

however, do not comment on the presence of this ridge on the basioccipital in *Pristerodon*, so its presence might be variable. Posterior to the intertuberal ridge, there is a deeper basioccipital collar-like excavation (bocex) that separates the basioccipital tubera from the basioccipital condyle. The basioccipital condyle in BP/1/2642 is spherical and is pierced by minute foramina (bocf) in ventral view. The fenestra ovalis (fo) is oval and its long axis extends mediolaterally.

In lateral view, the basioccipital tubera projects obliquely ventral to the horizontal plane, and its walls are thicker anteriorly than posteriorly (Figure 3.4D). In lateral view, the vestibule of the inner ear (ve) excavates a conical cavity on the basioccipital lateral wall (fo, Figure 3.4D).

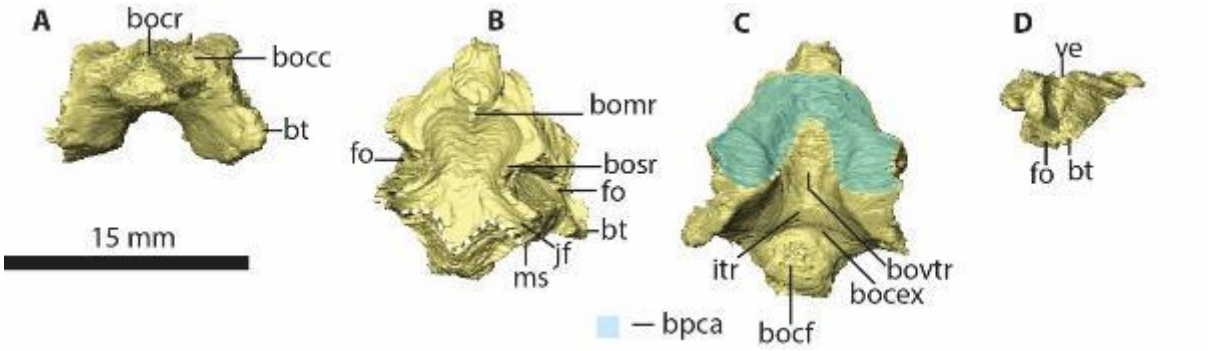


Figure 3. 4. The basioccipital of *Pristerodon mackayi* (BP/1/2642) in **(A)** posterior, **(B)** dorsal, **(C)** ventral, and **(D)** right lateral views. bocc, basioccipital condyle; bocex, basioccipital colar-like excavation; bocf, basioccipital condyle foramina; bocr, basioccipital condyle median ridge; bomr, basioccipital median ridge; bosr, basioccipital lateral ridges; bovtr, basioccipital ventral trough; bpca, basisphenoidal sutural area; bt, basioccipital tubera; itr, intertuberal ridge; fo, fenestra ovalis; jf, jugular foramen; ve, vestibule.

3.1.5. Exoccipital

The exoccipitals form the posterolateral portion of the braincase and constitute most of the ventral half of the foramen magnum and the dorsal third of the occipital condyle in most

dicynodonts, including *Pristerodon* (Cox 1965; Modesto et al. 2003, Fröbisch 2007, Castanhinha et al. 2013). It bounds the medial border of the jugular foramen. Typically, the exoccipital is traversed by the canal for the hypoglossal cranial nerve (CN XII) in dicynodonts (Castanhinha et al. 2013), but this could not be segmented in the specimen BP/1/2642 due to damage. The exoccipital contacts the supraoccipital dorsally, the opisthotic laterally and the basioccipital ventrally. The exoccipital is coossified to the supraoccipital and opisthotic anteriorly. The ventral suture with the basioccipital is M-shaped. The exoccipital in *Pristerodon* can be divided into two main components: the exoccipital condyle and the dorsal component.

In anterior view, each exoccipital is knob-like and is excavated by the jugular foramen (Figure 3.5). The exoccipital condyle is robust and sends a short tuber-like process (eoat) that overlaps the M-like posterodorsal edge of the basioccipital (Figure 3.5A). The base of the exoccipital condyle shows a sigmoidal outline in anterior view. The articular surface of the exoccipital condyle has a convex aspect. The dorsal component of the exoccipital has an expanded dorsal end at the contact with the supraoccipital in anterior view. The exoccipital forms the posterodorsal border of the jugular foramen (jf), which is located between the dorsal edge of the dorsal component and the exoccipital condyle in anterior view (Figure 3.5A). The foramen excavates a semi-cylindrical cavity in the exoccipital.

In posterior view, the foramen magnum (fm) is vertically elliptical and the exoccipital covers 40% of its ventral portion. The exoccipital is dorsoventrally short in posterior view (Figure 3.5B). The dorsal end of the exoccipital in posterior view coincides with the greater width of the foramen magnum, which is 6 mm long. The exoccipital condyle is typically reniform in dicynodonts but it is very damaged in BP/1/2642. Therefore, the exoccipital condyle of BP/1/2642 is formed by an oblique bulge (eobg) that is overlapped by the subvertical buttress (eobt) of the dorsal component. The dorsal component forms a subvertical

and hourglass-shaped buttress (eobt) that sutures with the supraoccipital dorsally and descends to overlap the exoccipital condyle. The dorsal component extends dorsally to just above the level of the dorsal margin of the jugular foramen. The two exoccipitals are coossified at the midline above the basioccipital (Figure 3.2/5).

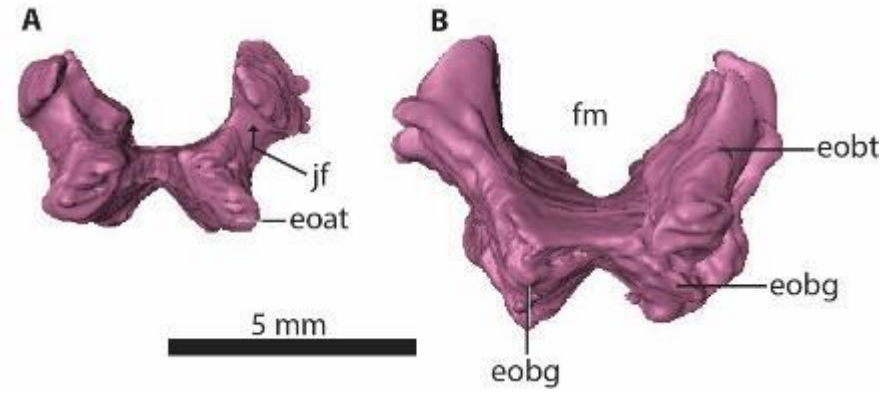


Figure 3. 5. The exoccipital of *Pristerodon mackayi* (BP/1/2642) in **(A)** anterior and **(B)** posterior views. eoat, exoccipital anterior tuberosity; eobg, exoccipital posterior bulge; eobt, exoccipital subvertical buttress; fm, foramen magnum; jf, jugular foramen.

3.1.6. Supraoccipital

The supraoccipital is the largest element of the occiput, forming the posterodorsal part of the braincase. The supraoccipital in *Pristerodon* is subvertically-oriented with a slight anterior tilt (Figure 3.6C). *Pristerodon* shows the typical anatomy of the dicynodont supraoccipital, which is divided into three main anatomical sub-units (e.g., Castanhinha et al. 2013; Macungo et al. 2020): one medial lobe and two lateral alae. The supraoccipital bounds the dorsal half of the foramen magnum. Its lateral wing borders the posttemporal fenestra dorsally, and hosts the posterior half of the floccular fossa, and the vestibular organ medially. Anteriorly, the supraoccipital contacts the prootic, and ventrally the opisthotic and exoccipital.

In anterior view the supraoccipital in *Pristerodon* is characterized by two anteriorly-projected crests (sap, Figure 3.6A/C) that lengthen ventrally to the dorsal process of the prootic. These crests are oblique and meet dorsally at the midline. They border an anteromedial triangular recess (sar) that is bounded ventrally by an incipient horizontal ridge (sor). The anterior face of the supraoccipital lateral alae is perforated by small circular oblique cavities for the insertion of the anterior semicircular canal (ascca) in anterior view. These cavities communicate internally to the large vertical one that accommodates the crus communis (cca, Figure 3.6A/B). The region where the crus communis is accommodated does not form a distinct buttress in *Pristerodon* unlike in emydopoids. Mediolaterally, the supraoccipital forms the posterior wall of the floccular fossa (flo), which has a circular outline and is 2.65 mm deep (Figure 3.6A/B).

In lateral view the anterior suture with the prootic is located at the top of a dorso-ventrally elongated recess (slr, Figure 3.6C). This suture is dorsoventrally oriented and appears completely coossified on CT images. The dorsoventral recess is also known as the venous groove in *Dicynodontoides* and other dicynodonts (Olson 1944; Cox 1959; Cluver 1971; King 1981; Surkov and Benton 2004) or as the anterior posttemporal fenestra groove in *Emydops* (Fröbisch and Reisz 2008). This recess is dorsoventrally oblique and as tall as the supraoccipital.

In posterior view, the supraoccipital of *Pristerodon* is taller than wider as it forms 60% of the dorsal margin of the tall and slightly compressed foramen magnum (Figure 3.6D). Its posture is more vertically-oriented compared to the emydopoids. The supraoccipital medial lobe is robust and has a rounded dorsal margin in posterior view (Figure 3.6D). The supraoccipital alae of *Pristerodon* are more laterally pointed and possess a horizontal process (spp), which expands laterally to border the dorsal margin of the posttemporal fenestra (ptf,

Figure 3.6D). Whereas the suture between the supraoccipital and the exoccipital is oblique in posterior view, it is horizontal between the supraoccipital and the opisthotic (Figure 3.2D).

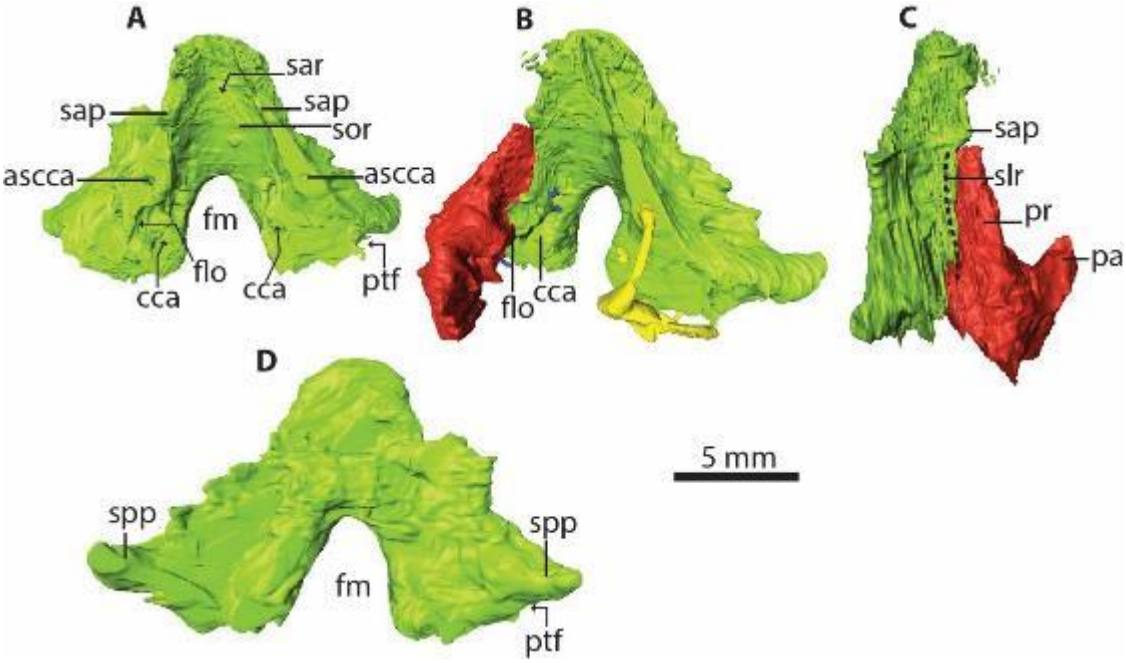


Figure 3. 6. The supraoccipital of *Pristerodon mackayi* (BP/1/2642) in **(A)** anterior, **(B)** internal, **(C)** right lateral and **(D)** posterior views. assca, attachment of the anterior semicircular canal; cca, attachment of the crus communis; flo, floccular fossa; fm, foramen magnum; pa, pila antotica; pr, prootic; ptf, posttemporal fenestra; sap, supraoccipital anteriorly projected crest; sar, supraoccipital anterior recess; slr, supraoccipital lateral recess; sor, supraoccipital anterior horizontal ridges; spp, supraoccipital posterior process.

3.1.7. Prootic

The prootic forms the anterior part of the braincase lateral wall and borders the foramen magnum anterolaterally. Its medial wall is excavated by the floccular fossa and is pierced by the anterior semicircular canal. Due to its complex morphology, the prootic is described as two anatomical subunits: the main body posteriorly and, the anterior ascending ramus that forms the pila antotica.

The main body forms the lateral flange posteriorly (Laaß et al. 2017). It is typically coossified to the opisthotic forming the periotic in dicynodonts (Surkov and Benton 2004; Morato 2006; Boos et al. 2016; Kammerer et al. 2016; Angielczyk and Kammerer 2017). However, in *Pristerodon* (specimen BP/1/2642) the sutures are not always discernible as they are coossified with the opisthotic in some places. As it sends a dorsal process (pdp) dorsally to contact the supraoccipital, the opisthotic and basioccipital ventrally, and the parabasisphenoid anteriorly, the lateral flange forms the anterolateral wall of the braincase. In anterior view, the lateral flange tapers dorsally resulting in a crescent shape, with the concavity facing medially. The prootic bulges (pab) at the lateral part of the crescent in anterior and dorsal views (Figure 3.7A). The pila antotica (pa) projects dorsally from the anterior-most part of the prootic. It is low in *Pristerodon* compared to that of the emydopoid taxa described below. It overlaps the clinoid process of the parabasisphenoid and has a convex anteromedial edge in anterior view (Figure 3.7A). The distance between the left and right pila antotica is short in BP/1/2642 (Figure 3.2A), as they curve slightly medially.

In lateral view, the posterior portion of the prootic is dorsoventrally elongated in *Pristerodon* (Figure 3.7B). The notch posterior to the pila antotica gave passage to the V^{th} cranial nerve (Figure 3.7B). The lateral face of the prootic just ventral to the trigeminal notch is depressed (prd). The prootic anterior portion i.e., the pila antotica is thick and pyramidal, and has a slightly depressed lateral surface (pad). At the edge of its ventral suture with the basioccipital, the prootic is traversed by the facial foramen (fa, Figure 3.7B). Whereas the posteroventral margin of the prootic is in sutural contact with the opisthotic, its posterodorsal margin sutures with the supraoccipital in posterior view. At its contacts with the opisthotic, the prootic borders the anterior wall of the posttemporal fenestra (ptf, Figure 3.2A). The prootic of *Pristerodon* is perforated by small oval subvertical recesses for the anterior and lateral semicircular canal at its posterodorsal and posteroventral corners, respectively (Figure 3.7C).

In ventral view, the prootic overlaps the basioccipital and basipostsphenoid, and forms the anterior wall of the fenestra ovalis (fo). The suture is slightly horizontal with the basioccipital (boa) and oblique with the basipostsphenoid (bsa, Figure 3.7D). The fenestra ovalis forms an upside-down dorso-ventrally elongated conical cavity. This cavity is smaller than in the emydopoids described below. The shape of the vestibule suggests that the vestibule (ve) of the inner ear was crescentic in *Pristerodon* with the concavity facing laterally.

The medial aspect of the posterior portion of the prootic is excavated by a shallow horizontal floccular fossa (flo) that is surrounded by the osseous duct for the anterior semicircular canal (Figure 3.7E).

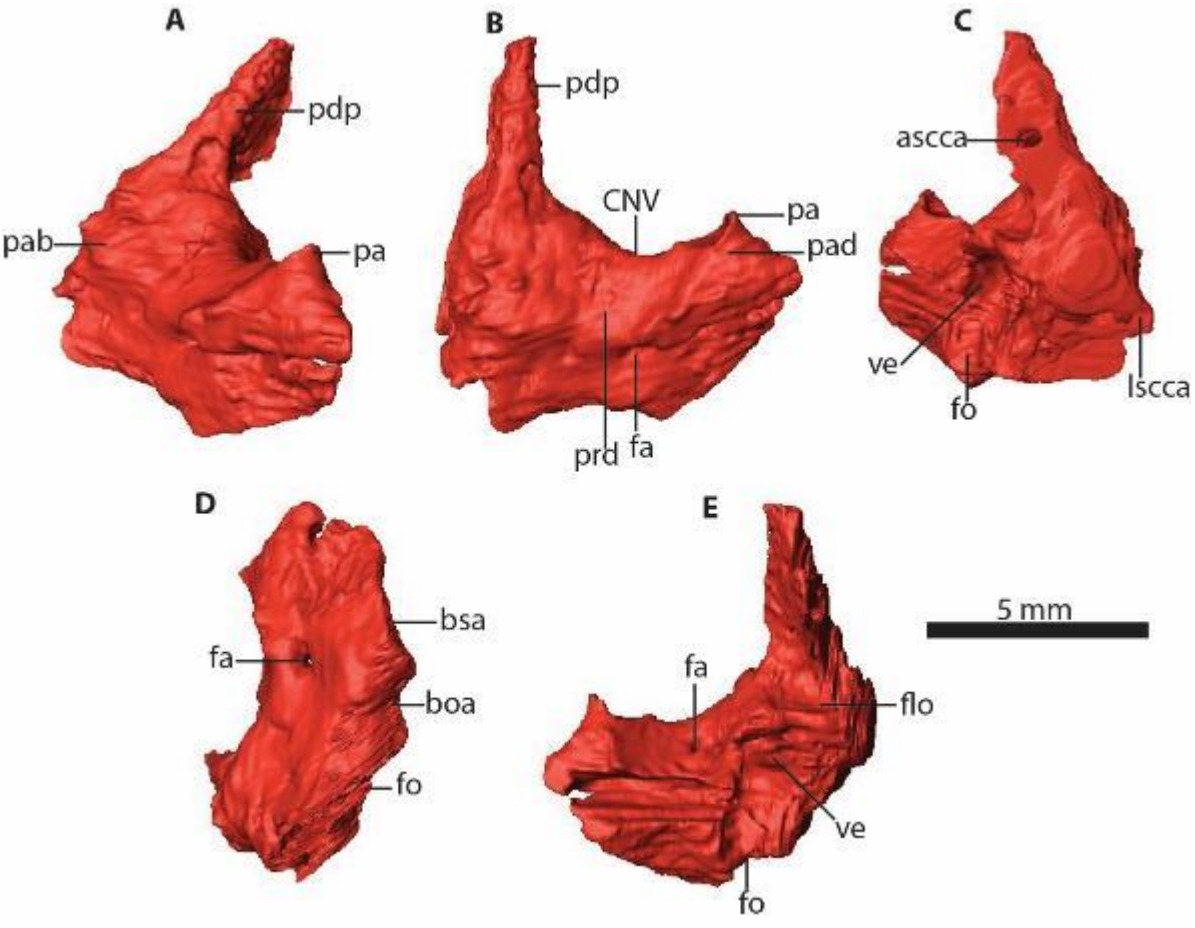


Figure 3. 7. The right prootic of *Pristerodon mackayi* (BP/1/2642) in **(A)** anterior, **(B)** lateral, **(C)** posterior **(D)** ventral and **(E)** medial views. assca, attachment of the anterior semicircular

canal; boa, basioccipital sutural area; bsa, parabasisphenoidal sutural area; CNV, passage of the cranial nerve five (V); fa, facial foramen; flo, floccular fossa; fo, fenestra ovalis; lscca, attachment of the lateral semicircular area; pa, pila antotica; pab, prootic anterior bulge; pad, pila antotica anterior depression; pdp, prootic dorsal process; prd, prootic lateral depression; ve, vestibule.

3.1.8. Opisthotic

The opisthotic in *Pristerodon* is a horizontal hour-glass-shaped bone in posterior view that forms the posterolateral wall of the braincase. It is located ventral to the supraoccipital and posterior to the prootic. The opisthotic contacts the exoccipital medially, and it sends a ventromedial process that contacts the basioccipital ventrally. The opisthotic borders the ventral margin of the posttemporal fenestra dorsally. Ventrally, it forms the posterior margin of the fenestra ovalis and the anterior margin of the jugular foramen.

The opisthotic shares an irregular suture with the prootic anteriorly (pra), which has a nearly semi-lunate shape (Figure 3.8A). This suture, gives an irregular aspect to the opisthotic in anterior view. On the dorsal margin of its anterior face, the opisthotic is penetrated by a small oval recess for the lateral semicircular canal (lscc), and by the ventral portion of the posterior semicircular canal (pscc) on its ventromedian part (Figure 3.8A). The ‘pscc’ excavates a larger recess than the ‘lscc’ in *Pristerodon* anterior view. Ventral to the entrance of the ‘pscc’, the opisthotic is excavated by a tuber-like conical vertical trough that hosted the vestibule of the inner ear (vea). The fenestra ovalis (fo) opens on the ventral margin of the vestibule and the ventromedial process of the opisthotic bounds its posterior wall. In lateral view, the opisthotic of *Pristerodon* has an oval outline (Figure 3.8B). Its lateral surface is smoothly concave to accommodate the articulation facet of the squamosal and quadrate (afac, Figure 3.8B).

The posterior aspect of the opisthotic is generally convex in *Pristerodon* (Figure 3.8C). The main body of the opisthotic is horizontal and expands laterally into the lateral vertical buttress (psb) in posterior view. It forms the ventral rim of the posttemporal fenestra (ptf). The lateral vertical buttress is the tallest part of the opisthotic in *Pristerodon* (Figure 3.8C). It is prominent ventrally where it forms the thick and tuber-like paroccipital process. At its medial edge, the main body of the opisthotic forms the ventromedial process (ovmp, Figure 3.8C). The ventromedial process of the opisthotic of *Pristerodon* is small, vertically oriented and its dorsal part is located ventral to the jugular foramen in posterior view (Figure 3.8C). This process shares a vertically-oriented suture with the basioccipital. There is a shallow vertical sulcus (osu) that excavates the opisthotic and separates the ventromedial process from the body of the opisthotic in posterior view (Figure 3.8C).

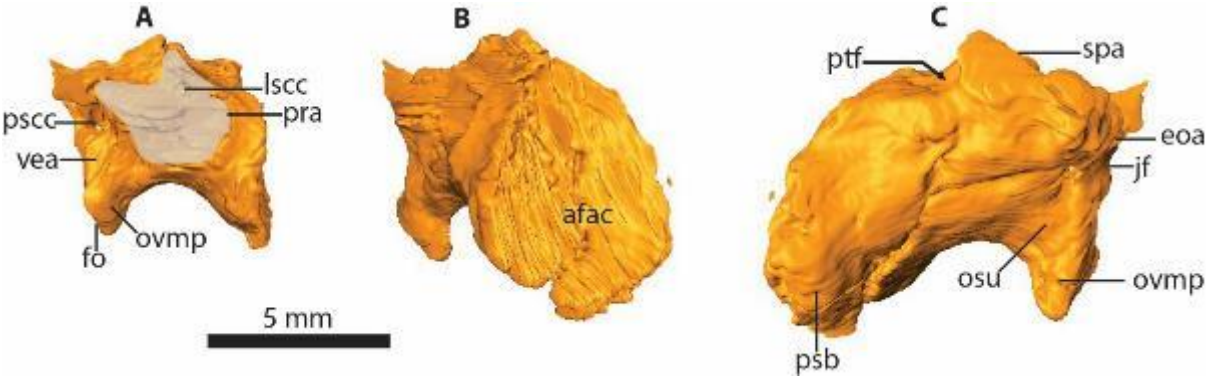


Figure 3. 8. The left opisthotic of *Pristerodon mackayi* (BP/1/2642) in **(A)** anterior, **(B)** lateral and **(C)** posterior views. afac, articulation facet concavity; eoa, exoccipital sutural area; fo, fenestra ovalis; jf, jugular foramen; lscc, attachment of the lateral semicircular canal; osu, opisthotic posterior vertical sulcus; ovmp, opisthotic ventromedial process; pra, prootic sutural area; psb, opisthotic lateral vertical buttress; pscc, attachment of the posterior semicircular canal; ptf, posttemporal fenestra; spa, supraoccipital sutural area; vea, vestibular area.

3.2. Anatomical description 2

SYSTEMATIC PALAEONTOLOGY

Order THERAPSIDA Broom, 1905

Suborder ANOMODONTIA Owen, 1859

Infraorder DICYNODONTIA Owen, 1859

Family MYOSAURIDAE Kitching, 1968

Myosaurus gracilis Haughton 1917

Specimens: BP/1/2690, BP/1/2701a (the description is a composite of the two specimens)

3.2.1. Orbitosphenoid

The orbitosphenoid of *Myosaurus* displays the typical Y-shape in anterior view. It is generally thicker than in *Pristerodon*, shorter dorsoventrally, but mediolaterally wider. As in other dicynodonts, the orbitosphenoid is composed of the vertical median process (the mesethmoid) anteriorly and the dorsally projected wings posteriorly (Castanhinha et al. 2013). The gutter that hosts the olfactory bulbs dorsally is wider than in *Pristerodon*. In anterior view, the orbitosphenoid has tall wings that open at a greater angle from the sagittal plane, which results in a broad olfactory cavity. The wings are less curved than in *Pristerodon* (Figure 3.9A). The median vertical process has a prominent vertical crest (obacr) on its anteriormost edge that is flanked by two lateral sulci (obasu) visible in anterior view. The dorsal aspect of the median process of the orbitosphenoid thickens dorsally in *Myosaurus* and bears a distinct horizontal fossa (obdfo, Figure 3.9B). Anterior to this fossa, an approximately 1.4 mm long spine projects anteriorly in the prolongation of the medial wall.

In lateral view, the orbitosphenoid is sub-rectangular in *Myosaurus*. It is short anteroposteriorly compared to *Kawingasaurus*. The dorsal margin of the wings is not horizontal like in *Pristerodon*, but slightly curved (Figure 3.9C). The plate-like vertical wall, which supports the wings of the orbitosphenoid, is dorsoventrally short in *Myosaurus* and it is

traversed by two oblique crests (ltcr) in lateral view (Figure 3.9C). The ventral-most crest is long, and the dorsal one is much shorter.

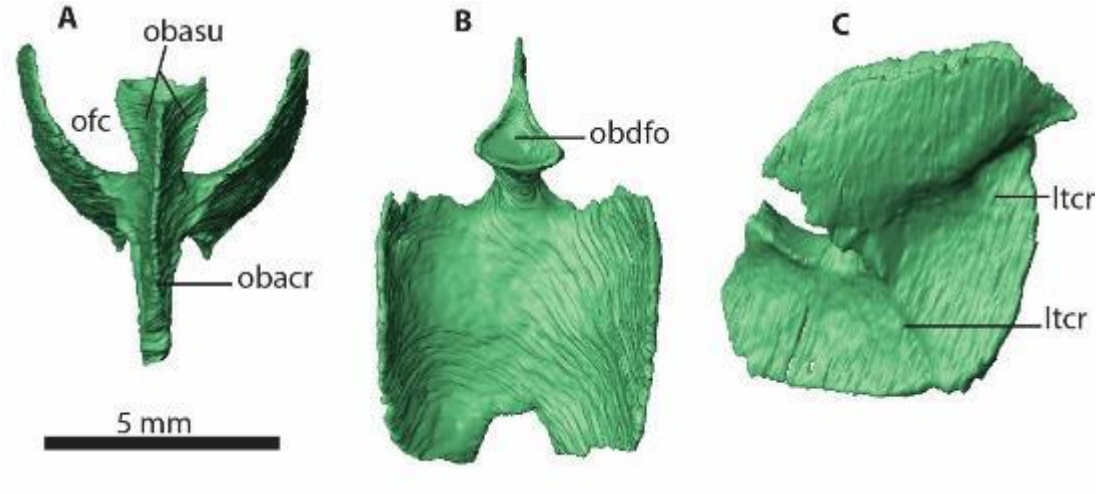


Figure 3. 9. The orbitosphenoid of *Myosaurus* (BP/1/2690) in **(A)** anterior, **(B)** dorsal and **(C)** right lateral views. obacr, orbitosphenoid vertical crest; obasu, orbitosphenoid lateral sulci; obdfo, orbitosphenoid dorsal fossa; ofc, olfactory cavity; ltcr, lateral wall oblique crests.

3.2.2. Pterygoid

The pterygoid in the two specimens of *Myosaurus* is well-preserved, except for the left quadrate ramus. It retains the X-shape dicynodont morphology. The palatal rami are more horizontal than in *Pristerodon* as they form an angle of 22º with the anteroposterior median axis of the skull only. The quadrate ramus angles ~61º with the sagittal axis of the skull and ~102º with the palatal ramus. The pterygoid in *Myosaurus* has a longer palatal ramus compared to the quadrate ramus (Figure 3.10D). In dorsal view, the palatal ramus is mediolaterally thinner in *Myosaurus* than in *Pristerodon*. On the anterior half of the palatal ramus, the pterygoid of *Myosaurus* is excavated by a narrow anteroposterior groove (pt gr) dorsally (Figure 3.10A). Posterior to this groove, there is the pterygoidal process (pt amp) that projects over the palatal ramus and terminates posteriorly at the anterior end of the pterygoid median plate in specimen

BP/1/2701a (Figure 3.10D). The quadrate ramus is coossified to a small portion of the epipterygoid dorsally.

In lateral view, the palatal ramus in *Myosaurus* is taller compared to the quadrate ramus. The specimens of *Myosaurus* described here do not present a ventral keel (Figure 3.10B/E). This is consistent with previous works on *Myosaurus*, in which this structure is not described (Haughton, 1917; Hammer and Cosgriff, 1981). The anteromedial pterygoidal process is triangular and gives a Y-shape to the pterygoid in lateral view (Figure 3.10E). This process is long and more developed dorsally than in *Pristerodon*. It angles 52º with the rest of the palatal ramus in *Myosaurus* BP/1/2701a. The quadrate ramus of the pterygoid (ptqr) attaches to the median pterygoid plate on the short posterior process of the median pterygoid plate. The quadrate ramus has a dorsoventrally flattened and pointed end in lateral view in BP/1/2701a (Figure 3.10E).

In ventral view, the palatal ramus of the pterygoid has a constant thickness (Figure 3.10C). The median plate of the pterygoid (ptmp) is narrow in *Myosaurus*. In ventral view, it contacts the basisphenoid along an interdigitating suture posteriorly and sends a short process posteriorly to meet the clinoid process of the basisphenoid (Figure 3.10C). *Myosaurus* has a V-shaped crista oesophagea (co) that meet at the midline posteriorly between the two carotid foramina and bifurcate anteriorly onto the palatal rami. The cristae are short anteriorly, i.e., they extend just to the anterior end of the pterygoid median plate. The crista oesophagea are incipient posteriorly, but they are prominent anteriorly. In BP/1/2690, the crista oesophagea is flat, but in the well-preserved specimen SAM-PK-K10974, the crista oesophagea forms a thin ridge. This difference may be the result of taphonomy or preparation. The suture between the two pterygoids is visible and marked by a poorly pronounced anteroposterior furrow (apf) at the midline (Figure 3.10C). The interpterygoid vacuity is narrower and more elongated in

Myosaurus than in *Pristerodon*. In ventral view, the quadrate ramus is expanded anteriorly and has a robust posterior edge.

Medially, the pterygoid is excavated by an anteroposterior muscle scars (msc) which probably hosted some fibers of the pterygoideus externus muscle (Figure 3.10C).

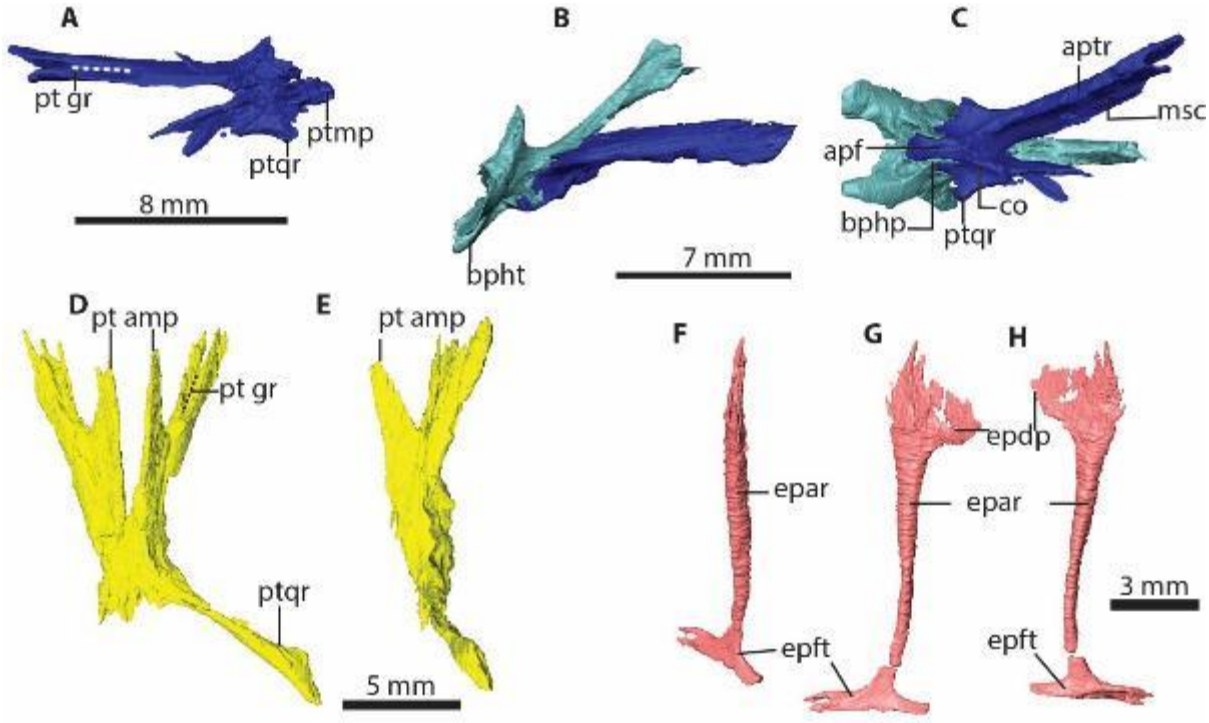


Figure 3. 10. The pterygoid of *Myosaurus* (BP/1/2690) in **(A)** dorsal, **(B)** right lateral and **(C)** ventral views; pterygoid of *Myosaurus* (BP/1/2701a) in **(D)** dorsal and **(E)** right lateral views; epipterygoid of *Myosaurus* BP/1/2701a in **(F)** anterior, **(G)** lateral and **(H)** medial views. apf, pterygoid anteroposterior furrow; aptr, anterior pterygoid rami; co, crista oesophagea; epar, epipterygoid ascending ramus; epdp, epipterygoid dorsal plate; epft, epipterygoid footplate; msc, muscle scars; pt amp, pterygoid anteromedial process; pt gr, pterygoid dorsal groove; ptmp, pterygoid median plate; ptqr, pterygoid quadrate ramus.

3.2.3. Epipterygoid

The epipterygoid is a vertically elongated braincase sidewall element that usually rests on the quadrate ramus ventrally and ascends to contacts the descending flanges of the parietal dorsally in dicynodonts (Keyser 1965, 1974; Angielczyk and Sullivan, 2008; Castanhinha et al. 2013; Angielczyk and Kammerer, 2017; Laaß and Kaestner, 2017; Angielczyk et al. 2019). The epipterygoid is preserved in specimen BP/1/2701a (Figure 3.10F, G, H) and is constituted of a subhorizontal footplate ventrally (epft) and a rod-like ascending ramus dorsally (epar). The footplate consists of a short anterior ramus and a posterior quadrate ramus that is broken off at nearly its mid-length (Figure 3.10G, H). The preserved portion of the quadrate ramus is taller and longer than the anterior ramus in lateral view (Figure 3.10G). The ventromedial surface of the footplate rests entirely on the dorsal aspect of the quadrate ramus of the pterygoid as in other emydopoids (Keyser 1965; Fourie 1991, 1993). The suture between the footplate and the quadrate ramus of the pterygoid follows the longitudinal plane of the skull. The epipterygoid footplate does not contact the parabasisphenoid in *Myosaurus*. The lateral surface of the epipterygoid is nearly flat but its medial surface is concave (Figure 3.10G, H). In dorsal view, the quadrate ramus of the epipterygoid footplate is mediolaterally wider than the anterior ramus.

In *Myosaurus*, the ascending ramus of the epipterygoid is longer and straighter than in *Kawingasaurus*, and forms a right angle with the footplate (Figure 3.10G). The ascending ramus has an anteroposteriorly wide base. Dorsally, it tapers considerably to become a rod-like bone at its mid-height and broadens more dorsally into a roughly inverted triangular-shaped dorsal process (epdp, Figure 3.10G, H). The dorsal process of the ascending ramus is slightly concave medially and articulates with the parietal laterally.

3.2.4. Parabasisphenoid

The parabasisphenoid complex of *Myosaurus* is well-preserved and has a subtriangular shape in both dorsal and ventral views. As usual in dicynodonts, the basipostsphenoid forms the posterior end of the bone, and the parasphenoid rostrum and basipresphenoid (PRB) forms its anterior part (Cox 1959).

The PRB is mediolaterally broad in *Myosaurus*. In dorsal view, it is excavated by an anteroposteriorly elongated and thin sulcus (pss). This sulcus is bordered by two low lateral crests (psc, Figure 3.11A). Posteriorly, this sulcus ends into a small anteroposteriorly oval foramen in the parasphenoid (psf). This pit opens on the ventral side of the bone within a circular cavity (Figure 3.11C). Whereas this pit is located anterior to the carotid foramina in BP/1/2690 (Figure 3.11A), it forms a notch on the anterior margin of the carotid foramina in BP/1/2701a. As such, it may represent a relictual pituitary fossa. In contrast to what is found in several dicynodont taxa, the PRB and the basipostsphenoid are fused in *Myosaurus*. The position of the carotid foramina is the only evidence to infer the position of the suture. The carotid foramina open dorsally into a single large circular orifice. Posterior to the carotid foramina, in dorsal view, lies the sella turcica (stu), which is a shallow excavation bordered posteriorly by a shallow inconspicuous ridge that corresponds to the dorsum sellae (Figure 3.11A). The sella turcica extends shortly anteriorly onto the carotid foramina but it is not confined anteriorly. There is no tuberculum sellae in *Myosaurus*. The sella turcica in *Myosaurus* is limited laterally by the dorsally projecting clinoid process (clp) of the basipostsphenoid. The clinoid process sharpens dorsally and its dorsal edge is turned medially. The clinoid process has a concave recess along with its dorsal extension and is separated from the pila antotica by a 0.3 mm gap. The clinoid processes are separated posteriorly by the dorsum sellae (ds, Figure 3.11A). The dorsum sellae is interrupted posteriorly by the transverse suture with the basioccipital in dorsal view. The basisphenoidal tubera (bpt) project posteroventrally

and have a slightly concave dorsal surface that articulates with the basioccipital. As such, the basisphenoidal tubera do not border the fenestra ovalis because the anteromedial wall of the fenestra is entirely formed by the basioccipital. In lateral view, the parasphenoid rostrum is straight but has a dorsoventrally expanded anterior tip (Figure 3.11B). The clinoid process notches the parasphenoid rostrum and forms a nearly vertical angle in *Myosaurus*.

In ventral view, the PRB tapers more anteriorly than posteriorly. It is excavated by a median trough that envelops the parasphenoid foramen (Figure 3.11C). The ventral aspect of the base of the PRB is not flat but is irregular due to the interdigitating suture with the pterygoid median plate (Figure 3.11C). This suture obscured most of the ventral anatomy of the PRB. The basipostsphenoid in *Myosaurus* does not form to the ventral depression of the basicranium. Instead, the basisphenoidal tubera only border the ventral depression laterally. The carotid foramina are bordered by thin ridges and they diverge ventrally and follow to some degree the basisphenoidal tubera (Figure 3.11C).

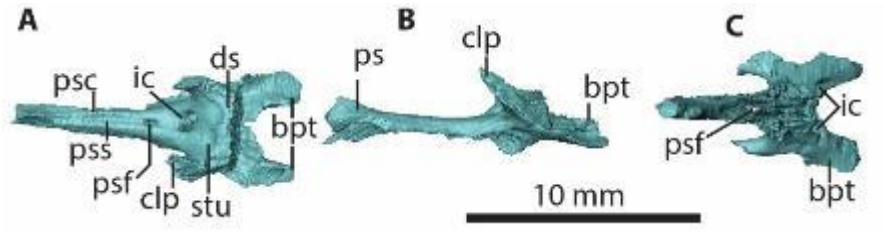


Figure 3. 11. The parabasisphenoid of *Myosaurus* (BP/1/2690) in **(A)** dorsal, **(B)** left lateral and **(C)** ventral views. bpt, basisphenoidal tubera; clp, clinoid process; ds, dorsum sellae; ic, internal carotid foramina; ps, parasphenoid rostrum; psc, parasphenoidal crests; psf, parasphenoidal foramen; pss, parasphenoidal sulcus; stu, sella turcica.

3.2.5. Basioccipital

The basioccipital in *Myosaurus* forms more than half the length of the braincase floor at the back of the skull. The basioccipital displays a subtrapezoidal shape in dorsal and ventral views, the posterior wall being the shortest. Its anterior and posterior aspects form an inverted U-shape. The basioccipital contacts the parabasisphenoid anteriorly, the opisthotic laterally, the prootic anterodorsally, and the exoccipital posterodorsally.

The basioccipital condyle is the most prominent structure in posterior view. The basioccipital condyle is excavated by two concavities (bocc) that host the exoccipital in posterior view (Figure 3.12A). Dorsal to these concavities, the condyle is traversed by the M-shaped ridge (bocdr) that articulates with the anterior tuberosity of the exoccipital (Figure 3.12B). In dorsal view, the dorsal surface of the basioccipital is slightly concave (Figure 3.12B). This concavity is separated in two by a blunt median ridge (bomr). The lateral margin of the basioccipital has sigmoidal ridges in dorsal view. The vestibule of the bony labyrinth (vea) deeply notches the lateral aspects of the basioccipital and opens ventrally as the fenestra ovalis (fo).

In ventral view, the basioccipital of *Myosaurus* is excavated by a Y-shaped depression (bod, Figure 3.12C). The two branches of the Y-shaped depression delineate the semi-spherical condyle posteriorly. Four nutritive foramina (bonf) aligned on the sagittal axis perforate the basioccipital along the median depression. The basioccipital contacts the parabasisphenoid anteroventrally along a wave-like suture with the basisphenoidal tubera extending backward to overlap the basioccipital tubera. The fenestra ovalis is ellipsoidal with its long diameter (3.3 mm by 1.5 mm) extending along the coronal axis of the skull.

In lateral view, the basioccipital is knob-like and is excavated by the jugular foramen dorsally (Figure 3.12D). The basioccipital forms the floor of the jugular foramen (jf). It has a minor contribution to the jugular foramen as the major portion is formed by the exoccipital and

opisthotic. The jugular foramen is located between the condyle and the basioccipital tuberum in lateral view (Figure 3.12D). This recess is large with a circular outline, and its diameter is 2.5 mm.

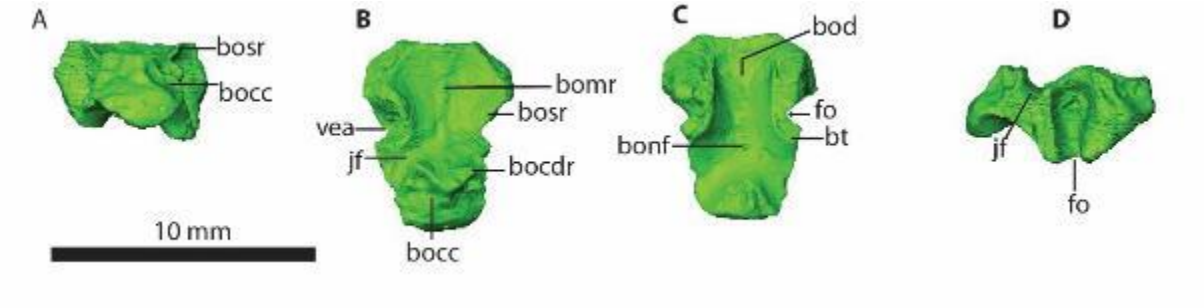


Figure 3. 12. The basioccipital of *Myosaurus* (BP/1/2690) in **(A)** posterior, **(B)** dorsal, **(C)** ventral and **(D)** right lateral views. bocc, basioccipital condyle; bod, basioccipital ventral depression; bodcr, basioccipital condyle dorsal ridge; bomr, basioccipital median ridge; bonf, basioccipital nutritive foramina; bosr, basioccipital lateral ridges; bt, basioccipital tubera; fo, fenestra ovalis; jf, jugular foramen; vea, vestibular area.

3.2.6. Exoccipital

As in other dicynodonts, the exoccipital in *Myosaurus* contributes to the occipital condyle and borders the ventral half of the foramen magnum. The exoccipital contacts the supraoccipital dorsally along an oblique suture, whereas it contacts the opisthotic laterally along a subvertical suture in posterior view. Ventrally, its suture with the basioccipital forms a saddle-like outline.

In anterior view, the two exoccipital condyles (eoc) meet at the midline. The exoccipital contributes to the posterior half of the jugular foramen (jf) which excavates a large subvertical semi-cylindrical cavity in the ventral aspect of the exoccipital in anterior view. The jugular foramen is bounded by the exoccipitals posteriorly, the opisthotic anteriorly, and the basioccipital laterally. The dorsal component has a subtriangular anterior face which is

perforated by a deep vertical cylindrical furrow (eovf) that hosts the posterior semicircular canal (Figure 3.13A/C).

In posterior view, the exoccipital condyles are semilunate and more prominent than the basioccipital condyle and they form the majority of the occipital condyle. Its dorsal surface is concave as it contributes to the ventral margin of the foramen magnum. The dorsal component of the exoccipital (eodc) is subrectangular in posterior view. It descends from the contact with the supraoccipital dorsally to form the dorsomedial border of the jugular foramen in posterior view (Figure 3.13B). The dorsal component of the exoccipital and the exoccipital condyle are separated by a shallow trench (eoptr) in posterior view.

In dorsal view, the exoccipital condyle forms a knob-like anterior tuberosity (eoat) located medially to the jugular foramen that contacts the dorsal aspect of the basioccipital ventrally (Figure 3.13C). In ventral view, there is a deep occipital pit (occp) in BP/1/2690 at the intersection of the two exoccipitals and the basioccipital (Figure 3.13D).

Medially, the exoccipital condyle is pierced by the hypoglossal foramen (hf). The ensuing canal is oriented obliquely connecting the jugular foramen to the foramen magnum (Figure 3.13E). The hypoglossal foramen is circular and its diameter is 0.5 mm in medial view.

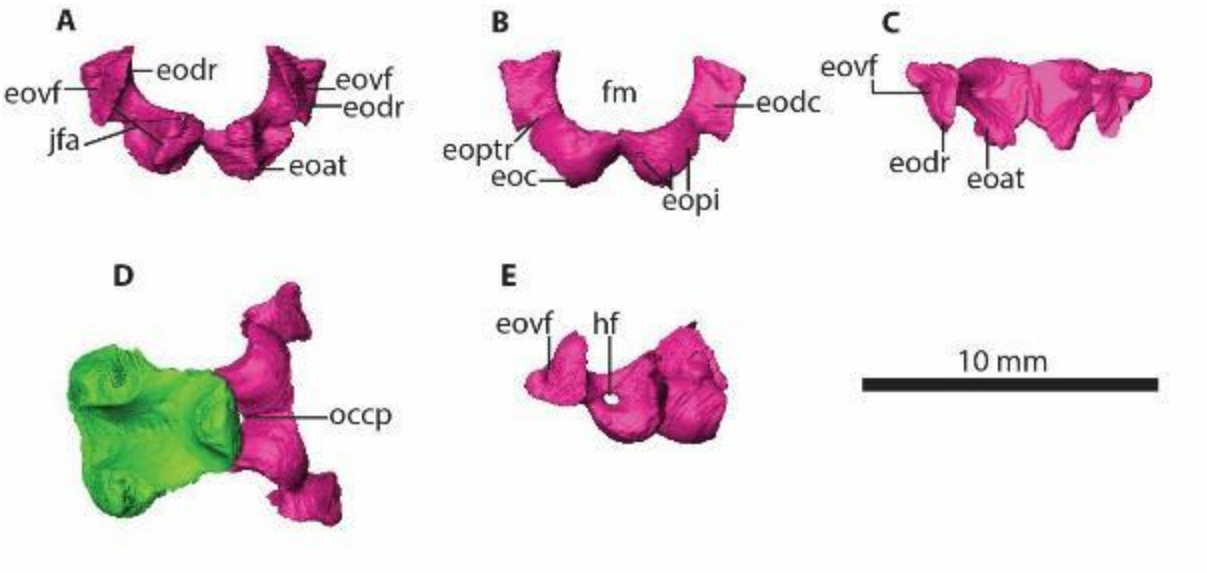


Figure 3. 13. The exoccipital of *Myosaurus* (BP/1/2690) in (A) anterior, (B) posterior, (C) dorsal, (D) ventral and (E) ventromedial views. eoat, exoccipital anterior tuberosity; eoc, exoccipital condyle; eodc, exoccipital dorsal component; eoptr, exoccipital posterior trench; eovf, exoccipital vertical furrow; fm, foramen magnum; hf, hypoglossal foramen; jf, jugular foramen; occp, occipital pit.

3.2.7. Supraoccipital

The supraoccipital has an inverted U-shape in anterior and posterior views as it forms the dorsal margin of the foramen magnum. The morphology of the posterior aspect of the supraoccipital of *Myosaurus* specimens BP/1/2690 and BP/1/2701a, as well as in other specimens (Haughton 1917), does not show a distinct medial lobe and lateral alae *per se*, because it has a rounded dorsal edge (Figure 3.14B). The main feature of the anterior view is a buttress that hosted the common crus of vestibular organ limited dorsally by crests, whereas the feature of the posterior surface is has a smoothly flatter aspect. The supraoccipital contacts the exoccipitals in an oblique suture in posterior view.

In anterior view, the supraoccipital bears a short descending process (sap) projecting from the anterolateral edge to the level of the contact with the prootic. Ventrally, the edge terminates by subcylindrical buttress oriented vertically and anteriorly (smb, Figure 3.14A). This buttress encircles the crus communis of the bony labyrinth and the anterior semicircular canal (ascc). Lateral to the buttress, lies the floccular fossa (flo), which separates the crus communis and the anterior semicircular canal. The floccular fossa is deep (2.2 mm), cylindrical and is oriented sub-obliquely to the horizontal plane. Its posterior half is flanked laterally by a sharp semicircular crest (sac) of the supraoccipital (Figure 3.14A).

In posterior view, there is a symmetrical pit (spi) on each side of the supraoccipital dorsal to the foramen magnum. These are interpreted as foramina which may have been for vessels bringing nutrients to the brain (Hammer and Cosgriff 1981; Angielczyk et al. 2009;

Angielczyk and Kammerer 2017) in other dicynodonts, however, in *Myosaurus* the pits do not perforate anteriorly. The supraoccipital is bounded laterally by shallow vertical depressions (svd) in posterior view that descend from the dorsal edge of the supraoccipital onto the exoccipital (Figure 3.14B). The lateroventral corner of the supraoccipital forms the posttemporal fenestra together with the exoccipitals, but the lateral wall of this fenestra is bounded by the opisthotic. As in other dicynodonts, the foramen magnum is dorsoventrally oval in posterior view. In *Myosaurus*, the foramen magnum is 3.9 mm at its widest point. Ventrally, the supraoccipital is excavated by a conspicuous sulcus for the posterior semicircular canal (psca, Figure 3.14C).

The supraoccipital has a lateral vertical recess (slr) formed by the lateral and anterior edges of the supraoccipital best seen in dorsal view (Figure 3.14D). The recess descends from the dorsalmost aspect of the supraoccipital to nearly half the height of the foramen magnum.

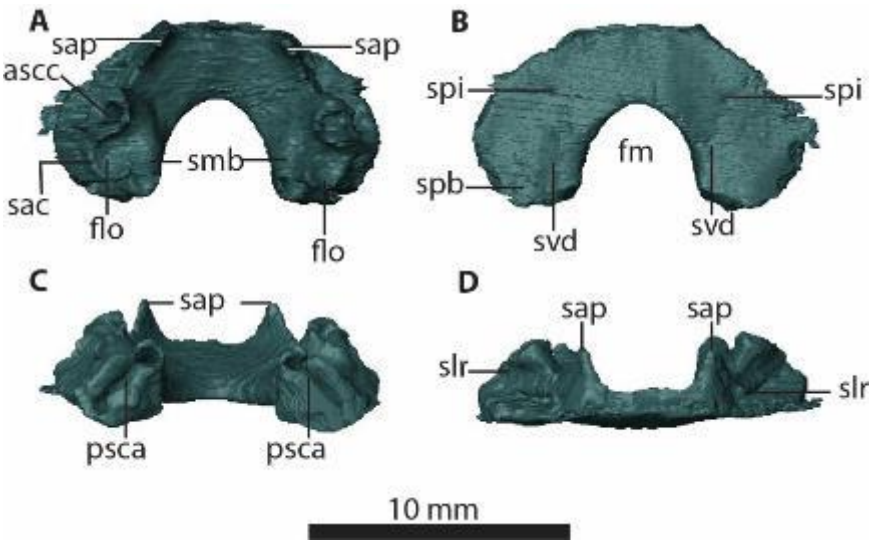


Figure 3. 14. The supraoccipital of *Myosaurus* (BP/1/2690) in **(A)** anterior, **(B)** posterior, **(C)** ventral and **(D)** dorsal views. assc, attachment of the anterior semicircular canal; flo, floccular fossa; fm, foramen magnum; psca, attachment of the posterior semicircular canal; sac, supraoccipital semicircular crests; sap, supraoccipital anteriorly projected crest; slr,

supraoccipital lateral recess; smb, supraoccipital subvertical buttress; spi, supraoccipital posterior pit; svd, supraoccipital posterior vertical depressions.

3.2.8. Prootic

The prootic of *Myosaurus* is a knob-like vertically oriented bone in lateral and medial views, that forms the lateral wall of the braincase. As typical in dicynodonts, the prootic borders the anterior wall of the foramen magnum. It is formed by the pila antotica anteriorly and the lateral flange posteriorly. The prootic of *Myosaurus* specimen BP/1/2690 is not completely fused to the surrounding bones (except the opisthotic) as it displays a gap of a few millimeters with the supraoccipital dorsally, the basioccipital and parabasisphenoid anteroventrally on CT-images.

In anterior view, the pila antotica (pa) of *Myosaurus* is tall, slightly curved medially, mediolaterally compressed, and tapers dorsally. Its anteroventral half is bordered by medial and lateral crests (prac) that join dorsally at half the pila antotica height, flanking a shallow vertical trough (Figure 3.15A).

In lateral view, the main body of the prootic sends a lateral flange (plf) posteriorly, that sutures with the opisthotic on its posteroventral part. The suture with the opisthotic is serrated and is oblique in lateral view (Figure 3.15B). The lateral flange has an S-like posterodorsal margin, and its dorsal and ventral margins are horizontal. Its anterior margin is straight and obliquely oriented in lateral view (Figure 3.15B). A notch for the passage of the trigeminal nerve (CN V) is present at the anteroventral part of the lateral flange and posterior to the pila antotica. In lateral view, the pila antotica of *Myosaurus* appears as an isosceles triangle, whereas the anterior border is relatively straight and the posterior border slightly convex (Figure 3.15B). The pila antotica typically overlaps the clinoid process of the basisphenoid but in BP/1/2690, they are separated by a 0.3 mm gap (gp, Figure 3.15D). The medial face of the prootic is slightly depressed in lateral view (best seen in dorsal view, Figure 3.15F), and ventral

to this depression, the prootic is perforated by the circular facial foramen (fa). Also, the prootic forms the lateral wall of the conical fenestra ovalis which opens on the ventral side of the bone.

In medial view, the posterior and anterior margins of the prootic are oblique, whereas the ventral margin is horizontal. The dorsal margin of the prootic is V-shaped as it is traversed by the trigeminal nerve (Figure 3.15C). The prootic forms the anterior wall of the horizontal, large and deep floccular fossa (flo) in medial view. The dorsal and ventral limits of the floccular fossa bear conjoined sigmoidal crests (prmc), the ventral one being the most prominent. The dorsal crest serves to articulate to the supraoccipital. The suture with the supraoccipital appears S-like in medial view (Figure 3.15C). A small circular cavity for the anterior semicircular canal (ascc) perforates the prootic dorsal to the floccular fossa in medial view. This cavity connects to a large conical one located ventrally to floccular fossa, which hosted the vestibule of the inner ear (vea, Figure 3.15C). As the sutural area between the prootic and opisthotic is visible in medial view, it appears trapezoidal. The base of the pila antotica is robust in medial view, and it overlaps the basioccipital along a nearly rectangular contact. Dorsal to this suture and anterior to the vestibule, is the facial foramen.

In posterior view, the prootic is excavated by a half-donut-like excavation (ppex), which exits through the posttemporal fenestra (Figure 3.15E). There is a bulge (prpb) at the concave part of the excavation which contributes to the anterior components of the posttemporal fenestra wall (Figure 3.15E). The prootic of BP/1/2690 is separated from the supraoccipital by a 0.4 mm gap posteriorly. Along its posteroventral corner, the prootic contacts the opisthotic in posterior view. This contact appears triangular. At the medial part of the suture, the prootic and opisthotic are perforated by the lateral semicircular canal (lsca, Figure 3.15E).

In dorsal view, the prootic forms a vertical buttress (pabt) and sends the lateral flange laterally. This buttress hosted the anterior semicircular canal. The area between the buttress and the lateral flange is depressed in dorsal view (Figure 3.15F).

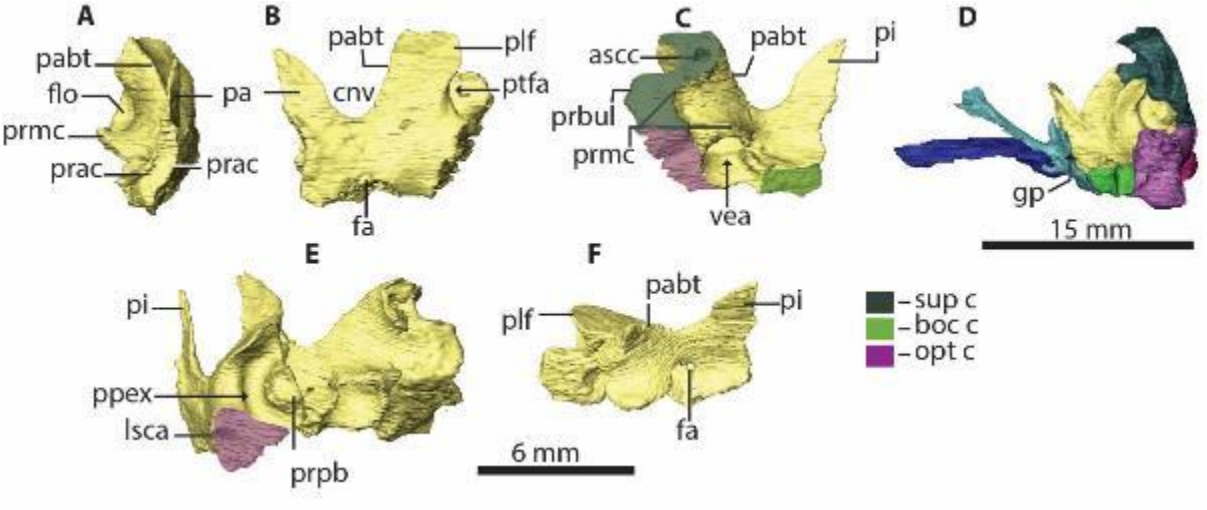


Figure 3. 15. The prootic of *Myosaurus gracilis* (BP/1/2690) in **(A)** anterior, **(B)** left lateral, **(C)** medial **(E)** posterior and **(F)** dorsal views; **(D)** the braincase of BP/1/2690 in left lateral view. assc, attachment of the anterior semicircular canal; boc c, sutural area of the prootic and the basioccipital; CNV, passage of the cranial nerve five (V); fa, facial foramen; flo, floccular fossa; gp, gap between the prootic and the clinoid process; lscca, attachment of the lateral semicircular area; pa, pila antotica; opt c, sutural area between prootic and opisthotic; pabt, prootic anterior buttress; plf, prootic lateral flange; ppex, prootic posterior excavation; prac, pila antotica anterior crests; prmc, prootic medial crest; prpb, prootic posterior bulge; sup c, sutural area of the prootic and supraoccipital; vea, vestibular area.

3.2.9. Opisthotic

The opisthotic in *Myosaurus* displays a subtrapezoidal shape in posterior view. It bears a well-developed ventromedial process. In anterior view, the lateral margin of the opisthotic forms the posteroventral wall of the posttemporal fenestra. The suture with the prootic is located in the middle of the anterior face of the opisthotic. This surface appears jagged in Figure 16A as

it represents an interdigitating suture and was thus different to segment out. The anteromedial aspect of the opisthotic is characterized by conjoined medial (omc) and lateral crests (olc). The lateral crest is sigmoidal while the medial one is linear and subvertically-oriented (Figure 3.16A, C). The lateral crest forms the lateral margin of the opisthotic that sutures with the supraoccipital. The medial one borders the articulation with the prootic. The two crests meet dorsally and ventrally to form a large cavity that hosts the vestibular organ (vea). The ventromedial process of the opisthotic (ovmp) is a thick and robust tuber-like knob in *Myosaurus*. The medial tip of the process expands anteroposteriorly to receive the basioccipital along its medial flat edge and the exoccipital condyle along its dorsal edge.

In posterior view, the opisthotic is shaped like a horizontal hourglass as its dorsal and ventral aspects are concave (Figure 3.16B/C). The ventral margin is the longest in posterior view. The stout oblique body (ob) is flanked by posteromedial (opmb) and lateral vertical buttresses (lvb). The posteromedial buttress of the opisthotic descends onto the dorsal component of the exoccipital ventrally, but remains separated from it by a 0.4 mm gap in specimen BP/1/2690. The lateral vertical buttress sutures with the squamosal and descends ventrally to articulates with the quadrate. The two opisthotic buttresses terminate dorsally forming rounded bulges visible in dorsal view (obu). These bulges comprise the posterior part of the posttemporal fenestra posterior to the prootic bulge. The posteromedial aspect of the opisthotic is excavated by an oblique slit sulcus (osu) that separates the main body of the opisthotic and the ventromedial process. This sulcus extends dorsally to join the exoccipital posterior trench. The ventromedial process is more vertical in specimen BP/1/2701a. In ventral view, the process borders the fenestra ovalis (fo) posteriorly, and the jugular foramen (jf) anteriorly (Figure 3.16D).

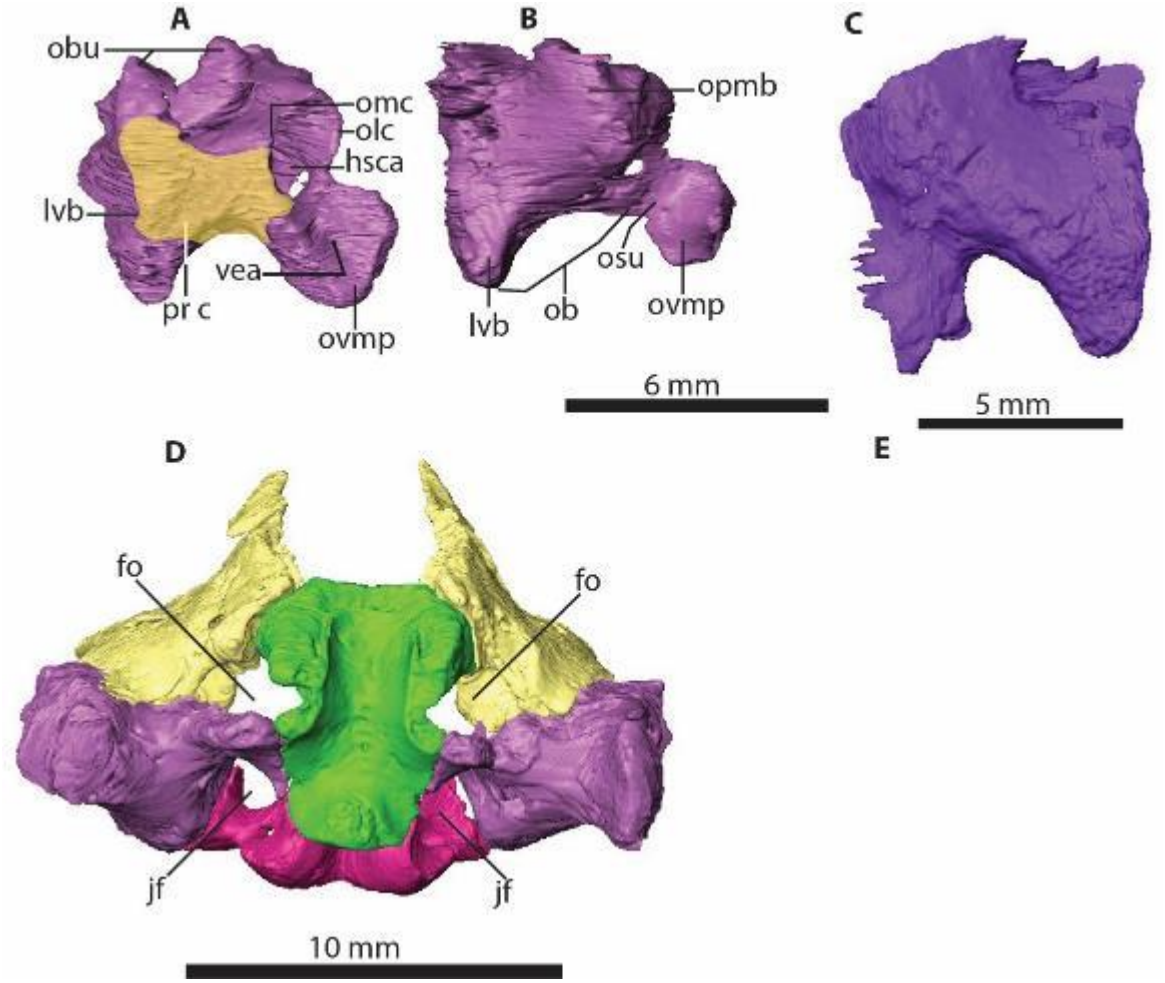


Figure 3. 16. The left opisthotic of *Myosaurus gracilis* (BP/1/2690) in **(A)** anterior and **(B)** posterior views; left opisthotic of (BP/1/2690) in **(C)** posterior; the braincase of (BP/1/2690) in **(D)** ventral views. fo, fenestra ovalis; jf, jugular foramen; lsca, attachment of the lateral semicircular canal; lvb, opisthotic lateral vertical buttress; ob, opisthotic body; obu, opisthotic bulges; olc, opisthotic lateral crest; omc, opisthotic medial crest; opmb, opisthotic posteromedial buttress; osu, opisthotic posterior vertical sulcus; ovmp, opisthotic ventromedial process; pr c, prootic sutural area.

3.3. Anatomical description 3

SYSTEMATIC PALAEONTOLOGY

Order THERAPSIDA Broom, 1905

Suborder ANOMODONTIA Owen, 1859

Infraorder DICYNODONTIA Owen, 1859

Superfamily EMYDOPOIDEA van Hoepen, 1934

Family CISTECEPHALIDAE Owen, 1876

Nov. gen, nov. spe.

Specimen: PK-16-1

3.3.1. Pterygoid

The pterygoid of the Malawian cistecephalid PK-16-1 has both palatal and quadrate rami well-preserved but is riddled by several small breaks and cracks. Its morphology is the typical dicynodont X-shape in dorsal and ventral views. The palatal rami extend anteriorly nearly parallel to each other along the sagittal axis whereas the quadrate rami open a greater angle between each other posteriorly. In PK-16-1, the two pterygoids diverge at an angle of 117º posteriorly. The Malawian cistecephalid does not preserve the pterygoid anteromedial process dorsally. Also, it does not form a distinct median plate *per se*, as the rami do not meet at the skull midline. In dorsal aspect, the palatal rami of the pterygoid are shorter and mediolaterally wider than the quadrate rami (Figure 3.17A).

In lateral view, the palatal ramus is tall in the Malawian cistecephalid PK-16-1, but the quadrate ramus is narrow. In PK-16-1, the lateral aspect of the quadrate ramus of the pterygoid is excavated by an anteroposterior shallow trench (pt ltr) that accommodates the epipterygoid footplate (Figure 3.17B).

In PK-16-1, the two pterygoids and the parabasisphenoid are coossified posteriorly in ventral view, but the right and left pterygoid halves are separated by a thin crest emerging from the basisphenoid. This condition is shared with *Cistecephaloides* (Cluver 1974a) but contrasts with that in *Cistecephalus* where the crest is absent (Keyser 1965). The pterygoid of the Malawian cistecephalid bears a longitudinal sulcus running at the base of the crista oesophagea on its ventral aspect (pt vsc, Figure 3.17C). The crista oesophagea (co) terminates posteriorly by overlapping the parabasisphenoid just anterior to the carotid foramina in ventral view, and extends anteriorly to almost one-fourth of the anterior extension of the palatal ramus. Such an anterior extension of the crista oesophagea is shared with the cistecephalid *Kembawacela*, but they differ in that the crista is posteriorly formed by the parabasisphenoid in *Kembawacela* (Angielczyk et al., 2019). The quadrate ramus of the pterygoid reaches the quadrate posteriorly and curves slightly medially in ventral view (Figure 3.17C).

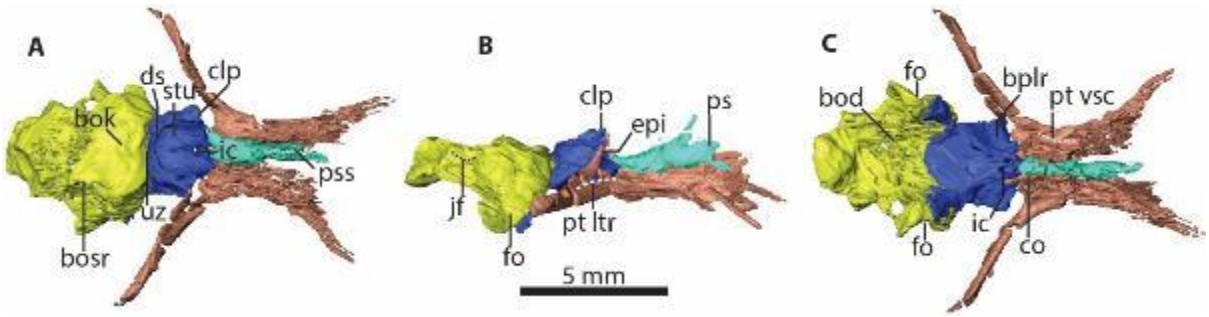


Figure 3. 17. The ventral region of the braincase of the Malawian cistecephalid (basisphenoid, parabasisphenoid and pterygoid) in **(A)** dorsal, **(B)** right lateral and **(C)** ventral views. bod, basioccipital ventral depression; bok, basioccipital dorsal knob; bosr, basioccipital lateral ridges; bplr, basisphenoidal lateral recess; clp, clinoid process; co, crista oesophagea; ds, dorsum sellae; epi, epipterygoid; fo, fenestra ovalis; jf, jugular foramen; ic, internal carotid foramina; ps, parasphenoid rostrum; pss, parasphenoid rostrum dorsal sulcus; pt ltr, pterygoid lateral trench; pt vsc pterygoid ventral sulcus; stu, sella turcica; uz, unossified zone.

3.3.2. Parabasisphenoid

The parabasisphenoid in the Malawian cistecephalid is riddled with minute fractures and it is partly coossified with the basioccipital posteriorly. Anteriorly, it shares an interdigitated suture with the pterygoid. The basipostsphenoid preserves the sella turcica (stu) bordered laterally by the clinoid process (clp) and the dorsum sellae posteriorly (ds).

The parasphenoid rostrum and basipresphenoid (PRB) is damaged and is bent slightly to the left, but it is visibly robust posteriorly and tapers considerably anteriorly. In dorsal view, the anterior half of the PRB is excavated by a shallow longitudinal sulcus medially (pss, Figure 3.17A). The parabasisphenoid complex is traversed by a fracture, which delimits the anterior wall of the carotid foramina dorsally. The two carotid canals open dorsally into a single orifice, but they split ventrally as in *Myosaurus*. In dorsal view, the sella turcica is shallow anteriorly where it is pierced by the carotid canals, but it is slightly deeper posteriorly. It is bordered anteriorly by the robust base of the PRB, the clinoid process laterally, and the dorsum sellae posteriorly. The clinoid process is subvertical, semicircular, and inclined anteromedially. Its dorsal surface is concave. The dorsum sellae is thin and convex posteriorly. Posterior to the dorsum sellae there is a mediolaterally-oriented gap (uz) that separates the basioccipital from the basisphenoid in dorsal view (Figure 3.17A). A similar gap was interpreted as an unossified zone in other synapsids (Olson 1944, Cluver 1971, Araújo et al 2017). In lateral view, the PRB forms an isosceles triangle, with the base placed anteriorly and the apex turned posteriorly (Figure 3.17B). Its anterior region deepens ventrally in lateral view, however, this may be a result of damage.

In ventral view, the posterior portion of the PRB forms a thin strip of bone that extends ventrally and separates the two pterygoids in ventral view (Figure 3.17C). The carotid foramina are oval in cross-section and the distance between the foramina is narrow in PK-16-1. Ventrally, the carotid foramina are asymmetric, i.e., they are not aligned along the coronal

plane (Figure 3.17C). The basisphenoidal tubera develop ventrally from just posterior to the carotid foramina, thicken posteriorly, and form distinct ventral blunt crests that are uniform in thickness through their anteroposterior length. In ventral view, the two tubera diverge posteriorly at a ~60º angle and they flank a shallow and wide excavation medially. The basisphenoidal tubera make up the ventral boundary of the lateral recess (bplr), which notches the basisphenoid posteriorly (Figure 3.17C).

3.3.3. Basioccipital

The basioccipital is subtrapezoidal in both dorsal and ventral views and its posterior portion contributes to the occipital condyle. In posterior view, the basioccipital condyle is wide, but smaller and less prominent compared to the exoccipital condyles. The basioccipital condyle is damaged such that its posterior-most surface was not determined. Its dorsal portion flares out laterally to accommodate the exoccipital condyles.

The basioccipital contacts the exoccipital posteriorly along a U-shape suture (us) in dorsal view. In dorsal view, the anterior half of the basioccipital is outlined by oblique lateral ridges (bosr, Figure 3.17A). As they are damaged, the ridges do not continue posteriorly, but they delimit a shallow, concave surface dorsally. A short, blunt anteroposterior knob (bok, Figure 3.17A) is visible inside the median concave surface of the basioccipital. The basioccipital has a short unossified area anterodorsally (uz, Figure 3.17A), whereas in other cistecephalids the basioccipital is coossified to the basisphenoid in dorsal view (Keyser 1965; Angielczyk et al. 2019).

In lateral view (Figure 3.17B), the basioccipital tubera slope almost vertically and its anterior wall is thicker than the posterior one. The basioccipital tubera form the medial wall of the fenestra ovalis. The fenestra ovalis is elliptical and is oriented obliquely, and its major diameter is 2.3 mm. The basioccipital has a very small contribution to the medial border of the

jugular foramen in the Malawian cistecephalid. Most of the ventral anatomy of the basioccipital is damaged in PK-16-1. The remaining features are the wide medial depression (bod) that separates the basioccipital tubera anteriorly, and delineates the basioccipital condyle posteriorly (Figure 3.17C). The ventral depression of the basioccipital reaches the wave-like suture with the basisphenoid anteriorly. It appears slightly deeper than the dorsal one, despite this region being damaged. In ventral view, the basioccipital condyle is subtriangular with the wide base forming the posterior margin (Figure 3.17C).

3.3.4. Exoccipital

The exoccipital forms the dorsal portion of the occipital condyle and extends dorsally to form the foramen magnum lateral walls. As it is damaged, the exoccipital appears knob-like in shape in both anterior and posterior views. Anteriorly, the exoccipital condyle bears a subvertical tuberosity (eoat) that flanks laterally the jugular foramen (jf) and forms the condyle anterior articular surface (Figure 3.18A). The exoccipital condyle has a flatter anterior surface caused by erosion. Little can be said about the anterior face of the dorsal component due to damage, except that it shows a lobate outline.

The exoccipital condyles are severely damaged in this specimen such that their midline contact has been broken. However, the sulcus on the posterior surface of the basioccipital condyle suggests that the two exoccipital were meeting medially as in other cistecephalids (Keyser 1965; Cluver 1974; Angielczyk et al. 2019). The left exoccipital is better preserved dorsally. Its dorsal portion forms a D-shaped structure (eodc, Figure 3.18B) in posterior view. The exoccipital dorsal component forms a convex suture with the opisthotic and supraoccipital laterally. This component is connected to the exoccipital condyle by a shallow exoccipital trench (eoptr) in posterior view (Figure 3.18B).

Medially, the right exoccipital condyle is pierced by two conspicuous foramina for the hypoglossal nerve and maybe an accompanying vessel (hf), which are separated ventrally by a thin crest (Figure 3.18C). The two foramina are oriented obliquely, and the lateral one is the largest. The lateral foramen is oval and its major diameter is 0.3 mm whereas the medial foramen is circular with a diameter of 0.1 mm.

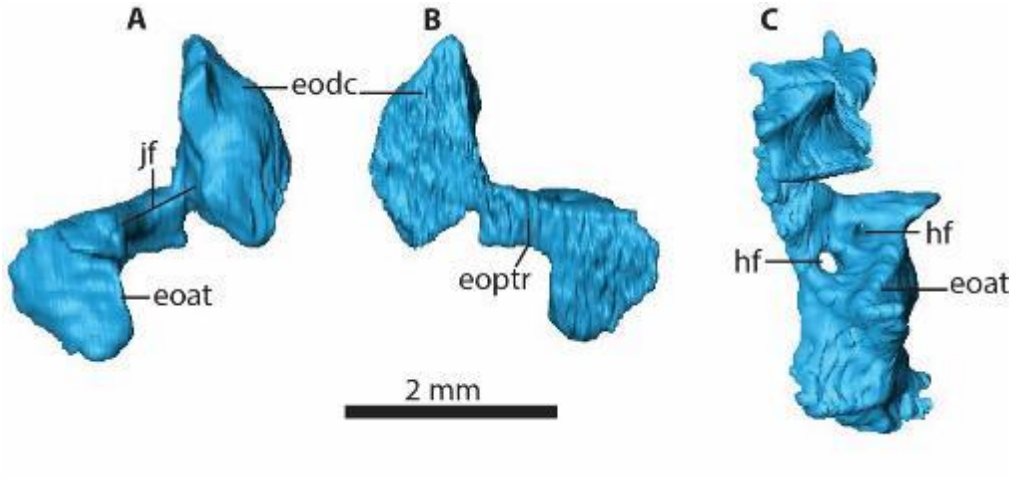


Figure 3. 18. The exoccipital of the Malawian cistecephalid (PK-16-1) in **(A)** anterior, **(B)** posterior and **(C)** medial views. eoat, exoccipital anterior tuberosity; eodc, exoccipital dorsal component; eoptr, exoccipital posterior trench; hf, hypoglossal foramen; jf, jugular foramen.

3.3.5. Supraoccipital

The supraoccipital shows the typical shortening and widening of the skull of the cistecephalid dicynodonts (Keyser 1965, Cluver 1974, Kammerer et al. 2016, Angielczyk et al. 2019). It is saddle-shaped in posterior view. The supraoccipital is eroded around the medial lobe and the dorsal portion of the left ala. The supraoccipital surrounds the dorsal half of the foramen magnum, however, the dorsal top of the foramen could not be determined in this specimen because of the damage. The supraoccipital contacts the exoccipital ventromedially along an

oblique suture and the opisthotic ventrally along a horizontal suture. It contacts the prootic anteriorly along a suture parallel to the coronal plane observed in lateral view.

In anterior view, the anterodorsal top of the medial lobe has two anteroposteriorly and dorsoventrally short descending processes (sap) that probably delimited the hindbrain in life as in *Kawingasaurus* (Figure 3.19F). The right process is deflected at its base and forms a notch with the anterior face of the supraoccipital ala, and forms also the anterodorsal border of the foramen magnum. The supraoccipital ala has a bulge anteriorly which forms the posterodorsal wall of the large and deep floccular fossa (flo) in PK-16-1. This bulge is also penetrated by the bony enclosure of the anterior semicircular canal (ascc) just dorsal to the floccular fossa (flo) and by the crus communis (cc) on the posterolateral edge of the floccular fossa (Figure 3.19F).

Laterally, the supraoccipital ala is excavated by the lateral recess (slr, Figure 3.19I) which is flanked by the supraoccipital posteriorly and notches the posttemporal fenestra.

In posterior view, the medial lobe of the supraoccipital expands dorsally toward the top of the skull and has a semicircular depression on its median posterodorsal region (ssd, Figure 3.19H). The lateral alae of the Malawian cistecephalid PK-16-1 supraoccipital are more extended and pointed laterally, and form the entire dorsal border of the posttemporal fenestra in posterior view (Figure 3.19H). The suture with the exoccipital is located anteriorly in the recess for the posterior semicircular canal (pscc).

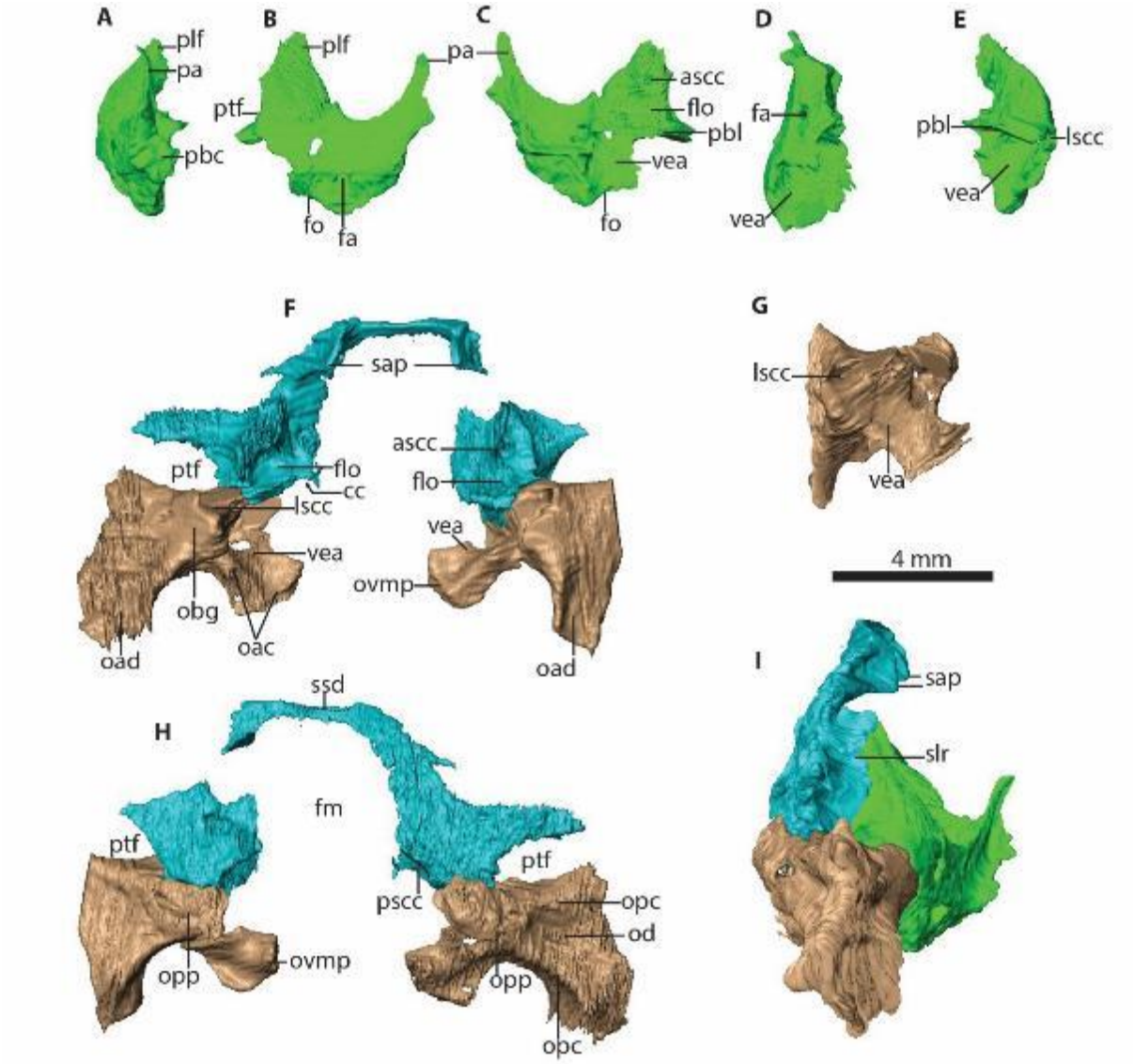


Figure 3. 19. The lateral and posterior wall of the braincase of the Malawian cistecephalid (PK-16-1). Right prootic in **(A)** anterior, **(B)** lateral, **(C)** medial, **(D)** ventral and **(E)** posterior views. Opisthotic and supraoccipital in **(F)** anterior, **(H)** posterior and **(I)** right lateral views; opisthotic in **(G)** medial view. ascc, attachment of the anterior semicircular canal; cc, attachment of the crus communis; fa, facial foramen; flo, floccular fossa; fm, foramen magnum; fo, fenestra ovalis; lscc, attachment of the lateral semicircular canal; oac, opisthotic anterior crests; oad, opisthotic anterior depression; obg, opisthotic anterior bulge; od, opisthotic posterior depression; opc, opisthotic posterior crests; opp, opisthotic posterior process; ovmp, opisthotic ventromedial process; pa, pila antotica; pbl, prootic blade-like process; plf, prootic lateral flange; pssc, attachment of the posterior semicircular canal; ptf, posttemporal fenestra; sap, supraoccipital anteriorly projected crest; slr, supraoccipital lateral recess; vea, vestibular area.

3.3.6. Prootic

The prootic is well-preserved in PK-16-1 and is formed by the lateral flange posteriorly and the anterodorsally-directed pila antotica. As is typical in dicynodonts, the prootic of PK-16-1 forms the anterolateral wall of the braincase as it borders the foramen magnum anteriorly. Contrary to the state in *Kawingasaurus*, the prootic in PK-16-1 is only strongly coossified to the supraoccipital and opisthotic, but a few millimeters gap separates it from the basioccipital and basisphenoid.

In anterior view the prootic is gently twisted medially in the Malawian cistecephalid. Its lateral flange (pfl) expands laterally in anterior view, resulting in a concave lateral margin of the bone (Figure 3.19A). The dorsal edge of the lateral flange of the prootic is slightly pointed and extended dorsally in anterior view. In anterior view, the pila antotica of the Malawian cistecephalid is vertically flat and mediolaterally compressed dorsally. The dorsalmost part of the pila antotica is bent laterally in anterior view (Figure 3.19A). Its anteroventral part is broad as it overlaps the parabasisphenoid. This overlay is not sutural as the two bones are separated by a ~0.5 mm gap.

In lateral view, the prootic appears U-shaped as it sends the lateral flange (plf) and the pila antotica (pa) dorsally separated by the trigeminal notch (Figure 3.19B). The lateral flange of the prootic tapers dorsally in lateral view, and its mid-height part is the widest point. Whereas the lateral margin of the prootic forms an oblique suture with the opisthotic, its ventral margin forms a horizontal contact with the basioccipital in lateral view (Figure 3.19B). Dorsal to the suture with the opisthotic, the prootic forms the anterior border of the posttemporal fenestra (ptf). The fenestra ovalis (fo) is formed at the intersection of the prootic-opisthotic-basioccipital, and the prootic forms the anterior border of it. Ventrally, the prootic is perforated by the facial foramen which is located dorsal to the fenestra ovalis (Figure 3.19B). The right

pila antotica is the best preserved in PK-16-1. It is obliquely oriented, tall, and tapers dorsally in lateral view. The medial face of the pila antotica ventral to the trigeminal notch is depressed in lateral view. The trigeminal notch is wider in the Malawian cistecephalid and *Kawingasaurus* than in *Myosaurus* and *Pristerodon*.

In medial view the floccular fossa (flo) excavated the internal aspect of the prootic horizontally (Figure 3.19C). The prootic forms about 60% of its anterior margin. The floccular fossa is 1.6 mm deep in PK-16-1. The prootic part that forms the floor of the floccular fossa is blade-like (pbl) in medial view (Figure 3.19C). This blade-like process roofs the vestibular cavity and separates it from the floccular fossa. In PK-16-1, the vestibule (vea) is large inflated and vertically-oriented as in other cistecephalids (Laaß and Kaestner 2017; Angielczyk et al. 2019). The prootic has a thicker aspect dorsal to the floccular fossa, where it is excavated by a small circular cavity for the anterior semicircular canal (ascc, Figure 3.19C).

In ventral view the prootic forms a concave contact with the basioccipital and parabasisphenoid. The facial foramen in PK-16-1 is small, circular and excavates the prootic vertically in ventral view (Figure 3.19D). The vestibule of the Malawian cistecephalid has a conical aspect observed ventrally.

In posterior view, the prootic has a concave lateral margin. Its dorsomedial margin is knob-like but the ventromedial one is nearly oblique (Figure 3.19E). At its mid-height, the prootic bears a horizontal blade-like process (pbl) that sutures with the supraoccipital and opisthotic. Dorsal to the blade, the prootic sutures with the supraoccipital, and ventral to the blade it sutures with the opisthotic. Also, the vestibule of the inner ear is visible ventrally to the blade in posterior view (Figure 3.19E). The lateral semicircular canal (lscc) perforates the prootic and opisthotic immediately ventral to the horizontal blade-like process.

3.3.7. Opisthotic

The opisthotic of the Malawian cistecephalid is hour-glass shaped in anterior and posterior views and its dorsal and ventral margins are convex. It can be divided into two subunits: the ventromedial process and the main body medially that sends two crests laterally.

The opisthotic is bulged anteriorly as it housed the vestibule of the inner ear (Figure 3.19F). This bulge (obg) serves as a sutural part with the prootic anteriorly. On its dorsal margin, the opisthotic bulge is perforated by a cavity for the lateral semicircular canal (lscc). This cavity connects to the vestibule (vea) on the anteromedial surface of the opisthotic. The vestibule is spherical and inflated as is typical for cistecephalids and excavates a shallow concavity on the anterior face of the ventromedial process of the opisthotic (Figure 3.19F). The vestibule is anteroventrally bordered by a V-like low crest (oac). The opisthotic seems to have housed only 40% of the vestibule leaving the other 60% portion to the prootic. Laterally to the bulge, the face of the opisthotic bears a vertical depression (oad) for articulation with the quadrate-quadratojugal complex in anterior view. The recess for the lateral semicircular canal of the Malawian cistecephalid PK-16-1 is small and oval in internal view (Figure 3.19G). At its ventralmost margin, the vestibule opens into a large elliptical fenestra ovalis, observed in ventral view.

In posterior view, the main body is a horizontal bulge-like process (opp, Figure 3.19H) located medially, which flattens dorsally to form the floor of the posttemporal fenestra (ptf) laterally and sutures with the supraoccipital dorsally. The posttemporal fenestra appears elliptical in posterior view, with the longest axis oriented horizontally (Figure 3.19H). Whereas the suture with the exoccipital appears oblique, the suture with the supraoccipital is horizontal in posterior view. The ventromedial part of the opisthotic forms a tuber-like subvertical ventromedial process (ovmp, Figure 3.19H) that curves slightly posteroventrally to form the anterior wall of the jugular foramen and the posterior border of the fenestra ovalis. This gentle

curvature of the process excludes the basioccipital from the jugular foramen in PK-16-1. The posterior aspect of the opisthotic in PK-16-1 bears two divergent crests (opc, Figure 3.19H) that flank a shallow horizontal depression (od, Figure 3.19H). The lower crest is shaped like a long rod that projects laterally in the oblique direction to suture with the squamosal and quadrate. In contrast, the topper crest is short, broader and horizontal.

3.4. Anatomical description 4

SYSTEMATIC PALAEONTOLOGY

Order THERAPSIDA Broom, 1905

Suborder ANOMODONTIA Owen, 1859

Infraorder DICYNODONTIA Owen, 1859

Superfamily EMYDOPOIDEA van Hoepen, 1934

Family CISTECEPHALIDAE Owen, 1876

Kawingasaurus fossilis (Cox, 1972)

Specimen: GPIT/RE/9272

Description

3.4.1. Orbitosphenoid

The orbitosphenoid is the complex composed of two dorsally directed wings posteriorly and the vertical median process anteriorly often called mesethmoid in cistecephalids (Keyser 1965; Laaß and Kaestner 2017; Angielczyk et al. 2019). It contacts the frontal dorsally and the parasphenoid ventrally. At its dorsal part, the orbitosphenoid hosts the olfactory bulbs. The orbitosphenoid is nearly rectangular in lateral view.

The wings in GPIT/RE/9272 preserve the usual Y-shape cross-section. The lateral wings are oriented almost vertically in anterior view and connect to the body of the bone at a

right angle (Figure 3.20A). The dorsal vertical portion of the wings is thinner, whereas the horizontal portion is thicker. In anterior view, the base of the wing is excavated by a shallow sulcus (obasu, Figure 3.20A) that descends for a short distance medioventrally. The anteriormost half of the orbitosphenoid is composed of the median vertical process which forms a horizontal dorsal plate (obpl) dorsally and descends to form a thick vertical plate ventrally that articulates to the parasphenoid rostrum (Figure 3.20A). The dorsal horizontal plate articulates with the frontal dorsally. The median process separated the olfactory cavities (ofc, Figure 3.20A) which are relatively enlarged in *Kawingasaurus*. In dorsal view, the horizontal plate of the vertical process is triangular in shape and is excavated by a long anteroposterior sulcus (dsu, Figure 3.20B).

In lateral view, the orbitosphenoid in *Kawingasaurus* is longer anteroposteriorly than in *Myosaurus*. The wings are well separated from the mesethmoid. The lateral surface of the wings is slightly convex. Their dorsal margin is horizontal and flat to articulates with the frontal, as in *Pristerodon*. The ventral margin of the wing expands posteriorly and horizontally, giving the wing a C-shaped posterior margin (Figure 3.20C). The anterior margin of the wings appears S-shaped in lateral view (Figure 3.20C). In dorsal view, the gutter formed by the two wings is anteroposteriorly very short and inclined posteriorly. There is a notch between the median vertical process and the orbitosphenoid wings in lateral view. In lateral view, the vertical plate of the median vertical process has a horizontally oval outline topped by the rectangular shape of the dorsal plate dorsally.

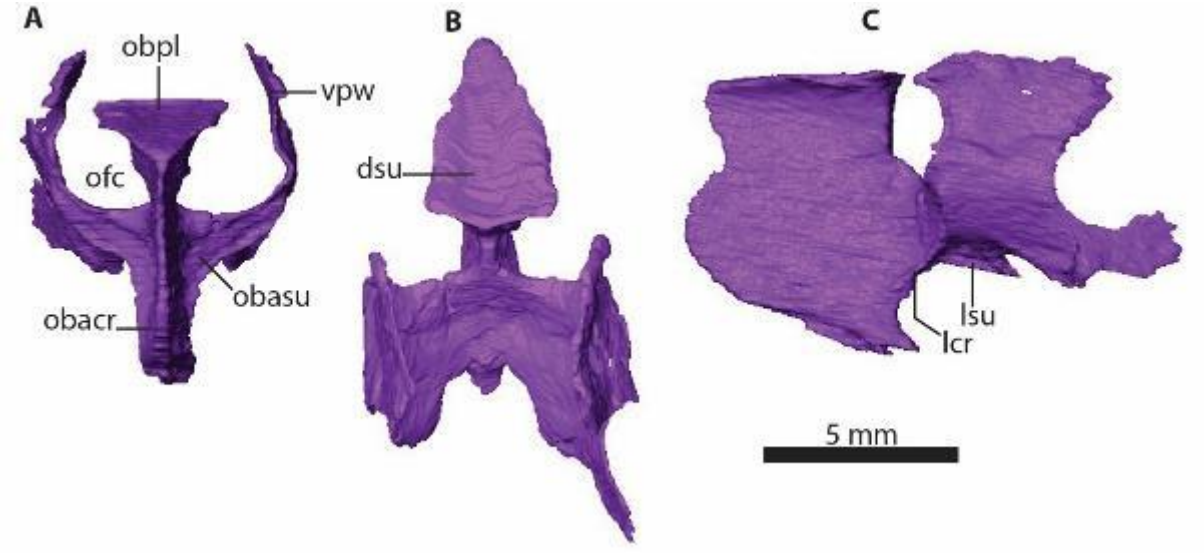


Figure 3. 20. The orbitosphenoid of *Kawingasaurus fossilis* (GPIT/RE/9272) in **(A)** anterior, **(B)** dorsal and **(C)** left lateral views. dsu, orbitosphenoid dorsal sulcus; nt, lateral notch; obacr, orbitosphenoid vertical crest; obasu, orbitosphenoid lateral sulci; obpl, orbitosphenoid dorsal plate; ofc, olfactory cavity; vpw, vertical process of the orbitosphenoid wing.

3.4.2. Pterygoid

The pterygoid displays the typical X-shape dicynodont morphology. In GPIT/RE/9272, the pterygoid is almost completely preserved except for the right quadrate ramus. The quadrate ramus in *Kawingasaurus* spreads at nearly 80º from the median sagittal plane. The anterior palatal ramus of the pterygoid has a concave lateral surface observed in dorsal view. It is overlapped by a thin and dorsally projecting lamina (pt dl, Figure 3.21A). This lamina is in a similar position as the anteromedial pterygoidal process described in *Pristerodon* and *Myosaurus*, but it has a more vertical orientation. The pterygoid dorsal lamina notches the anterior pterygoid ramus and an oval foramen (pt afo) is present at the anterior end of this intersection (Figure 3.21A). As mentioned in Cox (1972), the foramen pierces the pterygoid obliquely just ventral to the contact between the pterygoid and ectopterygoid. As the palatal ramus is notched by the dorsal lamina, it is taller than the quadrate ramus observed in lateral

view (Figure 3.21B). The posterior end of the quadrate ramus deepens ventromedially in lateral view. Medially, the posterior-most region of the quadrate ramus has a convex surface that articulates to the quadrate.

The palatal ramus of the pterygoid is thicker ventrally than the quadrate ramus and terminates anteriorly with an irregular suture with the ectopterygoid (ptve, Figure 3.21C). In *Kawingasaurus*, the pterygoid ventral keel is represented by a low and thin lamina (ptvl, Figure 3.21C) that runs ventrally and probably served as a point of attachment to the pterygoideus musculature in life. In ventral view, the two pterygoids meet at the midline of the median horizontal plate in *Kawingasaurus* as in most cistecephalids. The ventral exposure of the pterygoid median plate in *Kawingasaurus* is very short compared to the parabasisphenoid at the median sagittal axis (Figure 3.21C) as noted in (Angielczyk et al., 2019). *Kawingasaurus* lacks the crista oesophagea as the median horizontal plate of the pterygoid is flat (Figure 3.21C). Also, it lacks an interpterygoid vacuity as already noted by Cox (1972). This contrasts with the condition in other cistecephalids (Keyser 1965, Cluver 1974, Kammerer et al. 2016, Angielczyk et al., 2019), in which the vacuity is present albeit reduced. The quadrate ramus is broad posteriorly but mediolaterally compressed towards the median plate in ventral view.

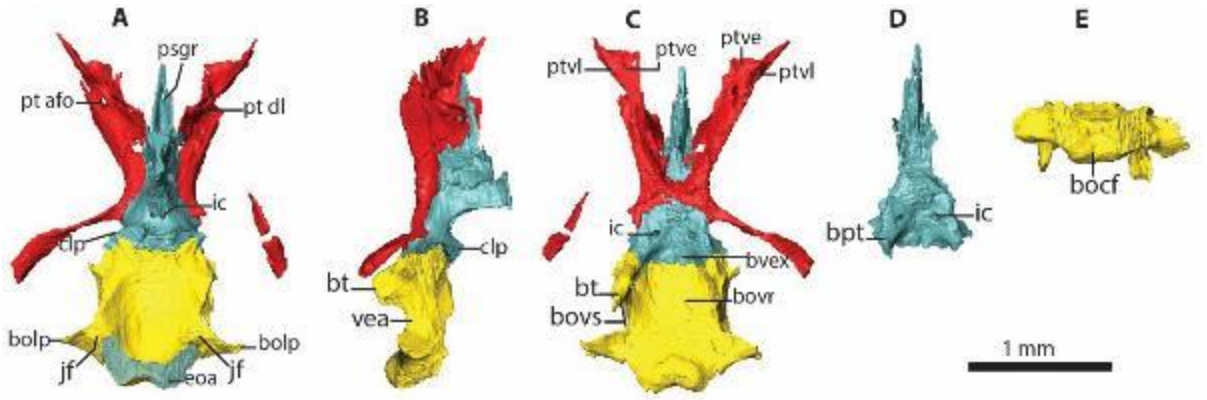


Figure 3. 21. The ventral portion of the braincase of *Kawingasaurus fossilis* (GPIT/RE/9272): basioccipital, parabasisphenoid and pterygoid in (A) dorsal, (B) left lateral and (C) ventral

views; parabasisphenoid in (D) ventral view; and basioccipital in (E) posterior view. bocf, basioccipital longitudinal furrow; bolp, basioccipital lateral process; bovr, basioccipital median ridge; bovs, basioccipital vestibular space; bpt, basisphenoidal tubera; bt, basioccipital tubera; bvex, basioccipital-basisphenoidal ventral excavation; clp, clinoid process; eoa, exoccipital sutural area; ic, internal carotid foramina; jf, jugular foramen; psgr, parasphenoidal groove; pt afo, pterygoid oval foramina; pt dl, pterygoid dorsal lamina; ptve, pterygoid ventral excavation; ptvl, pterygoid ventral lamina.

3.4.3. Epipterygoid

Specimen GPIT/RE/9272 has only the right epipterygoid preserved (Figure 3.22A, B). The epipterygoid consists of two subunits: the subhorizontal footplate and a vertical ascending process forming an inverted T-shape. The footplate of the epipterygoid in *Kawingasaurus* (epft, Figure 3.22A) is smoothly concave medially to articulate with the quadrate ramus of the pterygoid. Its anterior tip is short as it does not extend far anteriorly to the median plate of the pterygoid. The epipterygoid footplate tapers anteriorly and posteriorly (Figure 3.22A). The anterior portion of the epipterygoid footplate is shorter compared to the posterior one. The epipterygoid footplate shares no sutural contact with the parabasisphenoid medially. Its ventral outline is gently convex.

The ascending ramus of the epipterygoid (epar, Figure 3.22B) is a rod-like subunit that curves in slightly dorsomedially as in other dicynodonts (Figure 3.22B). The ramus is broken off dorsally and therefore its contact with the descending flange of the parietal cannot be determined in this specimen. However, it is suggested that this contact may have occurred from the dorsal process developed on the epipterygoid in *Kawingasaurus* (Laaß and Kaestner 2017). There is a small anteromedial angular process emerging from the base of the ascending ramus (epap, Figure 3.22B).

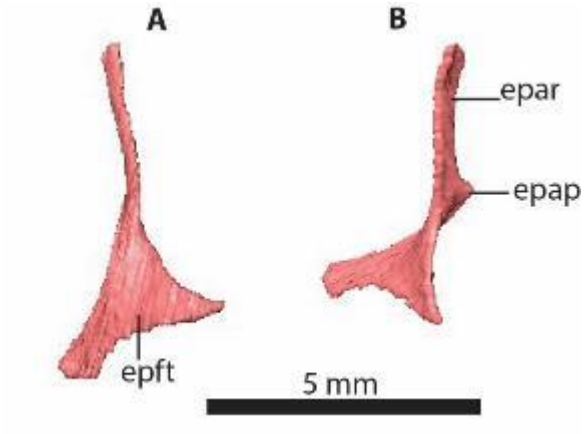


Figure 3. 22. The epipterygoid of the *Kawingasaurus fossilis* (GPIT/RE/9272) in **(A)** anterior and **(B)** right lateral views. epap, anteriomedial angular process of the epipterygoid; epar, ascending ramus of the epipterygoid; epft, epipterygoid footplate.

3.4.4. Parabasisphenoid

The PRB is coossified to the orbitosphenoid posterodorsally in *Kawingasaurus*. Also, the PRB is fused to the basipostsphenoid posteriorly as in *Myosaurus*. The PRB portion projects almost vertically in dorsal view, and is excavated by an anteroposterior groove (psgr) on its anterodorsal region (Figure 3.21A). This groove served for articulation with the orbitosphenoid. The PRB is subtriangular in lateral view. In ventral view, the PRB is wider posteriorly than anteriorly. Ventrally, it shares an interdigitated suture with the pterygoid.

No distinct separation between the PRB and the basipostsphenoid is visible in specimen GPIT/RE/9272. In dorsal view, the carotid foramina pierce the basisphenoid in two orifices separated by a median ridge (Figure 3.21A), unlike in *Myosaurus* and the Malawian cistecephalid. The carotid foramina are bordered by two lateral ridges that continue anteriorly and meet one another at the level of the suture with the vertical plate of the orbitosphenoid. Laaß and Kaestner (2017) suggested that the sagittal ridge at the sella turcica served to support the two lobes of the pituitary gland (hypophysis). However, the pituitary fossa is usually

divided into an anterior and posterior portion (Edinger 1942). Thus, the sagittal ridge in between the two carotid foramina must have separated these arteries instead of dividing the hypophysis. The region of the sella turcica is relatively small in *Kawingasaurus* with no anteroposterior median ridge on its posterior end as observed in the other emydopoids described here. In *Kawingasaurus*, the clinoid process (clp, Figure 3.21A) of the basisphenoid is firmly coossified to the pila antotica and projects dorsally, so the separation between the bones is difficult to ascertain. The dorsal edge of the dorsum sellae is thin and slightly convex in *Kawingasaurus*.

The PRB extends shortly anterior to the pterygoid median plate compared to *Myosaurus* in ventral view (Figure 3.21C). Its ventral aspect is generally subtriangular with the apex extended anteriorly (Figure 3.21D). The ventral surface of the PRB in *Kawingasaurus* is irregular as it shares an interdigitated suture with the vomer. The parabasisphenoid in *Kawingasaurus* is coossified with the pterygoid median plate anteriorly, and it is more exposed ventrally, i.e., the parabasisphenoid overlaps onto the pterygoid median plate and covers its anteriormost portion only (Figure 3.21C). Ventrally, the distance between the carotid foramina is wide in *Kawingasaurus* as the canals for the carotid arteries diverge laterally, unlike in the other emydopoids described here. The two basisphenoidal tubera (bpt) project ventrally just posterior to the carotid foramina in *Kawingasaurus* and cover the basioccipital in ventral view for a relatively short distance (Figure 3.21C). The basisphenoid tubera do not extend posterior to the level of the fenestra ovalis. The basisphenoidal tubera do not contribute extensively to the ventral anteroposterior excavation (bvex) in *Kawingasaurus*.

3.4.5. Basioccipital

The basioccipital is coossified to the parabasisphenoid and prootic in *Kawingasaurus*. It is very broad compared to the other dicynodonts described here. The basioccipital is divided into the

occipital condyle posteriorly, the basioccipital tubera laterally and the median concavity medially in ventral view.

In posterior view the occipital condyle is tripartite as the basioccipital forms the ventromedial part of the condyle and the exoccipitals form the two dorsolateral sides. The basioccipital condyle is less prominent compared to the exoccipital condyles in *Kawingasaurus*, but they all contribute to a broad excavation that forms a large occipital pit. The basioccipital condyle has a median longitudinal furrow (bocf, Figure 3.21E) in posterior view.

In dorsal view the basioccipital has a trapezoidal outline. It has a deep concave dorsomedial surface that accommodated the ventral part of the brain (Figure 3.21A). It sends two processes laterally (bolp, Figure 3.21A), which contact the opisthotic along a vertical suture and form the ventral floor of the jugular foramen (jf). The basioccipital extends anteriorly to contact the parabasisphenoid along a transverse suture. Its dorsolateral suture with the prootic forms a concave surface. The main basioccipital body together with the basioccipital condyle is overlapped by the exoccipital condyles dorsally. The suture with the exoccipital is U-shaped in dorsal view (eoa, Figure 3.21A).

In lateral view the basioccipital has an inverted crescent shape with the basioccipital tubera pointing ventrally (Figure 3.21B). It is excavated by a large and concave recess for the vestibule of the inner ear (vea) in lateral view. The major diameter of this recess is aligned with the anteroposterior skull axis and is 6 mm long. Posterior to the recess, there is a circular jugular foramen whose diameter is 1.7 mm.

In ventral view, the basioccipital median part has less deep concavity than its dorsal one and bears a faint median ridge (bovr, Figure 3.21C). The basioccipital condyle and the rest of the basioccipital main body are not separated by a sulcus in *Kawingasaurus*, unlike in *Myosaurus*. The basioccipital tubera project laterally, and form oblique tuberosities on each

side of the basioccipital. They border the spherical fenestra ovalis medially. Between the tubera and the basioccipital lateral process, there is a deep and hollow space (bovs, Figure 3.21C) through which the vestibule is visible on both sides of the basioccipital.

3.4.6. Exoccipital

The exoccipital in *Kawingasaurus* shows the typical dicynodont morphology, where it forms the dorsal thirds of the occipital condyle, the ventral part of the foramen magnum and the dorsal border of the jugular foramen. In anterior view, the exoccipital has a knob-like outline (Figure 3.23A). The dorsal component bears a thin oblique descending crest (eocr) that flanks an oval recess for the posterior semicircular canal (pscc) laterodorsally, and borders the jugular foramen (jf) ventromedially (Figure 3.23A). The anterior face of the exoccipital dorsal component is sutured to the vestibule of the inner ear. The anterior articular facet of the exoccipital condyle is concave.

In posterior view, the occipital condyle of *Kawingasaurus* is reniform as in other emydopoids (Angielczyk et al. 2005; Fröbisch, 2007). The intersection area between the three condyles is largely excavated in *Kawingasaurus* and the two exoccipitals meeting at midline form almost a horizontal dorsal border of the exoccipital condyles (Figure 3.23C). The two exoccipitals meet at the midline and exclude the basioccipital for the ventral border of the foramen magnum. The exoccipital dorsal component (eodc) extends for more than half the height of the foramen magnum and is subtriangular in posterior view (Figure 3.23C). The foramen magnum is vertically oval in *Kawingasaurus* and its base is the widest part, which is formed by the exoccipitals. The dorsal component of the exoccipital contacts the supraoccipital dorsally and opisthotic laterally along an oblique suture in posterior view. Ventral to this suture, and in the same orientation, is the posterior semicircular canal (pscc) penetrating the exoccipital.

Internally, the exoccipital condyle is perforated laterodorsally by the hypoglossal canal which is small with an oval outline (whose major diameter is 0.3 mm), and is oriented obliquely to the sagittal plane.

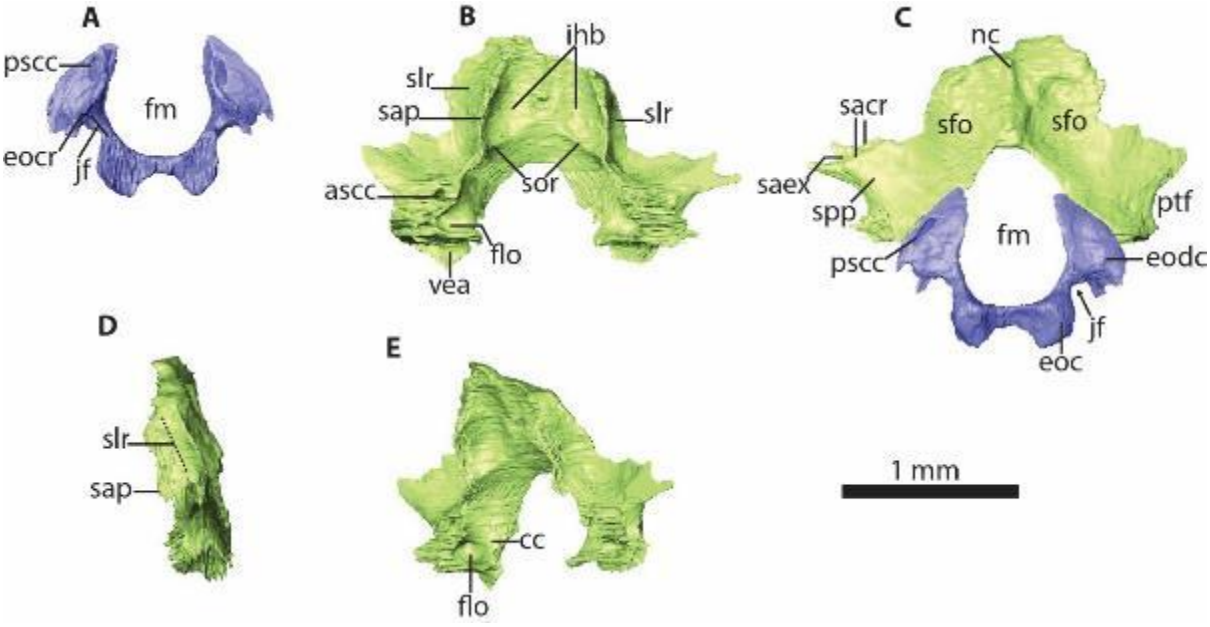


Figure 3. 23. The occiput region of *Kawingasaurus fossilis* (GPIT/RE/9272): exoccipital in **(A)** anterior view; supraoccipital in **(B)** anterior, **(C)** posterior, **(D)** left lateral and **(E)** medial views. ascc, attachment of the anterior semicircular canal; cc, attachment of the crus communis; eoc, exoccipital condyle; eocr, exoccipital descending crest; eodc, exoccipital dorsal component; flo, floccular fossa; fm, foramen magnum; ihb, impressions of the hindbrain; jf, jugular foramen; nc, nuchal crest; pscc, attachment of the posterior semicircular canal; ptf, posttemporal fenestra; saex, medial excavation of the supraoccipital lateral ala; sacr, crests of the supraoccipital ala; sap, supraoccipital anterior process of the median lobe; slr, supraoccipital lateral recess; sor, supraoccipital anterior oblique ridges; vea, vestibular area.

3.4.7. Supraoccipital

The supraoccipital is the largest element of the occiput which borders the dorsal half of the large foramen magnum, and the roof of the posttemporal fenestra. It is wider than tall in

posterior view as is typical for cistecephalids (Keyser 1965; Angielczyk et al. 2019) and has an overall saddle-shape outline. However, the left dorsalmost region of GPIT/RE/9272 supraoccipital is gently eroded. The supraoccipital contacts the prootic anteriorly along an intricate suture, the exoccipital and the opisthotic ventrally along a concave suture, the squamosal laterally, and the parietal dorsally along a nearly a suture aligned with the coronal plane.

The supraoccipital is composed of a median lobe and two lateral alae as in other dicynodonts (Castanhinha et al., 2013; Angielczyk and Kammerer, 2017; Macungo et al., 2020). The main feature of the anterior face of the medial lobe is the impressions of the hindbrain flanked by distinct processes, whereas its posterior aspect is marked by a broad nuchal crest. The lateral ala has a flat posterior surface, but its anterior aspect is complex as it housed part of the vestibular labyrinth.

In anterior view, the supraoccipital anterior process of the median lobe (sap, Figure 3.23B) descends vertically and broadens dorsally. The process is deflected laterally at its base to form the anterior border of the foramen magnum (Figure 3.23B). The two oblique ridges are faint in *Kawingasaurus* (sor, Figure 3.23B). They join together dorsomedially and connect the supraoccipital anterior process lateroventrally forming the dorsal border of the foramen magnum. Dorsal to these ridges, the anterior face of the supraoccipital is excavated by the impressions of the hindbrain (ihb, Figure 3.23B). The supraoccipital ala forms the posterior half and the floor of the floccular fossa (flo), which is located between the vestibule of the inner ear (vea) and the anterior semicircular canal (ascc). The floccular fossa is shallow, horizontal, and has a large face in GPIT/RE/9272; however, it is large relative to the skull in *Kawingasaurus* (Laaß and Kaestner 2017). The posterior half of the anterior semicircular canal perforates the supraoccipital obliquely, dorsal to the floccular fossa.

The vertical recess of the supraoccipital (slr, Figure 3.23B) is located between the anterior process and the lateral edge of the supraoccipital, and it descends to form a notch at the level where the alae join the medial lobe in lateral view (Figure 3.23B/D).

In posterior view, the two fossae are located dorsal to the foramen magnum (sfo, Figure 3.23C). They are deep, oval, and vertical and are separated by a medial nuchal crest (nc, Figure 3.23C), which is slightly broad ventrally. The supraoccipital alae project laterally bordering the posttemporal fenestra dorsally. In posterior view, they have subhorizontal dorsal edges and the lateral thick process (spp, Figure 3.23C) has a convex surface. The medial excavation on the dorsal surface of the left ala (saex, Figure 3.23C) descends mediolaterally and is flanked by crests (sacr) that unite at the dorsomedial edge of the excavation (Figure 3.23C). This dorsal excavation is not visible on the right ala due to damage but served to host part of the squamosal.

Internally, the supraoccipital forms the lateral wall of the crus communis (cc, Figure 3.23E) and the posterior semicircular canal, whose medial wall is formed by the exoccipital. The common crus is subvertical and forms a notch with the vestibule of the inner ear whereas the posterior semicircular canal perforates the supraoccipital obliquely.

3.4.8. Prootic

The prootic forms the anterior and lateral walls of the braincase. The prootic of *Kawingasaurus* is dorsoventrally taller and anteroposteriorly thinner than in the Malawian cistecephalid PK-16-1. In *Kawingasaurus* it shares a sutural contact with the supraoccipital and opisthotic posteriorly and with the basioccipital and parabasisphenoid ventrally. The suture with the opisthotic is vertical. The prootic is formed by the main body posteriorly and a triangular pila antotica anteriorly.

In anterior view, the morphology of the prootic in *Kawingasaurus* is unique among the dicynodonts described here as its main body (the lateral flange, Laaß and Kaestner 2017) is

formed by three subvertical buttresses (two lateral and one medial) that flank three sequential subvertical fossae (pvfo, Figure 3.24A/B). The medial buttress (pmbt) hosts the anterior semicircular canal and is located medially halfway between the prootic anterior buttress and the prootic lateral buttress (Figure 3.24A). The medial buttress is thicker than the other two, but the lateral buttress is the tallest. The prootic anterior buttress (pabt) descends anteroventrally and flares slightly horizontally to form the trigeminal notch. The lateral buttress (plbt) descends from the anterior border of the posttemporal fenestra to half the height of the prootic (Figure 3.24A) in anterior view. The fossa between the medial and lateral buttresses is shallower and broader than the anterior one. The prootic in *Kawingasaurus* forms the lateral wall of the large fenestra ovalis, which is circular. The lateral flange of the prootic forms a bulge ventrally (pbg), which surrounds the massive vestibule. At its surface, the bulge bents medially where it is excavated by the facial foramen. The facial foramen is located at the junction between the lateral flange of the prootic and the pila antotica. The anterior external surface of the facial foramen is excavated by a shallow groove (pg), probably for the facial nerve. The pila antotica of *Kawingasaurus* is formed by paired anterodorsally-directed ridges (pard) separated by a subvertical ellipsoidal depression (pade) visible in anterior and lateral views. These ridges meet dorsally and form an inclined plate-like element. The medial ridge of the pila antotica and the clinoid process of the basisphenoid are coossified, and it is thus difficult to determine the sutural contact between them. Laaß and Kaestner (2017) recognized a canal for the prootic sinus in the medial region of the pila antotica in *Kawingasaurus* (see also Laaß et al. 2017 for *Diictodon feliceps*). I can only identify an anteromedial fossa at the base of the pila antotica that could relate to the prootic sinus. However, this region is extremely difficult to separate from the basisphenoid and I cannot ascertain it belongs to the prootic. Therefore, this structure is interpreted with caution.

In lateral view, the prootic appears U-shaped as it sends the lateral flange and pila antotica dorsally, similar to PK-16-1 (Figure 3.24B). The wide trigeminal nerve transited on the dorsal concavity of the prootic in lateral view. At its dorsalmost part, the prootic forms the anterior border of the posttemporal fenestra in lateral view. As it descends ventrally the prootic forms the lateral wall of the fenestra ovalis.

As typical in dicynodonts the prootic of *Kawingasaurus* is excavated internally by the floccular fossa (flo) and forms its anterior wall in medial view (Figure 3.24C). The floccular fossa is slightly horizontal and is 2.2 mm deep in *Kawingasaurus*, somewhat deeper than PK-16-1. The face of the prootic below the trigeminal is depressed in medial view. The facial foramen (fa) perforates the prootic along this depressed surface (Figure 3.24C).

The lateral margin of the prootic is concave in posterior view. As the anterior margin delimits the floccular fossa and the medial depression, it forms a zig-zagged outline (Figure 3.24D). At its dorsal-most end, the prootic sutures with the supraoccipital in posterior view. Inside this suture, the prootic and the supraoccipital are perforated by a circular recess for the anterior semicircular canal (ascc). The anterior semicircular canal connects ventrally to the large, spherical and inflated vestibule.

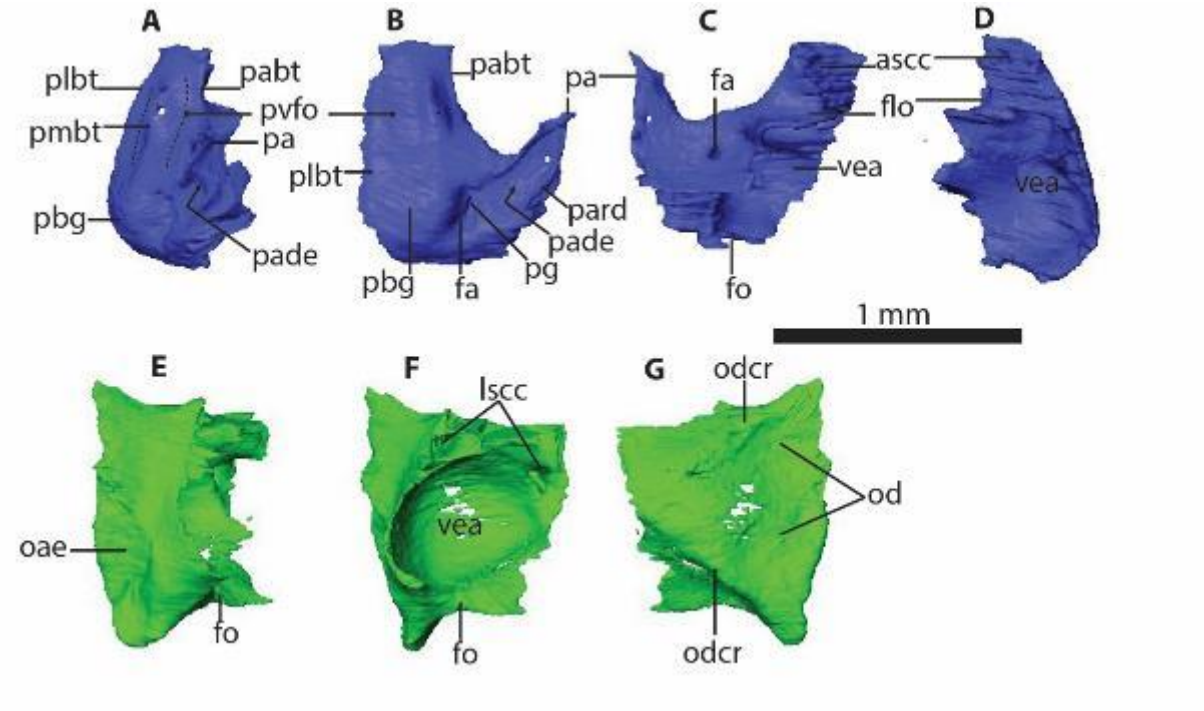


Figure 3. 24. The lateral wall of the braincase of *Kawingasaurus fossilis* (GPIT/RE/9272): prootic in **(A)** anterior, **(B)** lateral, **(C)**, medial, **(D)** posterior views; opisthotic in **(E)** anterior, **(F)** medial and **(G)** posterior views. ascc, attachment of the anterior semicircular canal; fa, facial foramen; flo, floccular fossa; fo, fenestra ovalis, lscc, attachment of the lateral semicircular canal; oae, opisthotic anterior depression; od, opisthotic depression; opc, opisthotic posterior crests; pa, pila antotica; pabt, prootic anterior buttress; pade, pila antotica ellipsoidal depression; pard, pila antotica anterodorsally-directed ridges; pbg, prootic anterior bulge; pg, prootic anterior groove; plbt, prootic lateral vertical buttress; pmbt, prootic medial vertical buttress; pvfo, prootic vertical fossa; vea, vestibular area.

3.4.9. Opisthotic

The opisthotic in *Kawingasaurus* is a subtrapezoidal element that forms the posterolateral wall of the braincase. It shares a sutural contact with the prootic anteriorly, the exoccipital and basioccipital medially, and the supraoccipital dorsally. The opisthotic hosts the vestibular organ internally and bounds the posttemporal fossa ventrally.

In anterior view the dorsal and ventral margins of the opisthotic are gently concaved (Figure 3.24E). The opisthotic possesses a tall vertical excavation (oae, Figure 3.24E) on its lateral part observed in anterior view. The ventral half of this excavation is for the articulation with the quadrate. The suture with the prootic is vertical and is located medial to the vertical excavation. Internally, the large, spherical and inflated vestibular cavity excavates the opisthotic (vea, Figure 3.24F). The opisthotic of *Kawingasaurus* hosted the major portion of the vestibule relative to the prootic. Dorsal to this cavity, the opisthotic is perforated by a circular recess which accommodated the lateral semicircular canal (lscc, Figure 3.24F).

In posterior view the opisthotic is tall and its lateral margin is the tallest part as it forms the deep paroccipital process (Figure 3.24G). In posterior view, the opisthotic expands laterally to form the floor of the posttemporal fenestra. The occipital surface of the opisthotic is concave in *Kawingasaurus* (Figure 3.24G). The posterior surface bears two divergent crests (opc, Figure 3.24G), that join medially at the contact with the exoccipital. The dorsal crest is subhorizontal and the ventral one is oblique relative to the sagittal plane. The two crest are separated laterally by two circular depressions (od, Figure 3.24G). Contrary to the Malawian cistecephalid, *Myosaurus* and *Pristerodon*, the opisthotic of *Kawingasaurus* does not present a ventromedial process. The opisthotic contacts the exoccipital on its medial margin along an oblique suture in posterior view. At the ventral end of this contact, the opisthotic borders the lateral wall of the circular large jugular foramen as in other dicynodonts. The medial margin of the opisthotic descends ventrally to form a convex suture with the basioccipital in posterior view. At its ventral part, the opisthotic forms the posterior border of the large fenestra ovalis (Figure 3.24F).

CHAPTER IV - DISCUSSION

4.1. Possible adaptations to fossoriality

It is relatively well established that cistecephalids were a specialized fossorial clade among emydopoid dicynodonts (Keyser 1965, Cox 1972, Cluver 1974a, Laaß and Schillinger 2015; Kammerer et al. 2016, Angielczyk et al. 2019). Fossoriality in cistecephalids has been mostly linked to specific postcranial adaptations (Cox 1972; Cluver 1978; Nasterlack et al. 2012), however, some of the new basicranial anatomical characters discussed below may represent adaptations to fossoriality.

4.1.1. Degree of coossification of the braincase

Coossification can be assessed by the degree of fusion between bones, which translates into how easily distinguishable the bones are on well-contrasted µCT data. Undistinguishable sutures between the braincase bones are interpreted as a high degree of coossification. In dicynodonts, a high degree of braincase bone coossification is interpreted as diagnostic for the entire clade (Olson 1944, Surkov and Benton 2004, Maisch and Gebauer 2005, Castanhinha et al. 2013; Kammerer et al. 2015, 2016, Boos et al. 2016, Angielczyk et al. 2017, Angielczyk and Kammerer 2017, Kammerer and Smith 2017, Olroyd et al. 2018, Kammerer 2019, Kammerer et al. 2019, Liu 2020). In basal dicynodonts, the opisthotic is indistinguishably fused to the surrounding bones (Sullivan 2000; Modesto et al. 2003; Angielczyk and Rubidge 2010), which results in the formation of the periotic when coossified to the prootic in some taxa (Agnew 1959; Surkov and Benton 2004). In most emydopoids the braincase elements are also coossified (Kammerer et al. 2015), and a single periotic bone is present (Fourie 1993; Angielczyk and Kammerer 2017). In this research, distinctions between bones were achieved by observing the type and orientation of the bone trabeculae in cases of fusion. In contrast, the two specimens of *Myosaurus* (BP/1/2690 and BP/1/2701a) show open sutures between the

bones such that the braincase is not as solidly ossified as is typical in other emydopoid taxa. As the degree of coossification depends on the ontogenetic stage, i.e., juvenile individuals being less co-ossified than the adult ones (Olson 1944; Sereno et al. 2009; Griffin et al. 2020), one could argue that the *Myosaurus* specimens represent juveniles. However, *Myosaurus* is only represented by diminutive skulls (Haughton 1917; Cluver 1974; Hammer and Cosgriff 1981), an interesting fact given that it was recently hypothesized that the early Triassic period could have been characterized by a high juvenile mortality rate in the lower Katberg Formation where *Myosaurus* is predominantly found (Botha and Smith, 2020; Botha, 2020). Another explanation is that *Myosaurus* shows paedomorphic patterns of skull ossification, retaining juvenile features while having reached sexual maturity already.

Similar to what is observed in modern taxa (amphisbaenians, badgers and some wombats) it would be expected that a specialized subterranean lifestyle would result in a more robustly build and coossified braincase in cistecephalids (Shimer 1903; Long 1972; Bemis et al. 1983; Tedford 2002; Kearney et al. 2005; Helgen et al. 2008; Maddin et al. 2011; Pardo et al. 2015). For instance, the braincase in caecilians (i.e., *os basale*) forms a single unit that represents the coossification of the supraoccipital, exoccipitals, basioccipital, basisphenoid, pleurosphenoid, parasphenoid, prootic, and opisthotic (Jenkins et al. 2007). These taxa used their head to dig and to compact the soil inside the tunnels, so the highly coossified braincase may be a result of adaptation to head-digging.

Cistecephalids such as *Cistecephalus*, *Cistecephaloides*, *Kawingasaurus*, *Kembawacela*, and *Sauroscaptor* have a strongly coossified basicranial axis as they display a coossification of the periotic to the other basicranial bones (Keyser 1965, Cox 1972, Cluver 1974, Kammerer et al. 2016, Laaß and Kaestner 2017, Angielczyk et al. 2019). *Kawingasaurus* shows the most extreme condition within the studied cistecephalids as its sphenethmoid complex is further coossified to the parasphenoid. However, a similar degree of coossification

found in most cistecephalids has also been described in the non-fossorial, or at least less specialized emydopoid *Emydops* (Fourie 1993). The dicynodontoid *Dicynodon* has an even more coossified braincase as its the supraoccipital and basioccipital are fused to the periotic (Ray and Chinsamy 2003; Kammerer 2019). This indicates that relatively high levels of coossification are present in various dicynodont taxa. On the other hand, some known burrowers, such as *Lystrosaurus*, display a less coossified braincase than the generalized dicynodont pattern (Ray et al. 2005; Botha et al. 2019), which could simply imply they were forelimb-diggers. As such, the extreme degree of coossification of the braincase in *Kawingasaurus* may indicate that GPIT/RE/9272 was an old adult compared to the other cistecephalids studied so far. The alternative hypothesis that the high degree of braincase coossification reflects that *Kawingasaurus* was better adapted to head-digging than any other studied dicynodonts, including other emydopoids, remains a possibility. Elevated levels of braincase coossification do not imply specifically fossoriality, but it represents a pre-requisite. Structural reinforcement of areas subjected to elevated stress and strain during head-digging movements is, therefore, necessary.

4.1.2 Cranial pneumaticity

A vast network of trabecular spaces inside the *Kawingasaurus* braincase was interpreted as an adaptation to low frequency hearing system within the burrow (Laaß 2014). A similar pattern is predicted to be found in the derived cistecephalid *Cistecephaloides*. Conversely, *Myosaurus* does not present trabecular space inside the bone. Cranial pneumaticity is also described in the braincase of the probainognatian cynodont *Pseudotherium* (Wallace 2018). Pneumatization of basicranial bones is described in subterraneans golden moles, *Talpa* and *Scalopus*, in which it is interpreted as an adaptation to hearing seismic waves (Mason 2001; 2003; 2006). In contrast, pneumatization of the braincase occurs in many non-fossorial taxa such as archosauriform reptiles (Witmer 1990, Elzanowski and Galton 1991), proboscideans (Benoit et al. 2013b),

macroscelids (Benoit et al. 2013a) in which it is also interpreted as an adaptation to low-frequency hearing (Kundrát and Janáček 2007). *Kawingasaurus* unique cranial pneumaticity supports an adaptation to low-frequency seismic hearing, which would be consistent with fossoriality; however, *Kawingasaurus* peculiar auditory adaptations cannot be generalized to all cistecephalids (Laaß 2014; Angielczyk at al. 2019).

4.1.3. Pineal foramen

The pineal foramen in cistecephalids is located considerably posterior when compared to most dicynodonts. The pineal foramen and related pineal organ typically regress with increasing subterranean behavior (Quay 1981; Benoit et al. 2016). The pineal foramen is located in a region of the skull that may mechanically be damaged during digging. The posterior location of the pineal foramen can also be a result of the reorganization of the brain and surrounding braincase bones (Araújo et al. 2021). This may account for its posterior location in *Sauroscaptor* and *Kembawacela* (Kammerer et al. 2016; Angielczyk et al. 2019), assuming that these taxa were diggers. Although, a posterior location of the pineal foramen is also present in biarmosuchians and some gorgonopsians, in which a subterranean lifestyle is not recognised (Sigogneau-Russell 1989; Rubidge and Sidor 2001). Another hypothesis is that because the pineal organ is photosensitive and monitors circadian rhythm, it is expected that subterranean species spending most of their lives in the dark would lose its function. The frequent absence of the pineal foramen in cistecephalids (Benoit et al., 2016) and the absence of a pineal foramen in the highly fossorial taxon *Kawingasaurus* (Cox 1972) support this hypothesis. An exception occurs in the South African *Kombuisia frerensis*, which lacks the pineal foramen but does not show any fossorial adaptations (Fröbisch 2007). Similarly, the pineal foramen is absent in mammals (e.g., in the Edentata anteater, sloth and armadillos, Oksche 1965; Quay 1965; Ralph 1975), and many non-fossorial lizards as well, whereas many fossorial reptiles still retain a pineal foramen (Eakin 1973, Benoit et al. 2016). The facultative fossorial *Lacertilia* has a

pineal foramen (Gundy and Wurst 1976a; 1976b; Benoit et al. 2016). Once again, despite not being direct evidence for fossoriality, the tendency for the loss or posterior location of the pineal foramen among cistecephalids, would be consistent with an inferred fossorial lifestyle but would not support it alone.

4.1.4. Development of an increased area for the atlantooccipital musculature attachment

The atlantooccipital musculature serves for flexion, extension, and rotation of the skull and first cervical vertebrae (Evans and Lahunta 2013). These muscles encompass the longissimus series, the transversospinalis, the rectus capitis lateralis, obliquus capitis cranialis, the obliquus capitis magnus, obliquus capitis superior, rectus capitis dorsalis minor, and rectus dorsalis major muscles in dicynodonts (Cox 1959; Renaut 2000). The muscle reconstructions of Cox (1959) and Renaut (2000) for dicynodonts seem to have equivalent insertion sites if considering the recently updated reviews for reptiles (Tsuihiji 2005; 2007; Jones et al. 2009) and extant fossorial mammalian taxa such as for moles (Whidden 2000). Two features characterise the insertion site of the atlantooccipital musculature particularly in cistecephalid dicynodonts: the presence and elaboration of the nuchal crest on the supraoccipital; and the presence of ridges and depressions on the posterior aspect of the opisthotic.

4.1.4.1. The occipital surface of the opisthotic

The external surface of the opisthotic is variable among emydopoids. Many emydopoids (e. g., *Emydops* and *Myosaurus*) have a relatively flat occipital plate when compared to cistecephalids (e.g., *Kawingasaurus*). In cistecephalids the posterior aspect of the opisthotic is characterized by conspicuous sulci and depressions. These contrasting morphologies imply an expansion of the atlantooccipital musculature, as sulci and depressions allow for further surface area for muscle attachment. The occipital surface of the paroccipital process, where some atlantooccipital muscles attach, is convex and featureless in the emydopoids *Emydops*,

Dicynodontoides, and *Compsodon*. Instead, the surface is flat in *Digalodon* (Kammerer et al. 2015) and *Myosaurus* (Figure 4.1G). The depression limited by bulging crests (Figure 4.1) present on the opisthotic posterior surface served for the accommodation of the atlantooccipital musculature in cistecephalids as in other dicynodonts (Cox 1959, 1965, Bandyopadhyay 1988, Renaut 2000). Similar elaboration of the posterior aspect of the paroccipital process is present in some lystrosaurids, such as, IVPP V3243 4; SAM-PK-K-11187 (Kenneth Angielczyk and Christian Kammerer pers. comm.). In dicynodonts, the rectus capitis lateralis, obliquus capitis cranialis, rectus dorsalis minor, obliquus capitis magnus, obliquus capitis superior, inserted on the posterior aspect of the paroccipital process (Renaut 2000). These muscles may have required an extensive area for their accommodation and resulted in these deep depressions and large corrugations on the posterior surface of the opisthotic in *Kawingasaurus* (Figure 4.1O), and other cistecephalids such as *Sauroscaptor*, *Kembawcela* and PK-16-1 (Kammerer et al. 2016; Angielczyk et al. 2019, Araújo et al. 2021; this study).

4.1.4.2. Development of nuchal crest

The gradual development of a nuchal crest is an additional feature of the occipital plate in cistecephalids. The nuchal crest is less developed in the basal emydopoids compared to the cistecephalids. The nuchal crest has been interpreted as an additional surface area for muscle attachment (Kammerer et al. 2016). In *Emydops*, *Myosaurus*, *Digalodon*, and *Compsodon*, the occipital surface of the supraoccipital is relatively flat (Figure 3.2, 3.14, 4.1), such that they do not have a nuchal crest. The nearly flat posterior aspect of the supraoccipital in these four taxa, suggests that the muscles attached to this region were not particularly well-developed and may have not required relatively larger space for accommodation. An exception occurs in the kingoriid *Dicynodontoides*, which despite having no elaborated nuchal crest, bears a dorsolaterally-oriented depression on the supraoccipital that hosted the rectus capitis dorsalis minor muscle (Cox 1959). In contrast, the nuchal crest is present in cistecephalids. It appears

undivided in *Cistecephaloides*, *Kawingasaurus*, and *Kembawacela* (Figure 4.1O, Cluver 1974a; Angielczyk et al. 2019) but bipartite in *Sauroscaptor* (Kammerer et al. 2016). The nuchal crest flanks two deep depressions laterally in cistecephalids (Keyser 1965; Cox 1972; Cluver 1974a; Kammerer et al. 2016; Angielczyk et al. 2019). These depressions increased the surface area for the atlantooccipital musculature, which may have generated power for digging with the head. In *Kawingasaurus* (Figure 4.1O), the depressions are deeper and vertically-oriented than other cistecephalids. As in Kannemeyeriiformes (Renault 2000), these fossae housed the rectus capitis dorsalis minor muscle and parts of the rectus dorsalis major (Evans and de Lahunta 2013).

Analogously, the nuchal crest is present on the posterodorsal part of the supraoccipital in extant mammalian fossorial taxa such as talpids, chrysochlorids, *Notoryctes*, *Necrolestes*, *Spalax* and the badger *Meles* (Rose and Emry 1983; Mecozzi et al. 2019) who, dispite being typically forelimb-diggers, require muscular reinforcement of the neck region. Similarly, at the occipital surface of the supraoccipital in amphisbaenians there is an ascending process that is analogous to the dicynodont nuchal crest (Müller et al. 2016; Abo-Eleneen et al. 2017). The development of a nuchal crest and its relative forward position in these taxa is associated with some head-digging requirements (Rose and Emry 1983), coincident with a fossorial lifestyle, even when forelimbs are the main mechanism of excavation. The typical mechanism of burrowing in the amphisbaenid *Leposternon microcephalum* consists of pitching head movements to compress the soils of the upper part of the animal's tunnel (Navas et al. 2004). The power generated for digging originates mostly from the longissimus muscle in that taxon. This mechanism is analogous to cistecephalid emydopoids, because they show a larger area for the insertion of these muscular systems (Cox 1959). The elaboration of the occipital region in *Kawingasaurus* is consistent with the accommodation of larger muscle mass for digging as they play a crucial role for force-generating capacity, as observed in *Notoryctes*, *Myospalax*

(Brodie 1950, Nevo 1979; Snively and Russell 2007, Werneburg 2019). However, due to the clear adaptations in the postcrania in various cistecephalids, it is more likely these taxa used both mechanisms of excavation, with possibly the head being a secondary assisting tool.

Importantly, deep nuchal ligament fossae and salient crests on the occiput are generally present in species with a large and heavy head such as elephants, tyrannosaurids, dinocephalians, gorgonopsians and kannemeyeriform dicynodonts (Renaut 2000; Renaut and Hancox 2001; Coria and Currie 2002; Brochu 2003; Hurum and Sabath 2003; Bever et al. 2013; Kammerer 2016; Kammerer et al. 2015, 2019; Fraser-King et al. 2019). However, the presence of these features in such small animals as cistecephalids would support a functional role unrelated to body mass, but rather related to lifestyle.

Pristerodon and other basal dicynodonts have a convex posterior aspect of the opisthotic and flatter posterior aspect of the supraoccipital (Barry 1974; Modesto et al. 2003; Angielczyk and Sullivan 2008; Angielczyk and Rubidge 2009; Castanhinha et al. 2013; Angielczyk et al. 2016; Boos et al. 2016; Macungo et al. 2020). This morphology is analogous to that of the basal emydopoids and is further comparable to that of the pylaecephalid *Diictodon* (Sullivan and Reisz 2005). Despite this similarity, *Diictodon* was recovered in helical burrows (Smith 1987, Sullivan et al. 2002), which could contradict that a salient nuchal crest is an adaptation to fossorial lifestyle. However, firstly, *Diictodon* could have been a facultative fossorial taxon, only using warrens for specific lifestyle tasks such as parental care, and shelter but does not feed in the burrows (Ray and Chinsamy 2003; Smith et al. 2021). Secondly, although it lacks some cranial adaptations to digging lifestyle, *Diictodon* forelimbs morphology is a reliable indicator of fossoriality as it has short limbs with major muscle attachment area, the posterolateral orientation of the humerus, and long and wide manus with long blunt claws (Ray and Chinsamy 2003). Indeed, comparing *Diictodon* and cistecephalids digging style based on the occipital surface, *Diictodon* was probably exclusively adapted to forelimb-

digging, whereas cistecephalids probably deployed more consistently head-digging. In dicynodonts, the longissimus muscular system reconstructed as inserting on the dorsolateral margin of the occiput, equivalent to the interparietal and tabular (Cox 1959). These muscles possibly adjoined to the rectus capitis system to generate power for digging in *Kawingasaurus*. However, in *Kawingasaurus* the more laterally located depression seems to indicate that the rectus capitis lateralis and the obliquus capitis cranialis were inserted on the opisthotic rather than on the opisthotic and exoccipital as observed in kannemeyeriiforms.

4.1.5. Rationale for fossorial adaptations in dicynodonts

Cistecephalids display both numerous cranial and post-cranial adaptations to fossoriality. They had an extreme posterior location or completely lost of their pineal foramen, and some species show a more pneumatized braincase, as exemplified by *Kawingasaurus*, which may be indicative of subterranean hearing. The enlarged forelimbs, robust humerus with major muscle attachment area, and broader manus of cistecephalids strongly suggest that they were forelimb-diggers. On the other hand, their more coossified skull and braincase, the presence of the nuchal crest and a vast area for the atlantooccipital musculature attachment, may indicate that cistecephalids were adapted to a head-digging strategy. Based on these lines of evidence, cistecephalids may have been potentially obligate or quasi-obligate fossorial species among dicynodonts, thus feeding within their tunnels. The presence of small orbits in *Kawingasaurus* and *Cistecephalus* and relatively small eyeball in *Kembawacela*, could imply that they did not rely on vision, such as *Spalax* and other moles. In contrast, other dicynodont taxa found in burrow casts display only post-cranial adaptations. *Diictodon* shows short limbs with major muscle attachment area, a posterolateral orientation of the humerus, and long and wide manus with long blunt claws (Smith 1987; Sullivan 2002; Ray and Chinsamy 2003; Smith et al. 2021), which suggests that it was a forelimb, and perhaps facultative digger. *Lystrosaurus* shows thick bone walls of the humerus and a spactulate structure of the claws that suggests that it was a

forelimb-digger species. Additionally, *Lystrosaurus* shows deep fossae and crests on the posterior aspect of the opisthotic, analogous to a vast area for the atlantooccipital musculature attachment, suggesting head-digging (or rooting behaviour) may have also been possible in this species. However, the skull shape of *Lystrosaurus* is too unique to infer head-digging, and it possesses relatively large orbits, a large pineal foramen, and its braincase is weakly coossified (Cluver 1971). Though *Lystrosaurus* was found in burrows (King and Cluver 1990; Groenewald 1991; Modesto and Botha 2010; Bordy et al. 2010; Botha-Brink 2017), I conclude that it was likely a facultative fossorial species. Further studies to test this hypothesis must be performed.

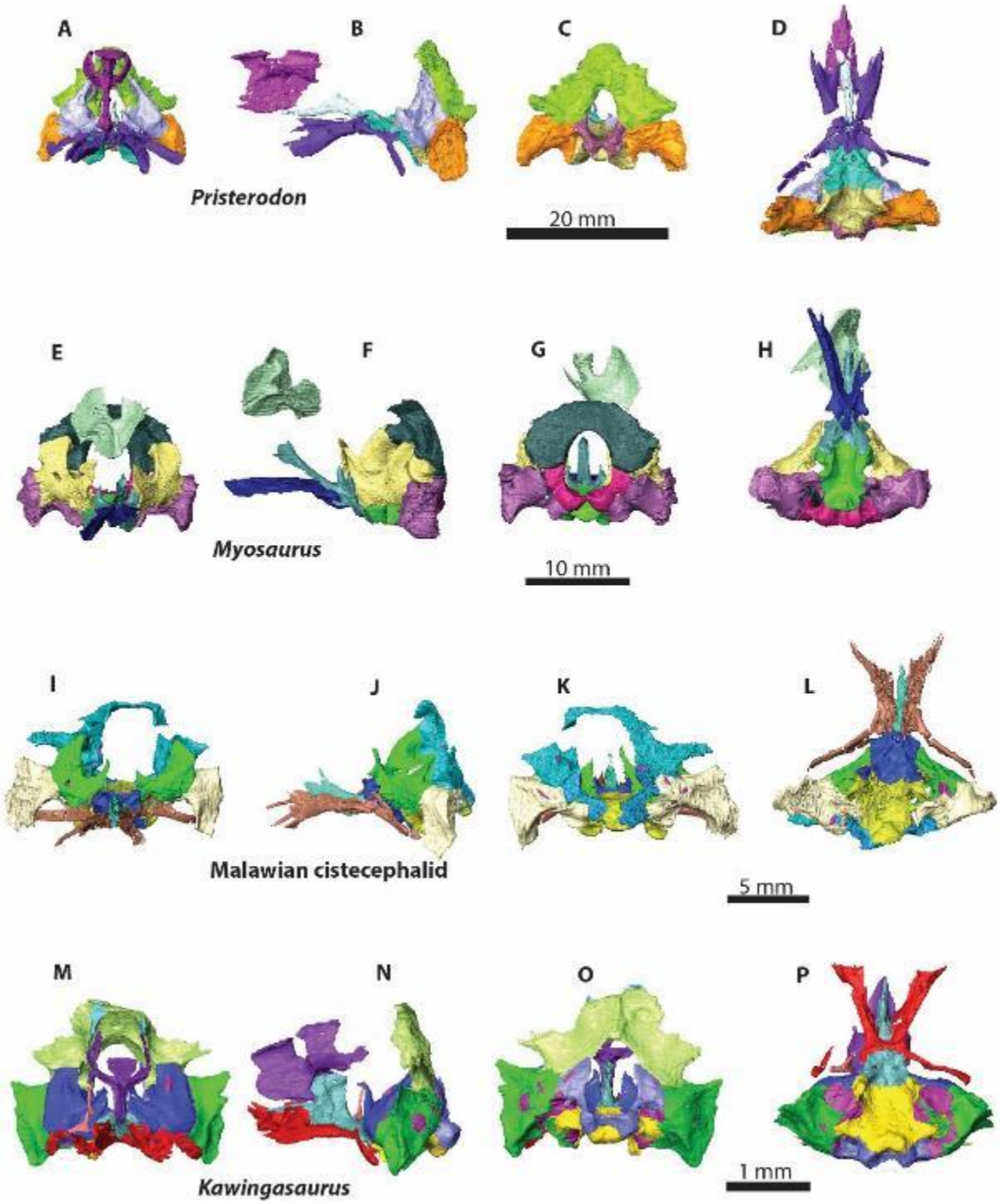


Figure 4. 1. Comparisons of the braincase between *Pristerodon* and emydopoids. *Pristerodon mackayi* (BP/1/2642) in **(A)** anterior, **(B)** left lateral, **(C)** posterior and **(D)** ventral views. *Myosaurus gracilis* (BP/1/2690) in **(E)** anterior, **(F)** left lateral, **(G)** posterior and **(H)** ventral views. The Malawian cistecephalid (PK-16-1) in **(I)** anterior, **(J)** left lateral, **(K)**, posterior and **(L)** ventral views. *Kawingasaurus fossilis* (GPIT/RE/9272) in **(M)** anterior, **(N)** left lateral, **(O)** posterior and **(P)** ventral views.

4.2. Emydopoidea inter- and intrarelationships

The phylogenetic instability of Emydopoidea, resulting in multiple published arrangements of their systematics, has long been an important source of debate. Emydopoidea was first proposed by Cluver and King (1983). Emydopoidea historically consisted of two main families: Emydopidae containing *Myosaurus* and *Emydops*; and the Cistecephalidae formed by *Cistecephalus*, *Cistecephaloides*, and *Kawingasaurus* (Cluver and King 1983). Later on, a third family was added to Emydopoidea, the Kingoriidae (Angielczyk and Kurkin 2003b; Angielczyk 2007; Fröbish 2007; Fröbish and Reisz 2008). It is further generally agreed that Emydopoidea is defined by four main families, namely: Emydopidae, Myosauridae, Kingoriidae and Cistecephalidae (Angielczyk 2007; Fröbish 2007; Fröbish and Reisz 2008; Kammerer and Angielczyk 2009; Kammerer et al. 2011; 2013; 2016; Angielczyk and Kammerer 2017; Angilczyk et al. 2019; Kammerer 2019a).

Phylogenetically, Emydopidae has been recovered as a basal clade of emydopoids, with the Kingoriidae, Myosauridade, and Cistecephalidae branching successively crownward (Angielczyk and Kurkin 2003b; Angielczyk 2007; Fröbish 2007; Fröbish and Reisz 2008; Kammerer and Angielczyk 2009; Kammerer et al. 2011; 2016; Angielczyk and Kammerer 2017; Kammerer 2019a), which is also consistent with the early occurrence of *Emydops* stratigraphically (Day and Smith 2020). On the other hand, recent analyses recovered Kingoriidae as the basalmost clade of Emydopoidea (Angielczyk and Cox 2015; Boos et al. 2016; Angielczyk et al. 2019) motivated by the retention of some plesiomorphic dicynodont characteristics such as the presence of a trough on the mid-ventral vomer plate and a mid-ventral vomerine plate with an expanded and oval-shaped area posterior to the junction with the premaxilla. In addition, there is some instability within the family Kingoriidae, such as debate over the inclusion of *Niassodon* (Castanhinha et al. 2013) and *Thliptosaurus* (Kammerer

2019a, but see this study). The recent placement of *Niassodon* as an endothiodontid seems more consistent with the presence of numerous postcanine teeth and the *Endothiodon*-like palatine (Boos et al. 2016; Araújo et al. 2018; Angielczyk et al. 2019; Macungo et al. 2020). The retention of plesiomorphic dicynodont characteristics among kingoriids probably accounts for their similarities to *Niassodon*. Another area of systematic instability is the position of the Cistecephalidae and Emydopidae with respect to *Myosaurus* (Surkov and Benton 2008). The position of *Myosaurus* alternate between a sister-relationship with Kingoriidae and Cistecephalidae (Angielczyk and Rubidge 2010; Kammerer et al. 2011). On the other hand, the systematics of Cistecephalidae have remained relatively consistent (Angielczyk 2007; Fröbish 2007; Fröbish and Reisz 2008; Kammerer and Angielczyk 2009; Kammerer et al. 2011), despite the recent addition of two new genera, i.e., *Sauroscaptor* and *Kembawacela* (Kammerer et al. 2016; Angielczyk et al. 2019), and possibly a third one, the Malawian cistecephalid PK-16-1 (Araújo et al. 2021). The highly diagnostic cistecephalid skull accounts to their derived cranial anatomy linked to multiple adaptations to fossoriality

4.2.1. Phylogeny results

This phylogenetic analyses resulted in four most parsimonious trees with a length of 1323.452 steps, with a consistency index of 0.227 and retention index of 0.709. The Bremer support indices can be read on Figure 4.2 and Figure S1. The resulting emydopoid relationship is almost topologically identical to that of Angielczyk et al. (2019), yet there are major changes concerning the position of *Thliptosaurus*, *Rastodon*, *Niassodon* and the formation of a polytomy among cistecephalids. The redefinition of the Emydopoidea based on this analysis is summarized by Figure 4.2, which includes, from the stemward to crownward direction: *Rastodon*, Kingoriidae, *Thliptosaurus*, *Digalodon*, Emydopidae, Myosauridae and Cistecephalidae. From my results, the presence of the divergent crests on the posterior surface of the opisthotic (character 180) supports the Cistecephalidae. My new character 181 is a

synapomorphy of the clade gathering the taxa more derived than *Thliptosaurus*. The distribution of the nuchal crest on the supraoccipital (character 183) separates the basal emydopoids from the derived cistecephalids. The region of the supraoccipital that may have hosted the nuchal crest is relatively low with shallower depressions in basal emydopoids, but a well-elaborated nuchal crest is present in all cistecephalids.

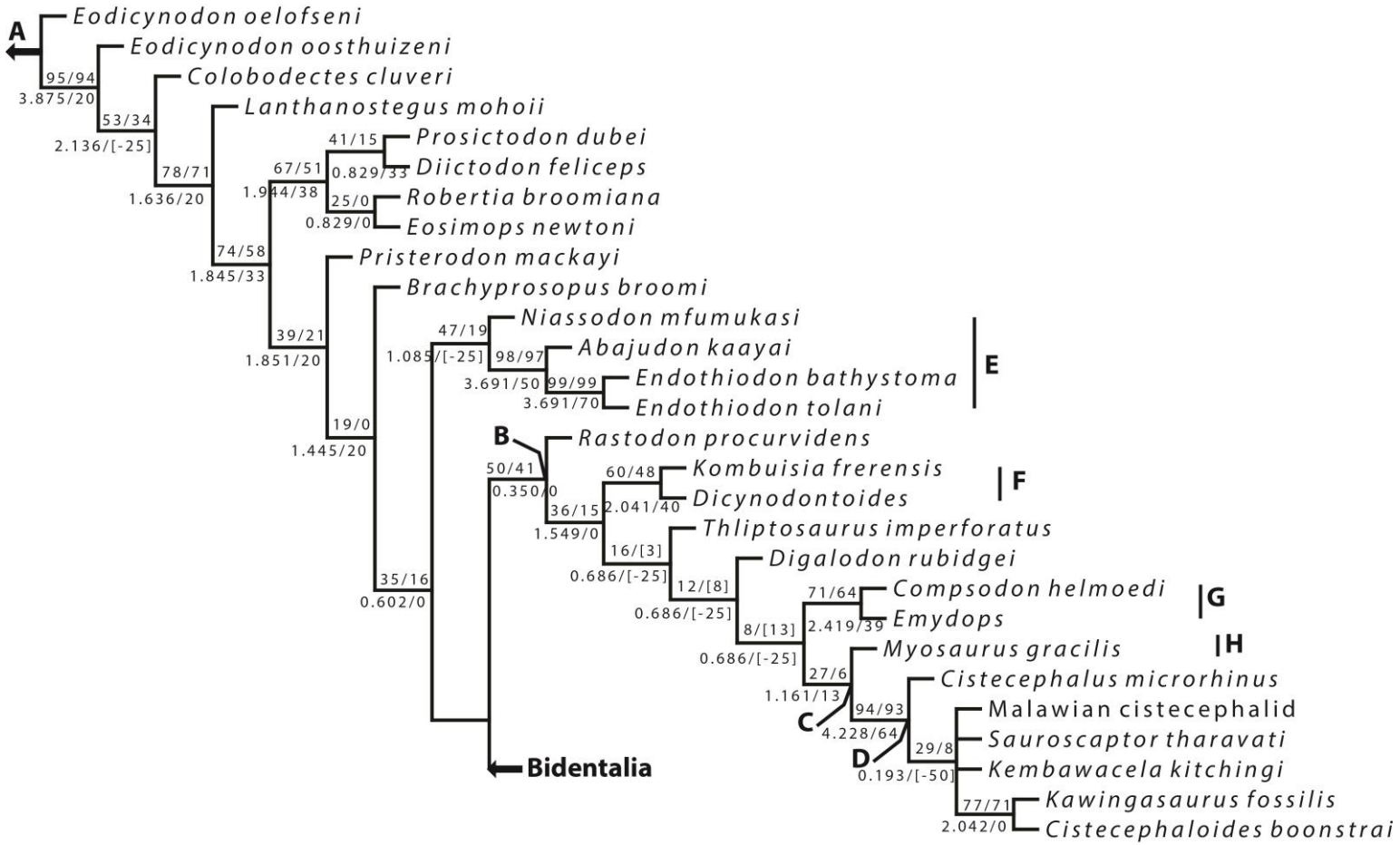


Figure 4. 25. Phylogenetic results simplified to highlight Emydopoidea intra- and interrelationships. Numbers at nodes represent: Symmetric Resampling values / CG values above nodes; Bremer Support values / Relative Bremer Support values below nodes. See appendices D, E and F for the complete trees. **A** – Dicynodontia; **B** – Emydopoidea; **C** – Kistecephalia; **D** – Cistecephalidae; **E** – Endothiodontia; **F** – Kingoriidae; **G** – Emydopidae; **H** – Myosauridae.

This result removes *Thliptosaurus imperforatus* from Kingoriidae (Kammerer 2019a) to become the sister-taxon to *Digalodon rubidgei* (Figure 4.2). *Digalodon* and *Thliptosaurus* have wide intertemporal regions, whereas this area is narrow in kingoriids (Boos et al. 2016). Also, *Thliptosaurus* shares a robust tuber-like opisthotic ventromedial process with *Digalodon* and other emydopoids except kingoriids (character 181); and the mandibular fenestra is only partially occluded as in *Digalodon* and the Emydopidae, wich contrasts with the completely occluded condition in kingoriids (see material and methods for details concerning rescoring of character 114).

Notably the Malawian cistecephalid, *Sauroscaptor tharavati* and *Kembawacela kitchingi* form a soft polytomy, which results from the addition of the the new characters and the Malawian cistecephalid (see appendix E for trees comparison) that has insufficiency of characters to support a definite relationship between the three taxa. For instance, the posterior aspect of the supraoccipital is badly preserved in the Malawian cistecephalid, such that I could not score the character 183 regarding the presence or absence of a nuchal crest. The composition of Kistecephalia has changed in our analyses now consisting of *Myosaurus* plus cistecephalids but excludes kingoriids (Figure 4.2). Kistecephalia was originally composed by *Myosaurus*, kingoriids and Cistecephalidae, with the exclusion of *Emydops* (Kammerer and Angielczyk 2009). I found that kingoriids are relatively more basal to Emydopidae (Boos et al. 2016; Angielczyk et al. 2019; Figure 4.2) due to their similarities with basal dicynodonts (characters mentioned above).

My analyses also excludes *Rastodon procurvidens* from its original position as a basal Bidentalia (Boos et al. 2016). The absence of an expanded area in the mid-ventral plate of the vomers supported *Rastodon* as bidentalian (Boos et al. 2016). However, that position has been recently challenged because the topological character also occurs in emydopoids and basal dicynodonts (Kammerer and Ordoñez 2021). The bidentalian position of *Rastodon* was also

retrieved in later phylogenetic analysis (e. g., Angielczyk and Kammerer 2017; Kammerer 2018; 2019a; 2019b; Kammerer et al. 2019; Kammerer and Ordoñez 2021), although *Rastodon* was already retrieved as a more basal dicynodont (Kammerer and Smith 2017). I retrieve *Rastodon procurvidens* as an emydopoid (Figure 4.2) based on the morphology of the occipital surface of the supraoccipital (character 183). *Rastodon* shares a nearly flat aspect of the supraoccipital with *Emydops, Compsodon, Digalodon, Kombuisia* and *Myosaurus*, i. e., these taxa lack the nuchal crest, but have very shallow vertical excavations on the occipital surface of the supraoccipital (Fourie 1993, Fröbish 2007; Fröbisch and Reisz 2008; Kammerer et al. 2015; Angielczyk and Kammerer 2017). Two other characters unite *Rastodon* to the Emydopoidea, despite not directly linked to the scope of this research. First, is the presence of a caniniform depression that has the form of a notch in palatal rim anterior to the caniniform process (discrete-state character 28). The second is the presence of the mandibular fenestra occluded by the dentary (discrete-state character 114, Kammerer and Ordoñez 2021), the last of which being found in the kingoriids *Dicynodontoides* and *Kombuisia*.

Finally, the former emydopoid *Niassodon* is recovered as an endothiodontid, consistent with other recent researches (Boos et al. 2016; Araújo et al. 2018; Kammerer 2019a). Even more recently *Niassodon* was, however, retrieved as the sister-taxon to Emydopoidea (Angielczyk et al. 2019), suggesting aspects of convergent evolution between endothiodontids and emydopoids.

CHAPTER V – CONCLUSION AND FUTURE WORKS

Conclusions

The emydopoid dicynodonts basicranial axis is here thoroughly analyzed thanks to µCT- and synchrotron scanning and segmentation. The cistecephalid basicranial axis reveals a derived anatomy among emydopoids and other dicynodonts. Some of these characters reflect fossorial adaptations. Cox (1972) and Cluver (1978) substantiated a forelimb-digging strategy in cistecephalids via muscle reconstruction. Here I hypothesise a complementary head-based burrowing strategy for cistecephalids. Cistecephalids share a highly coossified braincase, and increased area for the atlantooccipital musculature similar to extant fossorial taxa, such as moles, caecilians and amphisbaenians. I hypothesise that cistecephalids were likely obligate or quasi-obligate fossorial taxa, in contrast to possibly facultative fossorial, forelimb-digging taxa susch as *Lystrosaurus* and *Diictodon*. The addition to the definition of Emydopoidea of a transversally wider supraoccipital, and the modification of their occipital plate, is supported by my phylogenetic analyses. My tree recovers *Rastodon* as a basal member of Emydopoidea for the first time and suggests that the proposed addition of further internal characters using µCT techniques may help further resolve dicynodont interrelationships.

REFERENCES

Agnew, J. D. (1959). Cranio-osteological studies in *Dicynodon grimbeeki* with special reference to the sphenethmoid region and cranial kinesis. Dep. Zool. Univ. Pretoria

Anderson, J. S., Scott, D., Reisz, R. R. (2009). *Nannaroter mckinziei*, a new ostodolepid 'microsaur' (Tetrapoda, Lepospondyli, Recumbirostra) from the Early Permian of Richards Spur (Ft. Sill), Oklahoma. 29(2):379-388. DOI: 10.1671/039.029.0222

Angielczyk, K. D. (2007). New specimen of the Tanzanian dicynodont "*Cryptocynodon" parringtoni* Von Huene, 1942 (Therapsida, Anomodontia), with an expanded analysis of Permian dicynodont phylogeny. J. Vert. Paleontology. 27(1): 116-131. https://doi.org/10.1671/0272-4634(2007)27[116:NSOTTD]2.0.CO;2.

Angielczyk, K. D., Kammerer, C. F. (2017). The cranial morphology, phylogenetic position and biogeography of the Upper Permian dicynodont *Compsodon helmoedi* Van Hoepen (Therapsida, Anomodontia). Palaeontol. Assoc. 1-33. Doi: 10.1002/spp2.1087.

Angielczyk, K. D., Kurkin, A. A. (2003). Has the utility of *Dicynodon* for Late Permian terrestrial biostratigraphy been overstated? Geol. Soc. Am. 31:363-366

Angielczyk, K. D., Rubidge, B. (2009). The Permian dicynodont *Colobodectes cluveri* (Therapsida, Anomodontia), with notes on its ontogeny and stratigraphic range in the Karoo Basin, South Africa. J. Vert. Palaeontol. 29(4):1162-1173. DOI: 10.1671/039.029.0431.

Angielczyk, K. D., Rubidge, B. S. (2013). Skeletal morphology, phylogenetic relationships and stratigraphic range of *Eosimops newtoni* Broom, a pylaecephalid dicynodont (Therapsida, Anomodontia) from the Middle Permian of South Africa. J. Syst. Palaeontol. 11:2, 191-231. http://dx.doi.org/10.1080/14772019.2011.623723

Angielczyk, K. D., Sullivan, C. (2008). *Diictodon feliceps* (Owen, 1876), a dicynodont (Therapsida, Anomodontia) species with a Pangaean distribution. J. Vert. Paleontology 28(3):788-802. DOI:10.1671/0272-4634(2008)28[788:DFOADT]2.0.CO;2

Angielczyk, K. D., Benoit, J., Rubidge, B. S. (2019). A new tusked cistecephalid dicynodont (Therapsida, Anomodontia) from the upper Permian upper Madumabisa Mudstone Formation, Luangwa Basin, Zambia. Palaeontol. Assoc. 1-42. Doi: 10.1002/spp2.1285

Angielczyk, K. D., Cox, C. B. (2015). Distinctive emydopoid dicynodont (Therapsida, Anomodontia) mandibles from the Permian Ruhuhu and Usili Formations (Songea Group), Ruhuhu Basin, Tanzania. J. Vert. Paleontol. e1008699. DOI: 10.1080/02724634.2015.1008699

Angielczyk, K. D., Fröbisch, J., Smith, R. M. H. (2005). On the stratigraphic range of the dicynodont taxon *Emydops* (Therapsida: Anomodontia) in the Karoo Basin, South Africa. Palaeontol. afr. 41: 23-33

Angielczyk, K. D., Sidor, C. A., Nesbitt, S., J., Smith, R. M. H., Tsuji, L. A. (2009). Taxonomic revision and new observations on the dicynodont genus *Dicynodontoides*, the senior subjective synonym of *Kingoria* (Therapsida, Anomodontia). J. Vert. Paleontol. 29(4):1174-1187.

Araújo, R., Fernandez, V., Polcyn, M., Fröbisch, Martins, R. M. S. (2017). Aspects of gorgonopsian paleobiology and evolution: insights from the basicranium, occiput, osseous labyrinth, vasculature, and neuroanatomy. PeerJ 5:e3119; DOI 10.7717/peerj.3119.

Araújo, R., Fernandez, V., Rabbitt, R. D., Ekdale, E. G., Antunes, M. T., Castanhinha, R. et al. (2018). *Endonthiodon* cf. *bathystoma* (Synapsida: Dicynodontia) bony labyrinth anatomy, variation and body mass estimates. PlosOne 13: e0189883. https://doi.org/10.1371/journal.pone.0189883

Araújo, R., Macungo, Z., Fernandez, V., Chindebvu, E.G., Jacobs, L.L. (preprint 2021). A New Cistecephalid (dicynodontia: Emydopoidea) from the Upper Permian of Malawi. PaleorXiv. https://doi.org/10.31233/osf.io/2x4wb

Bandyopadhyay, S. (1988). The mammal-like reptile *Rechnisaurus* from the Triassic of India. Palaeontol. 32(2):305-312

Barry, T. H. (1967). The cranial morphology of the Permo-Triassic Anomodont *Pristerodon buffaloensis* with special reference to the neural endocranium and visceral arch skeleton. Ann. S. Afr. Mus. 50(7):131-161.

Barry, T. H. (1974). A new dicynodont ancestor from the Upper Ecca (Lower Middle Permian) of South Africa. Ann. S. Afr. Mus. 64, 117-136.

Beck, R. M. D., Loys, J., Brewer, P., Archer, M., Black, K. H., Tedford, R. H. (2020). A new family of diprotodontian marsupials from the latest Oligocene of Australia and the evolution of wombats, koalas, and their relatives (Vombatiformes). Sci. Rep. 10:9741. https://doi.org/10.1038/s41598-020-66425-8

Bellairs, A. d'A. (1949). The anterior brain-case and interorbital septum of Sauropsida, with a consideration of the origin of snakes. J. Linn. Soc. Zool. 41

Bellairs, A. d'A., Gans, C. (1983). A reinterpretation of the amphisbaenian orbitosphenoid. Nat. 302.

Bemis, W. E., Schwenk, K., Wake, M. H. (1983). Morphology and function of the feeding apparatus in *Dermophis mexinanus* (Amphibia: Gymnophione). Zool. J. Linn. Soc. 77, 75-96

Benoit, J., Merigeaud, S., Tabuce, R. (2013). Homoplasy in the ear region of Tethytheria and the systematic position of Embrithopoda (Mammalia, Afrotheria), *Geobios*, 644. http://dx.doi.org/10.1016/j.geobios.2013.07.002

Benoit, J., Crumpton, N., Merigeaud, S., Tabuce, R. (2013). Petrosal and bony labyrinth morphology supports paraphyly of *Elephantulus* within Macroscilididae (Mammalia, Afrotheria). J. Mamm. Evol. DOI 10.1007/s10914-013-9234-5

Benoit, J., Jasinoski, S. C. (2016). Picking up the pieces: the digital reconstruction of a destroyed holotype from its serial section drawings. Palaentol. Electron. 29.3.3T: 1-16

Benoit, J., Adbala, F., Manger, P. R., Rubidge, B. S. (2016). The sixth sense in mammalian forerunners: variability of the parietal foramen and evolution of the pineal eye in South African Permo-Triassic eutheriodont therapsids. Acta Palaeontol. Polonica 61:777-789

Benoit, J., Angieclzyk, K. D., Miyamae, J. A., Manger, P., Fernandez, V., Rubidge, B. (2018). Evolution of facial innervation in anomodont therapsids (Synapsida): Insights from X-ray computerized microtomography. J. Morphol. DOI: 10.1002/jmor.20804

Bever, G. S., Brusatte, S. L., Carr, T. D., Xu, X., Balanoff, A. M., Norell, M. A. (2013). The braincase anatomy of the Late Cretaceous dinosaur *Alioramus* (Theropoda: Tyrannosauroidea). BioOne.376(1):1-72. DOI: http://dx.doi.org/10.1206/810.1

Boos, A. D. S. (2012). Descrição osteológica de um exemplar de *Endothiodon* (Synapsida, Dicynodontia) proveniente da Serra do Cadeado (Formação Rio do Rasto, Permiano Superior) e suas implicações bioestratigráficas e paleobiogeográficas. Msc. Diss. Porto Alegre

Boos, A. D. S., Kammerer, C. F., Schultz, C. L., Soares, M. B., Ilha, A. L. R. (2016). A new Dicynodont (Therapsida: Anomodontia) from the Permian of Southern Brazil and Its Implications for Bidentalian Origins. PloS ONE. 11(5): e0155000. doi:10.1371/journal.pone.0155000.

Bordy, E. M. Sztanó, O., Rubidge, B. S., Bumby, A. (2010). Early Triassic vertebrate burrows from the Katberg Formation of the south-western Karoo Basin, South Africa. Lethaia. 44. DOI 10.1111/j.1502-3931.2010.00223.x

Botha-Brink, J. (2017). Burrowing in *Lystrosaurus*: preadaptation to a postextinction environment? J. Vert. Paleontol. 37:e1365080. https://doi.org/10.1080/02724634.2017.1365080.

Botha, J. (2020). The paleobiology and paleoecology of South African *Lystrosaurus*. PeerJ 8:e10408. http://doi.org/10.7717/peerj.10408

Botha, J., Huttenlocker, Adam, K., Smith, R. M. H., Prevec, R., Viglietti, P., et al. (2019). New geochemical and palaeontological data from the Permian-Triassic boundary in the South African Karoo Basin test the synchronicity of terrestrial and marina extinctions. Palaeontol. Palaeoclim. Palaeoecol. https://doi.org/10.1016/j.palaeo.2019.109467

Botha, J., Smith, R. M. H. (2020). Biostratigraphy of the *Lystrosaurus declives* Assemblage Zone (Beaufort Group, Karoo Supergroup), South Africa. Geol. Soc. S. Afr. 123(2), 207-216. doi:10.25131/sajg.123.0015

Bremer, K. (1994). Branch support and tree stability. Cladistics 10:295–304.

Brochu, C. A. (2003). Osteology of *Tyrannosaurus rex*: Insights from a nearly complete Skeleton and High-Resolution Computed Tomographic Analysis of the Skull. J. Vert. Paleontol. 22(4):1-138. http://dx.doi.org/10.1080/02724634.2003.10010947

Brock, G. T. (1939). The skull of *Acontias meleagris*, with a study of the affinities between lizards and snakes. J. Linn. Soc. Zool. 41.

Brodie, A. G. (1950). Anatomy and physiology of head and neck musculature.

Broom, R. (1905). On the use of the term *Anomodontia*. Rec. Albany Mus. 1, 266–269

Broom, R. (1913). On some new genera and species of dicynodont reptiles, with notes on a few others. Bull. Am. Mus. Nat. Hist. 32

Broom, R. (1915). On the Anomodont genera, *Pristerodon* and *Tropidostoma*. Proc. Zool. Soc. Lond. 355-361

Carlson, K. J., Stout, D., Jashashvili, T., De Ruiter, D. J., Tafforeau, P., Carlson, K. et al. (2011). The endocast of MH1, *Australopithecus sediba*. Sci. 333 :1402-1407.

Castanhinha, R., Araújo, R., Júnior, L. C., Angielczyk, K. D., Martins, G. G., Martins, Rui. M. et al. (2013). Bringing dicynodonts back to life: Paleobiology and Anatomy of a new Emydopoid genus from the Upper Permian of Mozambique. PLoS One 8 (12): e80974.

Catania, K. C. (2000). Epidermal sensory organs of moles, shrew-moles, and desmans: a study of the family Talpidae with comments on the function and evolution of Eimer's organ. Brains Behav. Evol. 56:146-174

Cau, A., Beyrand, V., Voeten, D.F., Fernandez, V., Tafforeau, P., Stein, K. et al. (2017). Synchrotron scanning reveals amphibious ecomorphology in a new clade of bird-like dinosaurs. Nat. 552(7685):395-399.

Christine, J. A. (2016). An overview of caecilians (Lissamphibia: Gymnophiona), with emphasis on selected topics. ETSU, DOI: 10.13140/RG.2.1.1553.0003

Cluver, M. A. (1971). The cranial morphology of the dicynodont genus *Lystrosaurus*. Ann. S. Afr. Mus. 56(5):155-274.

Cluver, M. A. (1974a). The skull and mandible of a new cistecephalid dicyndont. Ann. S. Afr. Mus. 64:137 – 155

Cluver, M. A. (1974b). The cranial morphology of the Lower Triassic dicynodont *Myosaurus gracilis*. Ann. S. Afr. Mus. 66:35-54.

Cluver, M. A. (1978). The skeleton of the mammal-like reptile *Cistecephalus* with evidence for a fossorial mode of life. Ann. S. Afr. Mus. 76(5): 213-246

Cluver, M. A., King, G. M. (1983). A reassessment of the relationships of Permian Dicynodontia (Reptilia, Therapsida) and a new classification of dicynodonts. Ann. S. Afr. Mus. 91, 195-273.

Coria, R. A., Currie, P. J. (2002). The braincase of *Giganotosaurus carolinii* (Dinosauria: Theropoda) from the Upper Cretaceous of Argentina. J. Vert. Palaeontol. 22(4):802-811. DOI: 10.1671/0272-4634(2002)022[0802:TBOGCD]2.0.CO;2

Cox, C. B. (1959). On the anatomy of a new dicynodont genus with evidence of the position of the tympanum. Proc. Zool. Soc. Lond. 132: 321- 367.

Cox, C. B. (1965). New Triassic dicynodonts from South America, their origins and relationships. Philos. Trans. R. Soc. Lond. B. 248, 457-514. doi: 10.1098/rstb.1965.0005.

Cox, C. B. (1972). A new digging dicynodont from the Upper Permian of Tanzania. In: Josey, K. A., Kemp, T. S. editors. Studies in Vertebrate Evolution. Edinburgh: Oliver and Boyd. pp 173-189.

Damiani, R., Modesto, S., Yates, A., Neveling, J. (2003). Earliest evidence of cynodont burrowing. Proc. R. Soc. Lond. B. 270:1747-1752. doi: 10.1098/rspb.2003.2427

Day, M. O., Smith, R. M. H. (2020). Biostratigraphy of the *Endothiodon* Assemblage Zone (Beaufort Group, Karoo Supergroup), South Africa. S. Afr. J. Geol. 123:165-180

Eakin, R. M. (1973). The third eye. 157 pp. University of California Press, Berkeley

Edinger, T. (1942). The pituitary body in giant animals fossil and living: a survey and a suggestion. The quarterly review of biology. 17(1):31-45. doi:1086/394644

Elzanowski, A., Galton, P. M. (1991). Braincase of *Enaliornis*, and early Cretaceous bird from England. J. Vert. Palaentol. 11:90-107.

Evans, H. E., De Lahunta, A. (2013). Miller's Anatomy of the Dog. St. Louis: Saunders/Elsevier

Fernandez, V., Abdala, F., Carlson, K. J., Rubidge, B.S., Yates, A., Tafforeau, P. (2013). Synchrotron reveals Early Triassic odd couple: injured amphibian and aestivating therapsid share burrow. PLoS One, 8(6), p.e64978.

Fernandez V., Tafforeau P. (2018). "Synchrotron X-Ray Micro Computed Tomography of Fossils Preserved on Slab." In 3rd Dimensional X-ray Computed Tomography Conference. Nottingham, UK.

Ferreira-Cardoso, S., Angielczyk, K. D., Araújo, R. (in prep.). Computed tomography-based re-description of the skull and mandible of the mid-Permian dicynodont *Dicynodon megalorhinus* (Broom, 1904) (nomen dubium). Palaeontol. afr.

Fourie, H. (1991). A detailed description of the skull of *Emydops* (Therapsida: Dicynodontia). Master's dissertation. University of the Witwatersrand.

Fourie, H. (1993). A detailed description of the internal structure of the skull of *Emydops* (Therapsida: Dicynodontia). Palaeontol. afr. 30, 103-111.

Fraser-King, S. W., Benoit, J., Day, M. O., Rubidge, B. S. (2019). Cranial morphology and phylogenetic relationship of the enigmatic dinocephalian *Styracocephalus platyrhynchus* from the Karoo Supergroup, South Africa. Palaeontol. afr. 54:14-29.

Freeman, P. W. (1979). Redescription and comparison of a highly fossorial mole, *Domninoides mimicus* (Insectivora, Talpidae), from the Clarendonian, Am. Mus. Novit. 2667, 1-16

Fröbisch, J. (2007). The cranial anatomy of *Kombuisia frerensis* Hotton (Synapsida, Dicynodontia) and a new phylogeny of anomodont therapsids. Zool. J. Linn. Soc. 150:117-144

Fröbisch, J., Reisz, R. R. (2008). A new species of *Emydops* (Synapsida, Anomodontia) and a discussion of dental variability and pathology in dicynodonts. J. Vertebr. Palaeontol. 28(3):770-787. DOI: 10.1671/0272-4634(2008)28[770:ANSOES]2.0.CO;2

Fröbisch, J., Angielczyk, K. D., Sidor, C. A. (2010). The Triassic dicynodont *Kombuisia* (Synapsida, Anomodontia) from Antartica, a refuge from the terrestrial Permian-Triassic mass extinction. Naturwissenschaften 97:187-196

Gans, C. (1978). The characteristics and affinities of the Amphisbaenia. Trans. Zool. Soc. Lond. 34(4):347-416

Goloboff, P. A. (1999). Analyzing large data sets in reasonable times: solutions for composite optima. Cladistics 15(4), 415-428.

Goloboff, P. A., Farris, J. S. (2001). Methods for quick consensus estimation. Cladistics 17(1), S26-S34.

Goloboff, P. A., Farris, J.S., Källersjö, M., Oxelman, B., Ramírez, M. J. Szumik, C. A. (2003). Improvements to resampling measures of group support. Cladistics 19(4), 324-332.

Goloboff, P. A., Catalano, S. A. (2016). TNT version 1.5, including a full implementation of phylogenetic morphometrics. Cladistics 32(3):221-238.

Grand, T. I., Barboza, P. S. (2001). Anatomy and development of the koala, *Phascolarctos cinereus*: an evolutionary perspective on the superfamily Vombatoidea. Anat. Embryol. 203, 211-223.

Griffin, C. T., Stocker, M. R., Colleary, C., Stefanic, C. M., Lessner, E. J., Riegler, M., et al. (2020). Assessing ontogenetic maturity in extinct saurian reptiles. Biol. Rev. 000-000. doi: 10.1111/brv.12666

Groenewald, G. H., Welman, J., MacEachern, J. A. (2001). Vertebrate burrow complexes from the Early Triassic *Cynognathus* Zone (Driekoppen Formation, Beaufort Group) of the Karoo Basin, South Africa. Palaios 16: 148–160

Groenewald, G. H. (1991). Burrow casts from the *Lystrosaurus-Procolophon* Assemblage-Zone, Karoo Sequence, South Africa. Koedoe 34:13-22

Gundy, G. C. Wurst, G. Z. (1976a). The occurrence of parietal eyes in recent Lacertilia (Reptilia). Soc. Stud. Amphib. Reptile. 10(2):113-121.

Gundy, G. C. Wurst, G. Z. (1976b). Parietal eye-pineal morphology in lizards and its physiological implications. Anat. Rec. 185:419-432

Hammer, W. R., Cosgriff, J. W. (1981). *Myosaurus gracilis*, an Anomodont reptile from the lower Triassic of Antarctica and South Africa. J. Palaeontol. 55(2):410-424.

Haughton, S. H. (1917). Investigations in South African Reptiles and Amphibia. Ann. S. Afr. Mus. 12(14):164-172

Helgen, K. M., Lim, N. T-L., Helgen, L. E. (2008). The hog-badger is not an edentate: systematics and evolution of the genus *Arctonyx* (Mammalia: Mustelidae). Zool. J. Linn. Soc. 154:353-385.

Hopson, J. A. (1979). Paleoneurology. In: Glans, C., Northcutt, R. G., Ulinski, P. (eds). Biology of the Reptilia. Acad. Press N. Y. 39-146.

Hurum, J. H., Sabath, K. (2003). Giant theropod dinosaurs from Asia and North America: skulls of *Tarbosaurus bataar* and *Tyrannosaurus rex* compared. Acta. Palaeontol. Pol. 48(2):161-190.

Huxley, T. H. (1868). On *Saurosternon bainii* and *Pristerodon mckayi*, two new fossil Lacertilian Reptiles from South Africa. Geol. Mag. 5 in phylogenetic analysis. Palaeontol. 47:619-639.

James, A. I., Eldridge, D. J. (2007). Reintroduction of fossorial native mammals and potential impacts on ecosystem processes in an Australian desert landscape. Biol. Conserv. 138:351-359

Jenkins, F. A., Walsh, D. M., Carroll, R. L. (2007). Anatomy of *Eocaecilia micropodia*, a limbed Caecilian of the Early Jurassic. Bull. Mus. Comp. Zool. 158:285-366

Jones, M. E. H., Curtis, N., O'Higgins, P., Fagan, M., Evans, S. E. (2009). The head and neck muscles associated with feeding in *Sphenodon* (Reptilia: Lepidosauria: Rhynchocephalia). Palaeontol. Electron. 12(2):7A-56. http://palaeo-electronica.org/2009_2/179/index.html

Kammerer, C. F. (2018). The first skeletal evidence of a dicynodont from the lower Eliot Formation of South Africa. Palaeontol. Afr. 52:102-128.

Kammerer, C. F. (2019a). A new dicynodont (Anomodontia: Emydopoidea) from the terminal Permian of KwaZulu-Natal, South Africa. Palaeontol. afr. 53:179-191

Kammerer, C. F. (2019b). Revison of the Tanzanian dicynodont *Dicynodon huenei* (Therapsida: Anomodontia) from the Permian Usili Formation. PeerJ 7:e7420. DOI 10.7717/peerj.7420

Kammerer, C. F., Angielczyk, K. D. (2009). A proposed higher taxonomy of anomodont therapsids. Zootaxa 2018:1-24

Kammerer, C. F., Angielczyk, K. D., Fröbisch, J. (2015a). Redescription of *Digalodon rubidgei*, an emydopoid dicyndont (Therapsida, Anomodontia) from the Late Permian of South Africa. Foss. Rec. 18:43-55.

Kammerer, C. F., Angielczyk, K. D., Fröbisch, J. (2011). A comprehensive taxonomic revision of *Dicynodon* (Therapsida, Anomodontia) and its implications for dicynodont phylogeny, biogeography, and biostratography. J. Vert. Paleontol. 31:1-158.

Kammerer, C. F., Bandyopadhyay, S., Ray, S. (2016). A new taxon of cistecephalid dicynodont from the Upper Permian Kundaram Formation of India. Palaeontol. Assoc. 1-16. doi: 10.1002/spp2.1055.

Kammerer, C. F., Fröbisch, J., Angielczyk, K. D. (2013). On the validity and phylogenetic position of *Eubrachiosaurus browni*, a kannemeyeriiform dicynodont (Anomodontia) from Triassic North America. PlosOne 8: e64203. doi:10.1371/journal.pone.0064203

Kammerer, C. F., Smith, R. M. H., Day, M. O., Rubidge, B. S. (2015). New information on the morophology and stratigraphic range of the Mid-Permian gorgonopsian *Euriphostoma microdon* Broom, 1911. Palaentol. 1-21

Kammerer, C. F., Smith, R. M. H. (2017). An early geikiid dicynodont from the *Tropidostoma* Assemblege Zone (late Permian) of South Africa. PeerJ5:e2913

Kammerer, C. F., Viglietti, P. A., Hancox, P. J., Butler, R. J., Choiniere, J. N. (2019). A new kannemeyeriiform dicynodont (*Ufudocyclops mukanelai*, gen. et. Sp. Nov.) from Subzone C of the *Cynognathus* Assemblage Zone, Triassic of South Africa, with implications for biostratigraphy correlation with other African Triassic Faunas. J. Vert. Paleontol. DOI: 10.1080/02724634.2019.1596921

Kammerer, C. F., Ordoñez, M. A. (2021). Dicynodonts (Therapsida: Anomodontia) of South America. J. S. Am. Earth Sci. https://doi.org/10.1016/j.jsames.2021.103171

Kearney, M., Maisano, J. A., Rowe, T. (2005). Cranial anatomy of the extinct amphisbaenian *Rhineura hatcherii* (Squamata, Amphisbaenia) based on high-resolution X-ray computed tomography. J. Morphol. 264:1-33

Kemp, T. S. (1969). On the functional morphology of the gorgonopsid skull. Philos. Trans. R. Soc. Lond. Biol. Sci. 256:1-83.

Keyser, A. W. (1965). On the morphology of the Anomodont genus *Cistecephalus* Owen 1876. University of Pretoria.

Keyser, A. W. (1974). Evolutionary trends in Triassic Dicynodontia (Reptilia Therapsida). Palaeontol. afr. 17:57-68.

King, G. M. (1988). Anomodontia. Encycl. Paleoherpetology, 17C: I – 174

King, G. M., Cluver, M. A. (1991). The aquatic *Lystrosaurus*: an alternative lifestyle. Hist. Biol. S. Afr. Mus. 4:323-341.

Kinlaw, A. E. (2006). Burrows of semi-fossorial vertebrates in upland communities of Central Florida: their architecture, dispersion and ecological consequences. Doctor Dissertation. University of Florida

Kitching, J.W. (1968). On the *Lystrosaurus* Zone and its fauna with special reference to some immature Lystrosauridae. Palaeontol. afr. 11:61–76

Kleinteich, T., Maddin, H. C., Herzen, J., Beckmann, F., Summers, A. P. (2012). Is solid always best? Cranial performance in solid and fenestrated caecilian skulls. J. Exp. Biol. 215, 833-844. doi:10.1242/jeb.065979

Kundrát, M., Janáček, J. (2007). Cranial pneumatization and auditory perceptions of the oviraptorid dinosaur *Conchoraptor gracilis* (Theropoda, Maniraptora) from the Late Cretaceous of Mongolia. Naturwissenschaften. 94:769-778. DOI 10.1007/s00114-007-0258-7

Laaß, M. (2014). Bone-conducting hearing and seismic sensitivity of the Late Permian anomodont *Kawingasaurus fossils*. J. Morphol. 276:121-143.

Laaß, M. (2015). Virtual reconstruction and description of the cranial endocast of *Pristerodon mackayi* (Therapsida, Anomodontia). J. Morphol. 276:1089-1099.

Laaß, M., Schillinger, B. (2015). Reconstructing the auditory apparatus of therapsids by means of neutron tomography. Phys. Procedia 69:628 – 635

Laaß, M., Kaestner, A. (2017). Evidence for convergent evolution of a neocortex-like structure in a late Permian therapsid. J. Morphol. 1-25. DOI: 10.1002/jmor.20712

Laaß, M., Schillinger, B., Kaestner, A. (2017). What did the "Unossified Zone" of the Non-Mammalian Therapsid Braincase House?. J. Morphol. 278(8):1020-1032.

Leigh, J. H., Wimbush, D. J., Wood, D. H., Holgate, M. D., Slee, A. V., Stanger, M. G. et al. (1987). Effects of Rabbit Grazing and Fire on a Sub-Alpine Environment. I. Herbaceous and Shrubby Vegetation. Aust. J. Bot. 35(4):433-64

Liu, J. (2021). The tetrapod fauna of the upper Permian Naobaogou Formation of China: 6. *Turfanodon jiufengensis* sp. Nov. (Dicynodontia). PeerJ 9:e10854. DOI 10.7717/peerj.10854

Long, C. A. (1972). Taxonomic revision of the North America Badgar, *Taxidea taxus*. Am. Soc. Mammal. 53(4):725-759

Lyckegaard A., Johnson, G., Tafforeau, P. (2011). Correction of ring artifacts in X-ray tomographic images. Int. J. Tomo. Stat. 18, 1-9.

Macungo, Z. A., Loide, I., Zunguza, S., Nhamutole, N., Maharaj, I. E. M., Mugabe, J. et al. (2020). *Endothiodon* (Therapsida, Anomodontia) specimens from the middle/late permian of

the Metangula Graben (Niassa Province, Mozambique) increase complexity to the taxonomy of the genus. J. Afr. Earth Sci. 163. https://doi.org/10.1016/j.jafrearsci.2019.103647

Maddin, H. C., Olori, J. C., Anderson, J. S. (2011). A redescription of *Corrolla craddocki* (Lepospondyli: Brachystelechidae) based on high-resolution CT, and the impacts of miniaturization and fossoriality on morphology. J. Morphol. 272:722-743

Maddin, H. C., Sherratt, E. (2014). Influence of fossoriality on inner ear morphology: insights from caecilian amphibians. J. Anat. 255:83-93

Maisch, M. W., Gebauer, E., V., I. (2005). Reappraisal of *Geikia locusticeps* (Therapsida: Dicynodontia) from the Upper Permian of Tanzania. Palaentol. 48 (2): 309-324

Martin, L. D., Bennett, D. K. (1977). The burrows of the Miocene beaver *Palaeocastor*, Western Nebraska, U.S.A. Palaeogeogr. Palaeoclimatol. Palaentol. 22:173-193

Mason, M. J. (2001). Middle ear structures in fossorial mammals: a comparison with non-fossorial species. J. Zool. 255:467-486.

Mason, M. J. (2003). Morphology of the middle ear of golden moles (Chrysochloridae). J. Zool., Lond. 260:391-403

Mason, M. J. (2006). Evolution of the middle apparatus in Talpid Moles. J. Morphol. 267:678-695.

Mecozzi, B., Coppola, D., Lurino, D. A., Sardella, R., Marinis, A. M. (2019). The Late Pleistocene European badger *Meles meles* from Grotta Laceduzza (Brindisi, Apulia, Southern Italy): the analysis of the morphological and biometric variability. Sci. Nat. 106(13). https://doi.org/10.1007/s00114-019-1604-2

Mirone, A., Brun, E., Gouillart, E., Tafforeau, P., Kieffer, J. (2014). The PyHST2 hybrid distributed code for high speed tomographic reconstruction with iterative reconstruction and a priori knowledge capabilities. *Nuclear Instruments and Methods in Physics Research Section B: Beam Interactions with Materials and Atoms.* 324:41-48.

Modesto, S., Rubidge, B., Visser, I., Welman, J. (2003). A new basal Dicynodont from the Upper Permian of South Africa. Palaeontol. 46:211-223.

Modesto S. P., Botha-Brink, J. (2010). A burrow cast with *Lystrosaurus* skeletal remains from the Lower Triassic of South Africa. Palaios 25:274–281

Morato, L. (2006). *Dinodontosaurus* (Synapsida, Dicynodontia): reconstituições morfológicas e aspectos biomecânicos. Master's dissertation. Universidade Federal do Rio Grande do Sul.

Müller, J., Hipsley, C. A. Maisano, J. A. (2016). Skull osteology of the Eocene amphisbaenian *Spathorhynchus fossorium* (Reptilia, Squamata) suggests convergent evolution and reversals of fossorial adaptations in worm lizards. J. Anat. doi: 10.1111/joa.12513

Müller, J., Hipsley, C. A., Head, J. J., Kardjilov, N., Hilger, A., Wuttke, M. et al. (2011). Eocene lizard from Germany reveals amphisbaenian origins. Nat. 473. doi:10.1038/nature09919

Nasterlack, T., Canoville, A., Chinsamy, A. (2012). New insights into the biology of the Permian genus *Cistecephalus* (Therapsida, Dicynodontia). J. Vert. Palentol. 32:6, 1396-1410.

Navas, C. A., Antoniazzi, M. M., Carvalho, J. E. (2004). Morphological and physiological specialization for digging in amphisbaenians, an ancient lineage of fossorial vertebrates. J. Exp. Biol. 207, 2433-2441. doi:10.1242/jeb.01041

Nevo, E. (1979). Adaptive convergence and divergence of subterranean mammals. Ann. Rev. Ecol. Syst. 10:269-308.

Oksche, A. (1965). Survey of the development and comparative morphology of the pineal organ. Prog. Brain Res. 10:3-28

Olroyd, A. L. Sidor, C. A., Angielczyk, K. D. (2018). New materials of the enigmatic dicynodont *Abajudon kaayai* (Therapsida, Anomodontia) from the lower Madumabisa Mudstone Formation, middle Permian of Zambia. J. Vert. Paleontol. DOI: 10.1080/02724634.2017.1403442

Olson, E. C. (1938). The occipital, otic, basicranial and pterygoid regions of the Gorgonopsia. J. Morphol. 62(2):141-175

Olson, E. C. (1944). The origin of mammals based upon the cranial morphology of the therapsid suborders. Special Papers—Geol. Soc. Am. 55:1 DOI 10.1130/GSAB-55-1.

Owen, R. (1859) On some reptilian remains from South Africa. Edinb. Philos. J. 10, 289–291

Owen, R., (1876). Descriptive and Illustrated Catalogue of the Fossil Reptilia of South Africa in the Collection of the British Museum. Taylor and Francis, London

Paganin, D., Mayo, S., Gureyev, T. E., Miller, P. R., Wilkins, S. W. (2002). Simultaneous phase and amplitude extraction from a single defocused image of a homogeneous object. J. Microsc. 206:33-40.

Pardo, J. D., Szostakiwskyj, M., Anderson, J. S. (2015). Cranial morphology of the Brachystelechid 'Microsaur' *Quasicaecilia texana* Carroll provides new insights into the diversity and evolution of braincase morphology in recumbirostran 'Microsaur'. PLoS ONE 10(6): e0130359. doi:10.1371/journal.pone.0130359

Quay, W. B. (1965). Histological structure and cytology of the pineal organ in birds and mammals. Prog. Brain Res. 10:49-84.

Quay, W. B. (1981). Pineal atrophy and other neuroendocrine and circumventricular features of the naked mole-rat, *Heterocephalus glaber* (Rüppell), a fossorial, equatorial rodent. J. Neural Transm. 52:107-115

Quintana, J., Köhler, M., Moyà-Solà, S. (2011). *Nuralagus rex*, gen. et sp. nov., an endemic insular giant rabbit from the Neogene of Minorca (Balearic Islands, Spain). J. Vert. Paleontol. 31(2):231-240. http://dx.doi.org/10.1080/02724634.2011.550367

Ralph, C. L. (1975). The pineal gland and geographical distribution of animals. Int. J. Biometeorol. 19(4):289-303.

Ray, S. (2001). Small Permian dicynodonts from India. Palaeontol. Soc. Jpn. 5,177-191.

Ray, S., Chinsamy, A. (2003). Functional aspects of the postcranial anatomy of the Permian dicynodont *Diictodon* and their ecological implications. Palaeontol. 46(1):151-183

Ray, S., Chinsamy, A., Bandyopadhyay, S. (2005). *Lystrosaurus murrayi* (Therapsida, Dicynodontia): bone histology, growth and lifestyle adaptations. Palaeontol. 48:1169-1185.

Renaut, A. J. (2000). A re-evaluation of the cranial morphology and taxonomy of the Triassic dicynodont genus *Kannemeyeria*. University of the Witwatersrand

Renaut, A. J., Hancox, P. J. (2001). Cranial description and taxonomic re-evaluation of *Kannemeyeria argentinensis* (Therapsida: Dicynodontia). Palaeont. afr. 37:81-91

Rodrigues, H. G., Šumbera, R., Hautier, L. (2016). Life in burrows channelled the Morphological evolution of the skull in rodents: the case of African mole-rats (Bathyergidae, Rodentia). J. Mammal Evol. 23, 175-189. DOI 10.1007/s10914-015-9305-x

Rose, J. A., Sandefur, M. Huskey, S., Demler, J. L., Butcher, M. T. (2013). Muscle architecture and out-force potential of the thoracic limb in the Eastern mole (*Scalopus aquaticus*). J. Morphol. 00:00-00. DOI 10.1002/jmor.20178

Rose, K. D., Emry, R. J. (1983). Extraordinary fossorial adaptations in the Oligocene Palaeanodonts *Epoicotherium* and *Xenocranium* (Mammalia). J. Morphol.175:33-56

Rubidge, B. S., Sidor, C. A. (2001). Evolutionary patterns among Permo-Triassic therapsids. Annu. Rev. Ecol. Syst. 32:449-80

Sansalone, G., Castiglione, S., Raia, P., Archer, M., Dickson, B., Hand, S. et al. (2020). Decoupling functional and morphological convergence, the study case of fossorial Mammalia. Front. Earth. Sci. 8:112. doi: 10.3389/feart.2020.00112

Sereno, P. C., Xijin, Z., Lin, T. (2009). A new psittacosaur from inner Mongolia and the parrot-like structure and function of the psittacosaur skull. Proc. R. Soc. B. 277:199-209. doi: 10.1098/rspb.2009.0691

Sherratt, E., Gower, D. J. (2014). Evolution of cranial shape in caecilians (Amphibia: Gymnophiona). Evol. Biol. DOI 10.1007/s11692-014-9287-2

Shimer, H. W. (1903). Adaptations to aquatic, arboreal, fossorial and cursorial habitats in mammals. Am. Nat. 37:444

Sigogneau-Russell D. (1989). Theriodontia I. In: Handbuch der Paläoherpetologie. Stuttgart: Gustav Fischer Verlag.

Smith, R. M. H. (1987). Helical burrow casts of Therapsid origin from the Beaufort group (Permian) of South Africa. Palaeogeogr. Palaeoclimatol. Palaeontol. 60:155-170

Smith, R. M. H., Angielczyk, K. D., Benoit, J., Fernandez, V. (2021). Neonate aggregation in the Permian dicynodont *Diictodon* (Therapsida, Anomodontia): evidence for a reproductive function for burrows? Palaeogeogr. Palaeoclimat. Palaeoecol. https://doi.org/10.1016/j.palaeo.2021.110311

Snively, E., Russell, A. P. (2007). Functional morphology of neck musculature in the Tyrannosauridae (Dinosauria, Theropoda) as determined via a hierarchical inferential approach. Zool. J. Linn. Soc. 151:175-808

Sullivan, C. (2000). Cranial anatomy of the Late Permian dicynodont *Diictodon*, and its bearing on aspects of the taxonomy, palaeobiology and phylogenetic relationships of the genus. Master's thesis, University of Toronto

Sullivan, C., Reisz, R. R. (2005). Cranial anatomy and taxonomy of the Late Permian dicynodont *Diictodon*. BioOne. 74:45-75. DOI: http://dx.doi.org/10.2992/0097-4463(2005)74[45:CAATOT]2.0.CO;2

Sullivan, C., Reisz, R. R., Smith, R. M. H. (2002). The Permian mammal-like herbivore *Diictodon*, the oldest known example of sexually dimorphic armament. Proc. R. Soc. Lond. 270:173-178. DOI 10.1098/rspb.2002.2189

Surkov, M. V., Benton, M. J. (2004). The basicranium of the dicynodonts (Synapsida) and its use in phylogenetic analysis. Palaeontol. 47(3):619-638

Surkov, M. V., Benton, M. J. (2008). Head kinematics and feeding adaptations of the Permian and Triassic dicynodonts. J. Vertebr. Paleontol. 28:1120-1129. DOI: 10.1671/0272-4634-28.4.1120

Strahan, R. (1995). The Mammals of Australia. Reed. Sydney.

Tedford, R. H. (2002). The basicranium of the giant Wombat *Phascolonus gigas* Owen (Vombatidae: Marsupialia) and its significance in phylogeny. Smithson. Contrib. Palaeobiol. 93:39-47

Tsuihiji, T. (2005). Homologies of the Transversospinalis muscles in the anterior presacral region of Sauria (Crown Diapsida). J. Morphol. 263:151-178

Tsuihiji, T. (2007). Homologies of the longissimus, iliocostalis, and hypaxial muscles in the anterior presacral region of extant Diapsida. J. Morphol. 268:986-1020

Van Staden S. L. (2014). The thoracic limb of the suricate (*Suricata suricatta*): osteology, radiologic anatomy, and functional morphologic changes. J. Zoo. Wildlife Med 45:476–486

Van Hoepen, E. C. N. (1934). Oor die indeling van die Dicynodontidae na aanleiding van nuwe vorme. Palaeontol. Navors. Nas. Mus. 2:67-101

Wallace, R. V. S. (2018). A new close mammal relative and the origin and evolution of the mammalian central nervous system. Master's dissertation, Univ. Texas

Walker, M. M., Louys, J., Herries, A. I. R., Price, G. J., Miszkiewicz, J. J. (2020). Humerus midshaft histology in a modern and fossil wombat. Aust. Mamm. https://doi.org/10.1071/AM20005

Werneburg, I. (2019). Morphofunctional categories and ontogenetic origin of temporal skull openings in Amniotes. Front. Earth Sci. 7:13. doi: 10.3389/feart.2019.00013

Whidden, H. P. (2000). Comparative myology of moles and the phylogeny of the Talpidae (Mammalia, Lipotyphla). Am. Mus Novit. 3294

White, A. M., Cameron, E. Z. (2008). Communal nesting is unrelated to burrow availability in the common warthog. Anim. Behav. xxx, 1-8

Witmer, L. M. (1990). The craniofacial air sac system of Mesozoic birds (Aves). Zool. J. Linn. Soc. 100:327-378

Woolnough, A. P., Steele, V. R. (2001). The palaeoecology of the Vombatidae: did giant wombats burrow?. Mamm. Rev. 31(1):33-45.

CHAPTER VI – APPENDICES

APPENDIX A

Notes on coding and character list for phylogenetic analysis of Kammerer and Ordoñez (2021).

Coding changes from previous (Kammerer, 2019) version of data matrix

Continuous characters

Rastodon procurvidens

1. 0.197 (was 0.221)

3. 0.199 (was 0.209)

4. 0.742 (was 0.444)

5. 0.558 (was 0.570)

6. 0.298 (was 0.258)

8. 0.122 (was 0.128)

9. 6.600 (was 6.300)

13. 0.798 (was 0.907)

15. 0.623 (was 0.824)

16. 0.667 (was 0.786)

Discrete state characters

Endothiodon tolani

55. 2 (was 1)

Rastodon procurvidens

16. 1 (was 0)

23. 1 (was ?)

28. 1 (was 0)

30. 1 (was 0)

49. 0 (was 1)

55. 1 (was 0)

71. 1 (was ?)

108. 1 (was 0)

114. 2 (was 1)

121. 4 (was 2)

Daqingshanodon limbus

55. 3 (was 0)

Keyseria benjamini

55. 1 (was 0)

Shansiodon

155. 0 (was 1)

Kannemeyeria lophorhinus

26. 1 (was 0)

29. 2 (was 1)

35. 1 (was 2)

42. 1 (was 0)

138. 1 (was 0)

Kannemeyeria simocephalus

26. 1 (was 0)

35. 1 (was 2)

39. 1 (was 0)

Rechnisaurus cristarhynchus

29. 2 (was ?)

Shaanbeikannemeyeria

29. 2 (was 1)

Sinokannemeyeria

29. 2 (was 1)

Uralokannemeyeria vjuschkovi

29. 2 (was ?)

Wadiasaurus indicus

29. 2 (was ?)

Jachaleria candelariensis

83. 1 (was ?)

Continuous characters

1. Length of preorbital region of skull relative to basal length of skull.
2. Relative length of premaxillary secondary palate.
3. Minimum width of interorbital skull roof relative to basal length of skull.
4. Relative width of temporal bar at level of postorbital bar versus the relative width at the junction of the intertemporal bar with the occipital plate.
5. Length of temporal fenestra relative to basal length of skull.
6. Relative position of pineal foramen, measured as the ratio of dorsal skull length posterior to the foramen versus dorsal skull length anterior to the foramen.
7. Height of anterior pterygoid keel in lateral view relative height of non-keel ramus.
8. Width of median pterygoid plate relative to basal skull length.
9. Angle formed by the posterior pterygoid rami.
10. Length of interpterygoid vacuity relative to basal length of skull.

11. Relative area of the internal nares.
12. Angle between ascending and zygomatic processes of the squamosal.
13. Angulation of the occiput relative to the palate, expressed the ratio of dorsal and basal lengths of the skull.
14. Ratio of height to length of mandibular fenestra in lateral view.
15. Ratio of height of dentary ramus to height of dentary symphysis.
16. Ratio of maximum height of postdentary bones (excluding reflected lamina of angular) to the height of the dentary ramus.
17. Ratio of minimum width of the scapula to maximum width of dorsal end of scapula.
18. Length of the deltopectoral crest relative to total length of the humerus.
19. Maximum width of the distal end of the radius relative to the maximum length of the radius.
20. Ratio of posterior iliac process length to acetabulum diameter.
21. Ratio of anterior iliac process Length to acetabulum diameter.
22. Length of trochanteric crest on femur relative to length of femur.
23. Breadth of scapula measured as ratio of maximal proximal width of scapula versus length of scapula (measured from dorsal edge of glenoid to proximal tip).

Discrete-state characters

1. Premaxillae unfused (0) or fused (1).
2. Paired anterior ridges on palatal surface of premaxilla absent (0), present and converge posteriorly (1), or present and do not converge (2).
3. Lateral anterior palatal ridges absent (0) or present (1).
4. Rounded depression on anterior palatal surface of premaxilla: absent (0); present (1).
5. Posterior median ridge on palatal surface of premaxilla absent (0), present with a

flattened, expanded anterior area (1), or present without a flattened, expanded anterior area (2).

6. Palatal surface of premaxilla with well-defined depressions with curved sides lateral to median ridge (if present) (0), with distinct accessory ridges lateral to medial ridge (1), or relatively flat with poorly defined or no depressions present (2).
7. Palatal surface of premaxilla with antero-posterior vascular groove lateral to median ridge (if present) absent (0); present (1).
8. Location of premaxillary teeth lateral (0), medial (1) or absent (2).
9. Posterior exposure of the premaxilla on the palate: absent (0), present (1).
10. Posterior process of the premaxilla with a non-bifurcated posterior tip (0) or with a bifurcated posterior tip (1).
11. Palatine shelf ventral to internal naris: absent (0), present (1).
12. Anterior tip of snout rounded (0), squared off (1), or with a deep central invagination, giving the snout a “hare-lip” appearance in anterior view (2).
13. Marked anterior expansion of preorbital region absent (0) or present (1).
14. Snout roughly parallel to long axis of skull (0) or strongly angled ventrally (1).
15. Height of canine-bearing portion of maxilla: relatively short (0); extremely deep, with long caniniform process, but with equally long premaxilla resulting in an overall tall snout (1); extremely long caniniform process offset from rest of snout (2).
16. Snout open to back of the skull (0) or anterior margin of orbit extended posteromedially to partly close off the snout from the rest of the skull (1).
17. Septomaxilla posterodorsal spur present and widely separates nasal and maxilla (0), spur present but does not separate maxilla and nasal (i.e., nasal-maxilla suture present and well defined in this region) (1), septomaxilla spur absent (2).
18. Notch on dorsal edge of narial opening absent (0) or present (1).

19. Postnarial excavation absent (0), present, relatively small, and rounded posteriorly (1), or present, very large, and elongate (2).
20. Maxillary alveolar region short, occupying less than 53% of the ventral length of the bone (0) or tooth bearing region long, occupying 72% or more of the ventral length of the bone (1).
21. Palatal surface of premaxilla exposed in lateral view (1) or not exposed in lateral view (0).
22. Maxillary canine present as large member of tooth series (0), absent (1), or present as tusk (2).
23. Maxillary non-caniniform teeth located near lateral margin of maxilla (0), located more medially, (1), or absent (2).
24. Shelf-like area lateral to the maxillary non-caniniform teeth absent (0) or present (1).
25. Fine serrations on maxillary teeth present (0), serrations absent (1), or coarse serrations present (2).
26. Sutural contact of maxilla and prefrontal present (0) or absent (1).
27. Caniniform process absent (0) or present (1).
28. Caniniform depression: has the form of an embayment bounded by a ridge medially of palatal rim anterior to caniniform process or tusk (1), has the form of a notch in palatal rim anterior to caninfiorm process (2), or absent (0).
29. Distinct lateral caniniform buttress absent (0), present (1), or present with posteroventral furrow (2).
30. Keel-like extension of the palatal rim posterior to the caniniform process absent (0) or present (1).
31. Postcaniniform crest absent (0) or present (1).
32. Ventral edge of the caniniform process or dorsal edge of the erupted portion of the canine

tusk anterior (0) to, or at the same level to slightly posterior to (1) the anterior orbital margin.

33. Nasals with a long median suture that separates the premaxilla from the frontals (0) or with a short median suture and frontals and premaxilla in close proximity (1) or without a median suture (2)
34. Nasal bosses absent (0), present as a median swelling with a continuous posterior margin (1), present as paired swellings near the dorsal or posterodorsal margin of external nares (2), present as paired swellings that meet in the midline to form a swollen anterodorsal surface on the snout (3).
35. Naso-frontal suture relatively straight, interdigitated, or gently bowed (0), with a distinct anterior process (1), or with a distinct posterior process (2).
36. Transverse crest approximately at level of naso-frontal suture absent (0); present and straightly transverse to curved with posterior convexity (1); present and strongly curved with posterior concavity (2).
37. Lacrimal does not contact septomaxilla (0) or does contact septomaxilla (1).
38. Prefrontal bosses absent (0), present but separate from nasals (1), or present and confluent with nasal bosses (2).
39. Raised, sometimes rugose, circumorbital rim absent (0) or present (1).
40. Frontal contribution to the dorsal rim of the orbit: broad, frontal forms a major part of the orbital rim (0); thin or absent, if present a thin frontal process extends laterally between the prefrontal and postorbital to reach the orbital margin (1).
41. Postfrontal bone present on dorsal surface of skull (0) or absent (1).
42. Postorbital bar without (0) or with thickenings and rugosities (1).
43. Mediolateral flattening and anteroposterior expansion of postorbital bar for most or all of its length absent (0) or present (1).

44. Temporal portion of skull roof relatively straight, without a strong break in slope (0), or temporal portion of skull roof angled dorsally with a strong break in slope near its anterior end (1).
45. Preparietal bone absent (0), present and flush with skull roof (1), present and depressed (2).
46. Lateral ridges bounding preparietal absent (0) or present (1).
47. Parietals' contribution to skull table transversely as broad as long (0), longer anteroposteriorly than broad (1), or shorter anteroposteriorly than broad (2).
48. Parietal posterolateral process slender and elongate (0), or short (1).
49. Parietals well exposed on the skull roof and relatively flat (0), parietals exposed in midline groove or channel (1), dorsal parietal exposure narrow and crest-like (2).
50. Postparietal bulges outwards as ovoid swellings at posterior end of sagittal crest: no (0); yes (1).
51. Orientation of the temporal portion of the postorbital: relatively flat, so that most of the exterior surface of the bone faces dorsally (0), close to vertical, so that most of the exterior surface of the bone faces laterally (1), or bi-planar, with approximately equally-sized dorsal and lateral surfaces that are close to perpendicular (2).
52. Postorbitals extend the entire length of intertemporal bar (0) or do not extend the entire length of intertemporal bar, such that the posterior portion of the bar is formed only by the parietals (1).
53. Fossa on the ventral surface of the intertemporal bar formed by the postorbital and parietal large (0), reduced (1), or absent (2).
54. Pineal foramen present (0); absent (1).
55. Circumpineal ornamentation: chimney-like boss (0); no boss, foramen flush with skull surface (1); dome- or collar-like boss, rugosity present (2); boss present with incomplete

border, more strongly developed on lateral edges of pineal foramen (3).

56. Orientation of pineal foramen: exits perpendicular to long axis of intertemporal bar (0); angled anterior to perpendicular relative to long axis of intertemporal bar (1).
57. Interparietal does not contribute to intertemporal skull roof (0), makes a small contribution to intertemporal skull roof (1), or makes a large contribution to intertemporal skull roof (2).
58. Squamosal without (0) or with (1) a small or (2) large lateral fossa for the origin of the lateral branch of the M. adductor mandibulae externus. ORDERED.
59. Distinct dorsolateral notch in squamosal below zygomatic arch in posterior view absent (0) or present (1).
60. Squamosal posteroventral process short such that there is relatively extensive exposure of quadrate and quadratojugal in posterior view and the quadrate foramen (if present) is visible in posterior view) (0) or long such that nearly all of the quadrate and quadratojugal are covered by the squamosal in posterior view and the quadrate foramen (if present) is not visible in posterior view (1).
61. Zygomatic portion of the squamosal without folded edge (0), out-turned to downturned (1) (*Oudenodon*, *Odontocylops*, etc.), or folded-over (2) (*Pelanomodon*, *Geikia*). ORDERED.
62. Dorsoventral expansion of squamosal posterior to postorbital bar: (0) absent (1) present.
63. Zygomatic process of squamosal parasagittally deep (0), narrow and rod-like (1), or transversely expanded (2).
64. Oblique ridge on lateral side of zygomatic arch giving triangular cross-section and overhanging a weak groove present (1) or absent (0).
65. Squamosal zygomatic process narrowly based and in line with occipital condyle (0) or widely based and flares posteriorly beyond occipital condyle (1).

66. Sutural contact of squamosal and maxilla absent (0) or present (1).
67. Squamosal separated by tabular bone from supraoccipital (0) or contacts supraoccipital (1).
68. Suborbital boss on jugal absent (0) or present (1).
69. Quadratojugal narrow and rod-like (0) or plate-like distally (1).
70. Quadrate with a dorsal lobe that has a convex, rounded anterior edge that rests against quadrate ramus of pterygoid (0) or with a dorsal lobe that is developed into a distinct process that extends anteriorly along the quadrate ramus of the pterygoid and is triangular to sub-triangular in shape (1).
71. Vomers unfused (0) or fused (1).
72. Mid-ventral plate of vomers with an expanded, oval-shaped area posterior to junction with premaxilla (0) or without a notable expanded area posterior to junction with premaxilla (1).
73. Mid-ventral plate of vomers relatively wide in ventral view (0), more narrow and blade-like in ventral view (1).
74. Trough on mid-ventral plate of vomers (i.e., ventral surface concave ventrally with raised edges): present (0) or absent (1).
75. Palatine dentition present (0) or absent (1).
76. Bone texture of the palatine: primarily smooth, without evidence of keratinized covering (0); relatively smooth but with fine pitting and texturing suggestive of a keratinized covering (1); rugose and textured (2).
77. Position of palatine: raised, central palatine boss present (0); entire palatine flush with surrounding palatal elements (1); raised posterior section with anterior section that is flush with the secondary palate (2).
78. Paired fossae on palatine surface absent (0); present (1).

79. Palatine widest at its approximate midpoint of length (0), widens posteriorly (1), width relatively constant for entire length (2), widens anteriorly forming a palatine pad (3). ORDERED.
80. Foramen on the palatal surface of the palatine absent (0) or present (1).
81. Lateral palatal foramen absent (0), present at level of the anterior, expanded palatal exposure of the palatines (1), present posterior and dorsal to the level of the anterior, expanded palatal exposure of the palatines (2).
82. Sutural contact of palatine and premaxilla absent (0) or present (1).
83. Labial fossa surrounded by maxilla, jugal, and palatine absent (0) or present (1).
84. Ectopterygoid extends further posteriorly than palatine in palatal aspect (0), or does not extend further posteriorly than palatine in palatal aspect (1), or absent (2).
85. Ectopterygoid dentition absent (0) or present (1).
86. Pterygoids contact anteriorly (0) or separated by vomers (1).
87. Transverse flange of pterygoid projects laterally, free of posterior ramus (0), projects laterally, bound by posterior ramus (1) does not project laterally (2).
88. Anterior pterygoid keel: absent (0); present (1).
89. Anterior pterygoid keel extending for most of the length of anterior ramus of pterygoid (0); anterior pterygoid keel restricted to the anterior tip of the anteritor ramus of the pterygoid (1).
90. Contact of pterygoid and maxilla absent (0) or present (1).
91. Converging ventral ridges on posterior portion of anterior pterygoid rami absent (0) or present (1).
92. Ventral surface of the median pterygoid plate depressed (0), smooth and flat (1), with a thin median ridge (2), with a wide, boss-like median ridge (3), or with a low rugose median swelling (4), or with a conical ventral projection (5), or with thin paried ridges

that are contiguous with the edges of the interpterygoid vacuity (6).

93. Pterygoid dentition present, conical (0); absent (1); present, bucco-lingually expanded.

94. Posterior edges of the interpterygoid vacuity located dorsal to the median pterygoid plate (0) or extended ventrally such that they are flush with the median pterygoid plate (1).

95. Development of the pila antotica as a rod-like process on the anterior edge of the periotic with a corresponding notch for the trigeminal never posterior to it (0), or pronounced pila antotica absent and trigeminal notch is a horizontal hollow in the anterior edge of the periotic (1).

96. Contact between periotic and parietal absent (0) or present (1).

97. Parasphenoid excluded from (0) or reaches (1) interpterygoid vacuity.

98. Basisphenoid contribution to the basisphenoid-basioccpital tubera slopes anterodorsally at a shallow angle, forming elongate ridges on the basicranium that are close to the same height as the tubera for most of their length (0), slopes anterodorsally at a steeper angle such that the parabasisphenoid conribution is still somewhat ridge-like but the portion of the ridge on the anterior surface of the tuber is more vertically-oriented (1), or is nearly vertical, forming very weak ridges if any (2).

99. Stapedial facet of basisphenoid-basioccipital tuber exposed laterally (0), exposed ventrolaterally (1), or exposed ventrolaterally and open distally (2).

100. Exposure of internal cartoid between mid-pterygoid plate and parasphenoid: directed laterally (0); directed medially (1).

101. Shape of basal tubera: bifurcating and posteriorly-directed(0); laterally directed anteroposteriorly elongate with relatively narrow edges (1); strongly rounded, such that anterior and posterior tips of tuber curve towards each other, nearly enclosing the stapedial facet; tuber inflated (2); elongate, nearly quadrangular, with tubera extremely close together (3).

102. Margin of fenestra ovalis formed predominantly by parabasisphenoid, with little or no contribution from basioccipital (0), formed by approximately equal portions of parabasisphenoid and basioccipital (1), or formed predominantly by basioccipital, with little or no contribution by parabasisphenoid (2).

103. Intertuberal ridge absent (0) or present (1).

104. Dorsal process on anterior end of epipterygoid footplate absent (0) or present (1).

105. Stapedial foramen present (0) or absent (1).

106. Dorsal process of the stapes present (0) or absent (1).

107. Tabular contacts opisthotic (0) or separated from opisthotic by squamosal (1).

108. Prootic bearing rectangular alar process that forms a plate raised above surface of temporal fenestra wall, in front of fossa: absent (0) present (1).

109. Exoccipital and basioccipital contributions to the occipital condyle distinct (0) or co-ossified into a single unit (1).

110. Occipital condyle round to subspherical in posterior view (0) or distinctly tri-radiate (1) in posterior view.

111. Circular central depression or fossa on the occipital condyle between the exoccipitals and basioccipital present (0) or absent (1).

112. Lateral edge of paroccipital process drawn into sharp posteriorly-directed process that is distinctly offset from the surface of the occipital plate: absent (0) present (1).

113. Floccular fossa present (0) or absent (1).

114. Mandibular fenestra absent (0), present (1), or present but occluded by a thin sheet of the dentary (2).

115. Jaw ramus straight in dorsal view, without strong lateral bends (0), or bends strongly laterally (1) posterior to symphysis.

116. Dentaries sutured (0) or fused (1) at symphysis.

117. Teeth present on dorsal surface of dentaries (0), medially displaced, sometimes on a swelling or shelf (1), or absent (2).

118. Fine serrations on dentary teeth present (0), serrations absent (1), or coarse serrations present (2).

119. Denticulated cingulum on dentary teeth absent (0) or present (1).

120. Anteriormost dentary tooth: not distinct from rest of tooth row (0); massively enlarged and incisiform (1).

121. Jaw symphysis terminates in dorsal platform bearing the incisors and canine elevated above level of posterior dentary ramus (0); Symphyseal region of lower jaw smoothly rounded and at same level as rest of dentary ramus in lateral view (1), with an upturned beak that is raised above the level of the dorsal surface of the jaw rami and has a scooped-out depression on its posterior surface (2), drawn into a sharp, spiky beak (3), or shovel-shaped beak with a rounded or squared-off edge and a weak depression on its posterior surface (4).

122. Curved ridge that follows the profile of the symphysis present on the edge between the anterior and lateral surfaces of the dentary absent (0) or present (1).

123. Boss present on ventral surface of anterior dentary ramus. absent (0) present (1).

124. Dentary table absent (0) or present (1).

125. Posterior dentary sulcus absent (0), present but does not extend past dentary teeth (if present) (1), present and extends past dentary teeth (if present), but is relatively wide and shallow (2), or present, extends past dentary teeth (if present) and is narrower and deeper (3).

126. Tall, dorsally-convex cutting blade on medial edge of dorsal surface of dentary absent (0) or present (1).

127. Lateral dentary shelf absent (0), present but relatively small (1), present and well

developed (2).

128. Anterodorsal edge of lateral dentary shelf relatively flat (0), with a groove (1), or developed into a rounded swelling (2).

129. Lateral dentary shelf relatively thick, with distinct dorsal and ventral surfaces above the mandibular fenestra (0) or a thin ventrolaterally-directed sheet that forms the dorsal margin of the mandibular fenestra (1).

130. Splenial symphysis unfused (0) or fused (1).

131. Spenial contribution to dentary symphysis: anterior process on splenial present in ventral view (0) or absent (1).

132. Exposed contribution of the angular to the symphysis: absent (0) present (1).

133. Coronoid bone present (0), or absent (1).

134. Angular with anterolateral trough for the posterior process of the dentary absent (0) or present (1).

135. Reflected lamina: (0) reflected lamina large, rounded, unornamented; (1) with perpendicular ridges; (2) with reticulate ridges; (3) triradiate, with distinct groove-ridge-groove morphology dorsoventrally arrayed along lamina; (4) small, tab-like (more elongate than rounded), unornamented (5); large, rounded, but with only a central groove bisecting the lamina.

136. Reflected lamina of angular closely approaches or touches articular (0) or widely separated from articular (1).

137. Prearticular with (0) or without (1) lateral exposure posteriorly.

138. Articular distinct (0) or at least partially fused to prearticular (1).

139. Surangular vertical lamina present and lateral to articular (0) or absent (1).

140. Jaw joint allows strictly orthal closure (0); allows parasagittal movement with joint surfaces of quadrate and articular approximately equal (1); allows parasagittal movement

with joint surfaces on articular large than that of quadrate (2). ORDERED.

141. Enlarged dentary caniniform present (0) or absent (1).

142. Number of sacral vertebrae three (0), four (1), five (2), or six or more (3).

143. Number of sternal bosses: 2 (0), 4(1).

144. Cleithrum absent (0) or present (1).

145. Anterior edge of scapula extended laterally to form a strong crest (1) or not (0).

146. Origin of triceps on posterior surface of scapula relatively low (0) or developed into a prominent posterior projection (1).

147. Acromion process: absent or very small (0) or present and well defined (1).

148. Procoracoid foramen or notch entirely contained within the procoracoid (0) or formed by contributions of the procoracoid and scapula in lateral view (1).

149. Procoracoid does not participate in formation of glenoid (0) or participates in formation of glenoid (1).

150. Proximal articular surface of humerus formed by a slightly convex area on proximal surface of the bone without much expansion onto the dorsal surface (0), somewhat expanded with some encroachment onto the dorsal surface (1), or strongly developed and set off from rest of humerus by a weak neck (2). ORDERED.

151. Insertion of M. subcoracoscapularis on humerus a rounded, rugose area on proximal end of humerus (0), short, pinna-like process (1); large elongate process (2). ORDERED.

152. Insertion of M. latissimus dorsi at rugose tuberosity on the posteroventral surface of humerus (0) or extended into a dorsoventrally flattened pinna-like process (1).

153. Anterior and distal edges of deltopectoral crest close to perpendicular (0) or very obtuse (1).

154. Ectepicondylar foramen on humerus present (0) or absent (1).

155. Radial and ulnar condyle continuous (0) or well ossified and separate (1) on ventral

surface of humerus.

156. Ulna with small olecranon process that does not extend far past the articular surface for the humerus (0), or with a large olecranon process that extends well past the articular surface for the humerus (1).

157. Distal carpal 5: present as a distinct element (0), not present as a distinct element (1).

158. Manual digit III, shape of second phalanx: short (disc-like) (0), absent (1).

159. Manual digit IV, phalangeal number: 5 (0), or 3 (1).

160. Dorsal edge of ilium: unnotched (0) or notched (1).

161. Pubic plate is significantly expanded anteroposteriorly, such that its length is comparable to that of ischium (0) or anteroposteriorly short, so that it is much shorter than ischium (1).

162. Pubic plate is significantly expanded ventrally such that it is nearly the same height as ischium (0) or reduced ventrally such that it is shorter than ischium (1).

163. Distinct cranial process on anterior end of pubis absent (0) or present (1).

164. Femoral head continuous with the dorsal margin of femur (0) or offset dorsally from dorsal margin (1).

165. Proximal articular surface of the femur present as a weak swelling that is mostly limited to the proximal surface of the bone (0) or present as a more rounded, hemispherical swelling that has some encroachment on the anterior surface of the femur (1).

166. Insertion of M. iliofemoralis present as a low rugosity on the dorsolateral portion of the femur (0), developed into a distinct crest that extends down part of the lateral surface of the femur (1) or a lateral crest that is split into a distinct first trochanter and third trochanter (2). ORDERED.

167. Pedal digit III, shape of second phalanx: short (disc-like) (0), absent (1).

168. Pedal digit IV, phalangeal number: 5 (0), 4 (1), or 3 (2).

169. Pedal digit IV, shape of second and third phalanges: long (0), short (1).

170. Pedal digit V, shape of second phalanx: short (0), absent (1).

171. Greatly enlarged vascular channels present (1) or absent (0).

172. Anterior face of dentary symphysis: unornamented (0), with median ridge (1).

173. Supinator process above ectepicondyle of humerus absent (0), present (1).

174. Morphology of supinator process: low, broadly separated from the shaft (0), tall and subvertical, with dorsal margin close to base of shaft (1), discrete, tab-like process occupying restricted portion of anterior face of distal humerus (2).

175. Angulation of subtemporal zygoma: horizontal to low-angle, such that dorsal margin of squamosal is ventral to skull roof in lateral view (0), steeply-angled, such that dorsal margin of squamosal is at the level of or dorsal to the skull roof in lateral view (1).

176. Median snout ridge: absent (0), restricted to premaxilla (1), present on premaxilla and nasal (2), present on premaxilla, nasal, and terminates in transversely-expanded boss on frontal (3). ORDERED.

177. Rostrum notch: absent (0), slightly embayed (1), strongly embayed (2).

178. Anteriorly-directed orbits: absent (0), present (1).

179. Straight zygoma: absent (0), present (1).

180. The paroccipital process is: convex and confluent with the lateral vertical process of the opisthotic in posterior view (0); flat with a lateral vertical buttress (1); concave with two laterally divergent crests (2).

181. Development of the small rod-like opisthotic ventromedial process: present (0); robust tuber-like knob (1); ventromedial process very reduced (2); ventromedial process absent (3).

182. The supraoccipital is dorsoventrally tall in occipital view (0); transversely wider (1).

183. The posterior surface of the supraoccipital medial lobe: is smooth or does not present a nuchal crest (0), is smoothly flat with lateral shallow vertical depression (1), or has a prominent vertical nuchal crest (2).

184. The pterygoid median plate bears a lateral lamina (0), or the lateral lamina is absent (1).

185. The pila antotica: is short and its base is robust and rounded (0), is narrow, long and rod-like (1), or is tall and anteroposteriorly expanded (2).

186. The anteromedial process of the pterygoid: is present (0), or is absent (1).

187. The tuberculum sellae: is present and forms crests (0); is absent (1).

188. The clinoid process: is short (0); or it is tall (1).

189. The dorsal component of the exoccipital and the exoccipital condyle: are fused to form an oblique buttress (0); or they are separated by a shallow trench (1).

190. The exoccipital dorsal component is short with minor contribution to the height of the foramen magnum (0); is tall, rectangular and covers half the foramen magnum height (1); or is tall, reniform and covers more than half the height of the foramen magnum (2).

APPENDIX B

EMYDOPOID BASICRANIAL CHARACTER EVOLUTION

EXTERNAL CHARACTERS

i) *Pristerodon* versus emydopoids

180 (New character) – The paroccipital process is: convex and confluent with the lateral vertical process of the opisthotic in posterior view (0); flat with a lateral vertical buttress (1); concave with two laterally divergent crests (2).

The paroccipital process is convex posteriorly and with a confluent lateral vertical process in basal forms such as *Pristerodon* (Figure 3.2D, 3.8C), but also *Niassodon*, *Eodicynodon*, *Brachyprosopus*, *Colobodectes*, *Endothiodon*, and *Diictodon* (Barry 1974; Sullivan 2000; Modesto et al. 2003; Angielczyk 2008; Angielczyk and Rubidge 2009; Castanhinha et al. 2013; Angielczyk et al. 2016; Macungo et al. 2020). However, the paroccipital process is flat posteriorly in *Myosaurus* specimen BP/1/2690, apart from the development of the lateral vertical process and the posterior subvertical buttress (Figure 3.16B). An extreme variation is observed in *Myosaurus* specimen BP/1/2701a which retains the plesiomorphic condition (Figure 3.16C). In *Digalodon*, the posterior surface of the opisthotic is also flat (Kammerer et al. 2015, Kammerer 2019). The kingoriid *Dicynodontoides* has a convex paroccipital process, but a bulging lateral vertical process (Cox 1959). *Compsodon* has the plesiomorphic condition, as it possesses the lateral vertical process that is not confluent with the paroccipital process (Angielczyk and Kammerer 2017). In the Malawian cistecephalid PK-16-1 and *Kawingasaurus*, the paroccipital process is concave. The paroccipital process bulges medially from where two sub-oblique crests develop laterally (opc, Figure 3.19H, 3.24G), which flank a depression between them (od, Figure 3.19H, 3.24G, Keyser 1965, Angielczyk et al. 2019). In summary, the posterior aspect of the opisthotic in basal dicynodonts is gently convex but

becomes flat and vertically taller with lateral vertical buttresses in basal emydopoids. The most extreme condition is observed in cistecephalids where the surface evolves to form crests separated by depressions.

181 (New character) – Development of the small rod-like opisthotic ventromedial process: present (0); robust tuber-like knob (1); ventromedial process very reduced (2); ventromedial process absent (3).

The opisthotic of *Pristerodon* develops a small vertical rod-like ventromedial process (Figure 3.2D, 3.8C), which borders the jugular foramen anteriorly and the fenestra ovalis posteriorly. This process is also present in the basal dicynodonts *Eodicynodon*, *Diictodon,* and *Brachyprosopus* (Barry 1974; Sullivan 2000; Sullivan and Reisz 2005; Angielczyk et al. 2016). In *Colobodectes*, *Endothiodon*, *Abajudon,* and *Niassodon* the ventromedial process is very reduced but it forms the floor of the jugular foramen (Modesto et al. 2003; Castanhinha et al. 2013; Olroyd et al. 2017; Macungo et al. 2020).

Myosaurus has a thick, robust tuber-like ventromedial process of the opisthotic (Figure 16) that develops as a somewhat separate entity of the main opisthotic body and limits the lateral expansion of the basioccipital tubera. This morphology is similar to *Compsodon* and *Digalodon*, where the process is separated from the opisthotic main body by a median sulcus (Kammerer et al. 2015a; Figure 3.1H, 3.2H, 3.4B in Angielczyk and Kammerer 2017). In *Thliptosaurus* (Kammerer 2019a), despite the occiput being weathered, the process seems thick as in *Myosaurus*. A small ventromedial projection of the opisthotic is further observed in *Emydops* and *Dicynodontoides* (Cox 1959; Fourie 1991), however, the severely damaged *Emydops oweni* (Fröbisch and Reisz 2008) prevents further analysis. The emydopoid *Kombuisia frerensis* lacks the opisthotic ventromedial process (Fröbisch 2006). The development of a robust opisthotic ventromedial process is observed in *Kembawacela* and

Cistecephaloides (Cluver 1974a; Angielczyk et al. 2019), but it is very reduced in the Malawian cistecephalid, *Sauroscaptor*, and *Cistecephalus* (plate II, in Keyser 1965; Kammerer et al. 2016). *Kawingasaurus* seems to lack the ventromedial process of the opisthotic as the basioccipital expands more laterally to form the floor of the jugular foramen (Figure 3.24G).

182 (New character) – The supraoccipital is dorsoventrally tall in occipital view (0); transversely wider (1).

The emydopoid supraoccipital morphology contrasts with that of the basal dicynodont *Pristerodon*, which is taller than wide in posterior view (Figure 3.2D, 3.6D). In *Diictodon*, the supraoccipital shows similar morphology to *Pristerodon*, as it also possesses a vertically elongated foramen magnum (Barry 1974; Sullivan and Reisz 2005, Ferreira-Cardoso et al. in press). *Colobodectes* and *Abajudon* have a less dorsoventrally elongated foramen magnum, being wider at the base, but tapering dorsally (Angielczyk and Rubidge 2009, Olroyd et al. 2018). *Colobodectes* and *Abajudon* have a supraoccipital that is, not significantly different from the condition in *Pristerodon*. *Brachyprosopus broomi* specimen FMNH UC 1561 has a tall supraoccipital, as in most other basal dicynodonts, but SAM-PK-K7607 seems to have a shorter supraoccipital, probably due to preservation artifact and compression of the specimen (Angielczyk et al. 2016). The endothiodont *Niassodon* also has an elongated foramen magnum, dorsoventrally tall supraoccipital, with yet well-developed lateral alae (Castanhinha et al. 2013). Despite *Niassodon* supraoccipital medial lobe being well-developed, the alae are the most prominent structures of the supraoccipital in posterior view, thus making the supraoccipital broader than tall. This is closer to the emydopoid condition.

The supraoccipital is the largest element of the occiput and its posterior aspect in emydopoid dicynodonts is broad but low. This condition of the supraoccipital is observed in *Myosaurus* (Figure 3.14B), including all basal emydopoid dicynodonts whose condition could

be properly assessed, namely *Emydops*, *Kombuisia*, *Digalodon*, *Compsodon* (Haughton 1917; Hammer and Cosgriff 1981; Fröbisch 2006; Fröbisch and Reisz 2008; Angielczyk and Kammerer 2017). Although *Emydops* (Fröbisch and Reisz 2008) seems to be devoid of medial lobe, we think that this interpretation is incorrect as it was probably only a result of fracturing. Along these lines, a transversely wider supraoccipital is observed in the cistecephalids *Cistecephalus*, *Cistecephaloides*, *Sauroscaptor*, *Kawingasaurus*, *Kembawacela*, and the Malawian cistecephalid PK-16-1 (Figure 3.19H, 3.23B; Keyser 1965; Cox 1972; Cluver 1974a; Kammerer et al. 2016; Angielczyk et al. 2019).

183 (New character) – The posterior surface of the supraoccipital medial lobe: is smooth or does not present a nuchal crest (0), is smoothly flat with lateral shallow vertical depression (1), or has a prominent vertical nuchal crest (2).

The absence of a nuchal crest in *Pristerodon* (Fig. 3.2D, 3.8D; Barry 1967; Cluver and King 1983) is shared by several other basal dicynodonts such as *Colobodectes*, *Brachyprosopus*, *Diictodon*, and *Niassodon* (Sullivan 2000; Modesto et al. 2003; Angielczyk 2008; Angielczyk and Rubidge 2009; Castanhinha et al. 2013; Angielczyk et al. 2016). In their description of *Pristerodon*, Barry (1967) and Cluver and King (1983) did not describe or illustrate any crest on the supraoccipital-interparietal region and we follow this interpretation.

The CT images of *Myosaurus* (Figure 3.14B) reveals a smoothly flat occipital surface of the supraoccipital, as it is excavated by very shallow vertical depressions on each side of the foramen magnum somewhat similar to *Emydops* (Fröbisch and Reisz 2008), thus raising the median surface of the supraoccipital. Cluver (1974a) described a crest descending from the interparietal to the supraoccipital in *Myosaurus* (see Figure 3 in Cluver 1974). *Kombuisia* follows the same morphology as *Myosaurus*. However, in *Kombuisia* specimen BP/1/430, the shallow excavations on the posterior surface of the supraoccipital are hard to determine as this

specimen was deformed by taphonomic distortion (Fröbisch 2007). Angielczyk and Kammerer et al. (2017) identified a distinct nuchal crest in the emydopoid *Compsodon*, but the suture between the interparietal and supraoccipital is hard to ascertain. In *Kawingasaurus* there is a prominent nuchal crest and lateral to it, there are two deep, large fossae in posterior view (Figure 3.23C). In other cistecephalids, the depressions are shallower. For instance, in *Kembawacela* and *Cistecephaloides* (Cluver 1974a; Angielczyk et al. 2019) the nuchal crest is not as prominent as in *Kawingasaurus*. There is a median ridge descending ventrally from the interparietal to overlap the supraoccipital in the serially sectioned *Cistecephalus* (Keyser 1965) that corresponds to the nuchal crest. So far, a prominent and distinctly divided nuchal crest is present in *Sauroscaptor* (Kammerer et al. 2016). The Malawian cistecephalid, on the other hand, has the dorsal-most edge of the supraoccipital weathered such that the presence of the nuchal crest is impossible to determine.

184 (New character) – The pterygoid median plate bears a lateral lamina (0), or the lateral lamina is absent (1).

The pterygoid in *Pristerodon* bears a wide and laterally expanded process that forms a lateral lamina (Figure 3.2C, Barry 1967). Similarly, in *Brachyprosopus*, *Diictodon* and *Niassodon* (Angielczyk et al. 2016; Sullivan and Reisz 2005), a wide lateral lamina of the pterygoid median plate is present. An expanded pterygoid lateral lamina is also present in *Eosimops* and *Colobodectes*, probably as a result of a lateral curvature of the anterolateral edge of the basisphenoid in ventral view (Modesto et al. 2003; Angielczyk and Rubidge 2013).

Myosaurus has a narrow pterygoid median plate which does not present a lateral lamina (Figure 3.10A/D). This condition is consistent with other emydopoid dicynodonts such as *Emydops*, *Compsodon*, *Digalodon*, and *Thliptosaurus*. In *Kombuisia frerensis* this region is severely affected by damage such that the interpretation was limited in this taxon (Fröbish

2007), but intriguingly the median plate is greatly expanded in *Kombuisia antarctica* (Fröbish et al. 2010). The narrowing of the pterygoid median plate and the absence of the pterygoid lateral lamina in emydopoids is further consistent with cistecephalids *Kawingasaurus*, *Kembawacela*, *Cistecephaloides*, *Sauroscaptor* and *Cistecephalus* (Figure 3.21A/C; Keyser 1965; Cluver 1974a; Kammerer et al. 2016; Angielczyk et al. 2019). This condition is also observed in the Malawian cistecephalid associated with a loss of a distinct pterygoid median plate in this taxon as the pterygoid rami do not meet medially (Figure 3.17A/C).

INTERNAL CHARACTERS

Using Computed Tomography technologies for the anatomical description and character assessment, I propose new phylogenetic characters or add novel anatomical information to the known structures. Despite being visible in some prepared specimens, often the features described are so delicate that they could be damaged during preparation. Therefore, I recommend CT-scans of all dicynodonts to properly address the following characters.

185 (New character) – The pila antotica: is short and its base is robust and rounded (0), is narrow, long and rod-like (1), or is tall and anteroposteriorly expanded (2).

The presence of a pila antotica is included in the most recent phylogenetic analyses as a character (char. 95, Kammerer 2019; Araújo et al. 2021) with two character-states: Development of the pila antotica as a rod-like process on the anterior edge of the periotic with a corresponding notch for the trigeminal nerve posterior to it (0), or pronounced pila antotica absent and trigeminal notch is a horizontal hollow in the anterior edge of the periotic (1). In this study, we intend to further detail the morphology of the pila antotica.

The pila antotica is short in *Pristerodon* and its base is rounded and more robust than that of emydopoids. This condition is also present in *Diictodon* (Barry 1974; Sullivan 2000;

Sullivan and Reisz 2005). A short pila antotica is present in *Colobodectes* (Modesto et al. 2003; Angielczyk and Rubidge 2009), despite these specimens being severely damaged. Other basal dicynodont taxa developed a narrow, long, and rod-like pila antotica, namely *Eosimops*, *Brachyprosopus*, and *Niassodon* (Angielczyk and Rubidge 2013; Castanhinha et al. 2013; Angielczyk et al. 2016).

However, an elaborated pila antotica seems to be a common feature among emydopoids whose condition was assessed. The pila antotica is tall and angles ~60º from the anterior prootic margin in *Myosaurus* and *Compsodon*. In *Myosaurus*, the pila antotica is depressed and bordered by crests on its anterior aspect (Figure 3.15A/B). However, the pila antotica in *Emydops* seems to retain a rod-like aspect (Fröbisch and Reisz 2008). The emydopoids *Kombuisia*, *Digalodon*, and *Thliptosaurus* have their pila antoticae obscured by a matrix that makes it impossible to examine this character (Fröbisch 2007; Kammerer et al. 2015; Kammerer 2019). However, *Cistecephalus*, *Kembawacela*, the Malawian cistecephalid PK-16-1, and *Kawingasaurus* possess a tall, anteroposteriorly expanded pila antotica that inclines slightly medially and, its lateral aspect is also excavated by a subvertical trough (Figure 3.19B, 3.24B; Keyser 1965; Angielczyk et al. 2019).

186 (New character) – The anteromedial process of the pterygoid: is present (0), or is absent (1).

The anterior ramus of the pterygoid in *Pristerodon* develops a small dorsal anteromedial process (Figure 3.2B; Cluver and King 1983), which is not present in any other basal dicynodonts as far as we could assess. The very large pterygoid anteromedial process is developed in the basal emydopoid *Myosaurus* specimen BP/1/2701a (Figure 3.10D/E). However, although present in *Compsodon* (Angielczyk and Kammerer 2017), the photographs

prevented determining the extension of the process in this taxon. The anteromedial pterygoid process is not observed in any cistecephalid emydopoid described here.

187 (New character) – The tuberculum sellae: is present and forms crests (0); is absent (1).

The tuberculum sellae region in *Pristerodon* is formed by thin crests that fuse at the midline to form the anterior border of the sella turcica region just anterior to the carotid foramina (Figure 3.3A). This condition conforms to the basal dicynodont *Diictodon* (Sullivan and Reisz 2005), but in *Niassodon*, the region anterior to the carotid foramina extends anteriorly as a trough bordered laterally by crests which fade more anteriorly (Castanhinha et al. 2013). Therefore, for this character, *Niassodon* has a transitional morphology between basal dicynodonts and the emydopoid construction, as it seems to lack a distinct tuberculum sellae.

The absence of the tuberculum sellae is observed in *Myosaurus* (Figure 3.11A), as the region anterior to the carotid foramina is smooth, possessing rather a long anteroposterior excavation. In the Malawian cistecephalid PK-16-1, the region is formed by the robust base of the parasphenoid rostrum (Figure 3.17A). Also, the dorsal surface of the parasphenoid rostrum base is flat in the Malawian cistecephalid PK-16-1, which results in the absence of the tuberculum sellae. *Kawingasaurus* has a short region anterior to the carotid canals, composed of ascending ridges that contact the orbitosphenoid dorsally (Figure 3.21A). Also, the sella turcica region is delimited by the carotid canals anteriorly in *Kawingasaurus*, such that there is no development of the tuberculum sellae.

188 (New character) – The clinoid process: is short (0); or it is tall (1)

Pristerodon has a thin, crest-like, and incipiently developed clinoid process, despite the region being somewhat damaged (Figure 3.3A/B). The clinoid process is also present and minimally developed in *Diictodon* and *Niassodon* (Sullivan 2000; Castanhinha et al. 2013). A more

developed clinoid process is present in emydopoid dicynodonts. *Myosaurus* has tall and a subvertical clinoid process which sharpens dorsally and is excavated by a recess along with its dorsal extension (Figure 3.11A/B). The Malawian cistecephalid clinoid process morphology conforms to that of *Myosaurus*, except for the height as here the process is cut-off transversely by damage in its dorsal aspect (Figure 3.17A/B). In *Kawingasaurus*, however, the clinoid process and the prootic are coossified. Despite this coossification, the clinoid process is tall but more vertical in *Kawingasaurus* than in other taxa (Figure 3.21A/B).

189 (New character) – The dorsal component of the exoccipital and the exoccipital condyle: are fused to form an oblique buttress (0); or they are separated by a shallow trench (1)

The exoccipital of *Pristerodon* forms a subvertical buttress on its posterior aspect which unites the dorsal component and exoccipital condyle into a single element (Figure 3.2D, 3.5B). This morphology contrasts with that of the more basal dicynodonts *Niassodon* and *Diictodon* (Sullivan and Reisz 2005; Castanhinha et al. 2013), as they appear separated by a very shallow trench in these taxa. Of interest, the emydopoids morphology is nearly similar to that of *Diictodon* and *Niassodon*. In *Myosaurus*, the Malawian cistecephalid and *Kawingasaurus*, the dorsal component and the exoccipital condyle are united by a median shallow oblique trench in posterior view (Figure 3.13B, 3.18B, 3.23C).

190 (New character) – The exoccipital dorsal component is short with minor contribution to the height of the foramen magnum (0); is tall, rectangular and covers half the foramen magnum height (1); or is tall, reniform and covers more than half the height of the foramen magnum (2).

The very small exoccipital contribution to the height of the foramen magnum unite *Pristerodon* to other basal dicynodonts such as *Brachyprosopus* and *Niassodon* (Castanhinha et al. 2013; Angielczyk et al. 2016). However, unclear sutures between the dorsal component and the supraoccipital and opisthotic make the determination of the shape and dorsal extension of the components in other basal dicynodonts difficult (Sullivan and Reisz 2005; Angielczyk and Rubidge 2010, Olroyd et al. 2018). This requires the use of micro-CT techniques to assess the sutures in this region.

Myosaurus has a tall and rectangular exoccipital dorsal component which covers nearly half the foramen magnum height in posterior view (Figure 3.13). This component forms right angles along its lateral margins in *Compsodon* and *Kombuisia* (Fröbisch 2007; Angielczyk and Kammerer 2017). The basal emydopoid *Emydops* conforms to the morphology observed in *Myosaurus* (Fourie 1991). Conversely, the exoccipital in *Digalodon* is tall and its posterior aspect is reniform, somewhat similar to *Kembawacela*, the Malawian cistecephalid and *Kawingasaurus* (Figure 3.23C; Angielczyk et al. 2019; Araújo et al. in press). Cistecephalids have a more dorsally extended exoccipital dorsal component as revealed in the Malawian cistecephalid, *Kawingasaurus*, *Kembawacela*, and in *Sauroscaptor* specimen ISI R231, which gives it a major contribution to the foramen magnum borders. However, *Cistecephaloides* and *Cistecephalus* (Keyser 1965; Cluver 1974a) have unclear sutures along the posterior aspect of the exoccipital.

CODED MATRIX

nstates 32

xread

213 119

& [cont]

Biarmosuchus_tener 0.693 ? 0.261 ? 0.148 0.029 ? ? 5.8 ? ? ? 1.06 ? 0.502 1.87 ? 0.446 ? 0.553 0.426 0.0 ?

Hipposaurus_boonstrai 0.606 ? 0.263 0.842 0.19 0.046 ? ? 3.5 ? ? ? 1.07 ? 0.539 2.63 0.667 0.367 0.125 ? ? 0.0 0.222

Archaeosyodon_praeventor ? ? ? ? ? 0.104 ? ? 5.6 ? ? ? ? ? 0.92 ? ? ? ? ? ? ? ? ?

Titanophoneus_potens 0.758 ? 0.244 0.7 0.227 0.051 ? ? 6.2 ? ? ? 1.16 ? 0.855 1.62 0.5 0.292 0.274 0.5 ? 0.0 0.343

Gorgonops_torvus 0.504 ? 0.29 1.15 0.305 0.072 ? ? 8.5 ? ? ? 0.977 ? ? ? ? 0.329 ? ? ? ? ?

Lycosuchus_vanderrieti 0.509 ? 0.261 0.333 0.352 0.303 ? ? 7.7 0.094 ? ? 1.06 ? 0.595 1.71 0.5 0.333 0.294 ? ? 0.0 0.4

Glanosuchus_macrops 0.547 ? 0.145 0.25 0.367 0.218 ? ? 5.3 0.05 ? ? 1.02 ? 0.718 2.12 0.545 0.309 0.2 0.833 ? 0.0 0.342

Biseridens_qilianicus ? ? ? 1.032 ? 0.094 ? ? ? ? ? 11.0 ? ? 0.956 ? ? ? ? ? ? ? ?

Anomocephalus_africanus ?

Tiarajudens_eccentricus ? ? ? ? ? ? ? ? ? ? ? ? ? ? ? ? ? ? ? 0.396 0.164 ? ? ? ?

Otsheria_netzvetajevi 0.381 5.425 0.231 ? 0.512 0.108 ? 0.181 5.3 0.108 10.95 15.5 0.86 ? ? ? ? ? ? ? ? ? ?

Ulemica 0.47 5.364 0.125 1.06 0.407 0.102 ? 0.216 4.9 ? 10.905 15.4 1.098 0.294 0.964 1.135 ? ? ? ? ? ? ?

Suminia_getmanovi 0.336 4.879 0.205 ? 0.23 0.105 ? 0.198 5.0 0.09 10.455 11.6 0.902 0.395 0.899 1.136 0.558 0.299 0.133 0.709 0.966 0.0 0.186

Patranomodon_nyaphulii 0.29 ? 0.228 0.914 0.272 0.076 ? 0.202 6.0 0.043 11.029 13.7 0.744 0.476 1.25 1.059 ? ? ? ? ? 0.0 ?

Galeops_whaitsi 0.339 5.325 0.18 ? 0.327 ? ? 0.136 4.1 ? 10.385 ? ? 0.489 0.831 0.968 0.646 0.356 0.181 ? ? ? 0.257

Galepus_jouberti ? ? ? 0.855 ? ? ? ? ? ? ? ? ? ? ? ? ? 0.351 0.149 ? ? 0.0 ?

Galechirus_scholtzi ? ? ? ? ? ? ? ? ? ? ? ? ? 0.355 0.865 0.7 ? 0.401 0.206 ? ? 0.0 ?

Eodicynodon_oelofseni 0.351 ? ? 0.968 0.435 ? 2.47 ? ? ? ? 12.0 ? 0.259 0.708 ? ? ? ? ? ? ? ?

Eodicynodon_oosthuizeni 0.322 5.555 0.234 0.908 0.518 0.111 2.501 0.14 8.2 0.182 10.457 9.0 0.847 0.253 0.698 1.061 0.446 0.509 0.244 0.3 0.5 0.0 0.475

Colobodectes_cluveri 0.203 5.714 0.195 ? 0.52 0.269 2.07 0.142 6.6 0.206 10.177 ? 0.948 ? ? ? ? ? ? ? ? ?

Lanthanostegus_mohoii ? ? ? 0.661 ? ? 2.434 ? ? ? ? ? ? ? ? ? ? ? ? ? ? ? ?

Eosimops_newtoni 0.186 5.89 0.243 0.795 0.541 0.257 2.014 0.126 8.1 0.172 9.402 11.3 0.831 0.402 0.803 0.904 0.633 0.466 0.26 ? ? 0.0 0.444

Diictodon_feliceps 0.247 5.925 0.223 0.64 0.534 0.273 1.702 0.135 8.0 0.214 9.418 11.9 0.881 0.257 0.742 0.901 0.443 0.486 0.297 0.67 1.388 0.0 0.366

Robertia_broomiana 0.237 5.863 0.197 0.721 0.555 0.259 1.681 0.108 8.6 0.199 9.417 9.8 0.85 0.132 0.711 0.868 0.487 0.502 0.227 ? ? 0.0 0.309

Prosictodon_dubei 0.238 5.807 0.171 0.864 0.548 0.228 2.469 0.098 8.1 0.131 9.78 9.3 0.881 ? 0.834 0.637 ? ? ? ? ? ? ?

Abajudon_kaayai 0.279 5.215 0.277 1.03 0.412 0.126 2.844 0.146 9.4 0.173 ? 8.0 0.907 0.302 0.898 1.016 ? ? ? ? ? ? ?

Niassodon_mfumukasi ? ? ? 0.867 ? ? 1.548 ? 8.4 ? ? 9.5 0.697 0.29 0.859 0.938 ? ? ? 0.214 1.145 ? ?

Brachyprosopus_broomi 0.231 5.81 0.19 0.998 0.515 0.338 1.847 0.129 6.8 0.15 9.687 10.6 0.898 0.132 0.715 0.824 0.612 0.437 ? ? ? 0.0 0.315

Endothiodon_tolani 0.328 ? ? 0.396 ? 0.025 1.505 0.109 10.6 ? ? ? 0.902 0.319 0.723 0.825 ? ? ? ? ? ? ?

Endothiodon_bathystoma 0.335 5.396 0.378 0.268 0.599 0.4 1.457 0.111 8.1 0.147 9.694 7.1 0.988 0.373 0.798 0.73 0.554 0.491 0.406 0.301 0.964 0.0 0.414

Pristerodon_mackayi 0.225 5.874 0.184 1.026 0.582 0.222 1.751 0.123 10.0 0.206 9.578 11.2 0.813 0.208 0.723 0.928 0.594 0.43 0.277 0.275 0.5 0.0 0.275

Emydops 0.22 5.872 0.204 0.906 0.537 0.166 1.646 0.118 9.8 0.176 9.667 9.3 0.84 0.398 0.692 0.955 0.668 0.428 0.23 0.454 1.283 0.0 0.353

Compsodon_helmoedi 0.196 5.874 0.207 1.066 0.431 0.187 1.71 0.082 10.3 0.22 9.858 11.0 0.817 ? ? ? ? ? ? ? ? ?

Digalodon_rubidgei 0.354 6.155 0.294 0.899 0.473 0.139 1.565 0.134 ? 0.173 ? ? 0.871 0.293 ? ? ? ? ? ? ? ? ?

Thliptosaurus_imperforatus 0.279 ? 0.198 0.84 0.407 ? 1.5 0.116 ? ? ? ? ? ? 0.75 0.667 ? ? ? ? ? ? ?

Rastodon_procurvidens 0.197 ? 0.199 0.742 0.558 0.298 ? 0.123 6.600 0.105 ? 12.0 0.798 0.1 0.623 0.667 ? ? ? ? ? ? ?

Dicynodontoides 0.269 5.95 0.24 0.764 0.539 0.211 1.492 0.085 8.823 0.181 9.814 11.9 0.887 ? 0.726 0.924 0.304 0.497 ? 0.167 2.5 0.406 0.359

Kombuisia_frerensis 0.193 5.976 0.202 0.4 0.555 ? 1.589 0.195 ? ? 9.645 ? 0.746 ? 0.684 ? ? ? ? ? ? ? ?

Myosaurus_gracilis 0.26 5.902 0.275 1.032 0.483 0.108 1.59 0.085 9.6 0.208 9.775 9.6 0.853 0.348 0.958 0.942 0.586 ? ? ? ? ? 0.208

Kembawacela_kitchingi 0.372 5.948 0.383 1.487 0.357 0.042 1.455 0.132 10.55 ? 10.173 11.65 0.969 0.415 0.726 0.99 ? ? ? 0.818 1.48 ? ?

Cistecephalus_microrhinus 0.279 6.056 0.289 1.139 0.509 0.088 1.49 0.117 9.55 ? 9.965 10.2 0.872 0.38 0.687 0.789 0.485 0.403 0.317 0.754 1.857 0.0 0.324

Sauroscaptor_tharavati 0.281 ? 0.298 1.339 0.421 0.048 ? ? ? ? ? ? 0.912 0.564 0.73 0.714 ? ? ? ? ? ? ?

Cistecephaloides_boonstrai 0.311 6.047 0.425 1.319 0.372 0.04 ? 0.194 ? ? 10.305 12.5 0.632 0.346 0.796 0.914 ? ? ? ? ? ? ?

Kawingasaurus_fossilis 0.308 5.933 0.33 1.404 0.34 ? 1.5 0.135 10.7 ? 10.119 10.0 0.836 0.286 ? 0.964 0.298 0.419 ? ? ? ? 0.446

Daqingshanodon_limbus 0.282 6.112 0.26 0.619 0.442 0.18 1.528 0.08 ? 0.189 9.34 10.3 0.808 0.212 0.677 0.819 ? ? ? ? ? ? ?

Keyseria_benjamini 0.244 6.155 0.159 1.034 0.605 0.203 1.6 0.083 6.3 ? ? 9.0 0.831 ? ? ? ? ? ? ? ? ? ?

Rhachiocephalus_magnus 0.329 6.094 0.271 0.738 0.598 0.606 1.48 0.094 8.8 0.143 9.17 12.8 1.011 0.167 0.838 0.777 0.501 0.506 ? ? ? ? 0.372

Kitchinganomodon_crassus 0.32 6.137 0.318 0.708 0.566 0.752 1.556 0.108 7.4 0.07 9.747 11.1 0.936 0.165 0.843 0.752 ? 0.466 ? ? ? ? ?

Oudenodon_bainii 0.281 6.054 0.173 0.844 0.609 0.271 1.458 0.092 8.1 0.141 9.219 11.3 0.864 0.264 0.798 0.745 0.57 0.491 0.366 0.514 0.765 0.353 0.411

Tropidostoma_dubium 0.284 5.989 0.197 0.899 0.565 0.277 1.436 0.098 8.8 0.14 9.106 12.4 0.875 0.237 0.758 0.766 0.531 0.503 ? 0.474 1.368 0.345 0.378

Australobarbarus 0.333 6.058 0.183 0.697 0.561 0.298 1.324 0.101 6.1 0.16 9.822 13.35 0.882 0.193 0.624 0.694 0.466 0.485 ? 0.848 1.033 0.333 0.391

Syops_vanhoepeni ? ? ? 0.484 ? 0.343 ? ? ? ? ? ? ? ? ? ? ? ? ? ? ? ?

Odontocyclops_whaitsi 0.376 6.066 0.232 0.988 0.551 0.232 1.448 0.092 10.1 0.131 9.74 12.3 0.929 0.213 0.787 0.731 0.551 0.518 0.427 0.435 1.13 0.426 0.491

Idelesaurus_tataricus 0.367 5.967 0.175 1.022 0.5 0.174 1.497 0.107 8.25 0.173 10.118 13.5 0.969 0.204 0.693 0.764 ? ? ? ? ? ? ?

Bulbasaurus_phylloxyron 0.284 6.003 0.25 0.562 0.534 0.233 1.362 0.112 10.333 0.052 9.851 14.78 0.887 ? 0.643 ? ? ? ? ? ? ? ?

Aulacephalodon_bainii 0.3 6.089 0.323 0.892 0.583 0.204 1.425 0.117 6.8 0.122 9.48 13.5 0.822 0.172 0.76 0.785 0.55 0.532 0.348 0.714 1.067 0.395 0.491

Pelanomodon_moschops 0.289 6.093 0.305 0.912 0.584 0.213 1.468 0.104 9.4 0.155 9.414 12.3 0.801 ? 0.856 0.742 ? ? ? ? ? ? ?

Geikia_locusticeps 0.256 6.049 0.278 0.908 0.514 0.251 1.627 0.104 8.72 0.141 9.392 13.9 0.756 0.205 0.818 0.848 ? ? ? ? ? ? ?

Geikia_elginensis 0.366 ? 0.521 0.846 0.529 ? 1.429 ? ? ? ? 13.1 0.829 0.212 0.9 0.987 ? ? ? ? ? ? ?

Elph_borealis 0.279 5.927 0.186 0.64 0.544 0.29 1.515 0.157 8.9 ? ? 13.0 0.914 ? 0.781 ? ? ? ? ? ? ? ?

Interpresosaurus_blomi ?

Katumbia_parringtoni 0.196 5.868 0.22 0.527 0.541 0.347 1.489 0.112 9.3 0.132 9.928 14.4 ? ? 0.833 0.822 ? ? ? ? ? ? ?

Delectosaurus_arefjevi 0.369 5.861 0.258 0.702 0.546 0.334 1.618 0.119 7.8 0.13 9.798 14.7 0.985 ? ? ? ? ? ? ? ? ? ?

Dicynodon_lacerticeps 0.324 5.982 0.253 0.607 0.546 0.359 1.485 0.117 7.7 0.121 9.869 11.9 0.926 0.241 0.749 0.766 ? ? ? ? ? ? ?

Dicynodon_angielczyki 0.308 5.937 0.253 0.524 0.569 0.359 1.351 0.105 7.56 0.114 9.95 12.0 0.965 0.219 0.808 ? 0.476 ? ? ? ? ? ?

Daptocephalus_huenei 0.292 6.091 0.23 0.564 0.569 0.414 1.25 0.123 ? 0.117 9.68 ? 1.024 ? ? ? ? 0.543 ? ? ? ? ?

Daptocephalus_leoniceps 0.268 6.091 0.237 0.539 0.567 0.437 1.5 0.118 6.4 0.111 9.378 ? 0.8584 0.238 0.763 0.75 ? 0.545 ? ? 1.667 ? ?

Dinanomodon_gilli 0.337 6.17 0.205 0.48 0.577 0.522 1.347 0.116 7.8 0.107 9.751 9.9 1.047 0.186 ? 0.724 ? ? ? ? ? ? ?

Peramodon_amalitzkii 0.272 ? 0.224 0.563 0.553 0.369 ? ? ? ? ? 9.5 0.839 0.167 0.676 0.68 0.463 ? ? ? ? ? 0.494

Taoheodon_baizhijuni 0.24 6.1 0.237 ? ? 0.26 1.18 0.11 ? 0.105 9.64 ? 0.91 0.285 ? ? ? ? ? ? ? ? ?

Counillonia_superoculis 0.297 5.068 ? ? 0.276 0.134 ? 0.131 8.333 0.14 ? 9.616 0.876 ? ? ? ? ? ? ? ? ? ?

Repelinosaurus_robustus 0.2 ? 0.295 ? 0.408 0.281 ? ? ? ? ? 14.698 0.829 ? ? ? ? ? ? ? ? ? ?

Vivaxosaurus_trautscholdi 0.38 6.019 0.23 0.685 0.481 0.285 1.824 0.116 7.9 0.121 10.203 13.9 1.041 0.203 0.702 0.731 0.317 0.544 ? ? ? ? 0.641

Jimusaria_sinkianensis 0.307 ? 0.278 0.672 0.767 0.464 1.443 0.089 7.2 0.098 ? 8.9 0.992 0.251 ? 0.699 ? ? ? ? ? ? ?

Sintocephalus_alticeps 0.354 5.969 0.244 0.516 0.522 0.294 1.338 0.124 6.5 0.132 9.399 9.6 1.022 ? ? ? ? ? ? ? ? ? ?

Basilodon_woodwardi 0.315 5.994 0.212 0.722 0.497 0.225 1.305 0.128 5.7 0.139 9.599 12.6 0.814 ? ? ? ? ? ? ? ? ? ?

Turfanodon_bogdaensis 0.320 6.160 0.285 0.640 0.567 0.416 1.380 0.121 8.500 0.078 9.470 10.000 0.895-0.920 ? ? ? ? ? ? ? ? ? ? ? ?

Turfanodon_jiufengensis 0.270-0.340 6.060-6.320 0.322 0.944 0.340 0.418 1.535-1.610 0.110-0.124 6.000 ? 9.500 ? 0.809-1.010 0.196-0.290 ? 0.810 ? ? ? ? ? ? ?

Gordonia_traquairi 0.252 ? 0.139 0.65 0.604 0.309 ? ? ? ? ? ? 0.924 0.188 ? 0.773 0.543 0.49 0.144 ? ? ? 0.476

Euptychognathus_bathyrhynchus 0.336 6.028 0.13 0.562 0.56 0.238 1.559 0.091 6.5 0.084 9.663 10.25 0.792 ? 0.79 0.815 ? ? ? ? ? ? ?

Lystrosaurus_hedini 0.32 6.111 0.414 0.705 0.413 0.146 1.471 0.174 9.2 0.079 10.203 11.4 0.673 0.294 0.691 0.781 ? ? ? ? ? ? ?

Lystrosaurus_maccaigi 0.274 6.072 0.347 0.656 0.325 0.108 1.764 0.165 8.4 0.123 10.022 10.9 0.805 0.354 0.711 0.706 ? 0.526 0.54 ? ? 0.389 ?

Lystrosaurus_curvatus 0.315 6.005 0.383 0.689 0.417 0.119 1.664 0.162 7.4 0.086 10.145 8.6 0.906 0.289 0.767 0.643 0.473 0.485 0.465 0.787 1.484 0.313 0.489

Lystrosaurus_declivis 0.347 5.954 0.424 0.705 0.415 0.112 2.141 0.157 8.8 0.097 10.309 9.7 0.874 0.315 0.757 0.711 0.418 0.458 0.478 0.75 1.3 0.347 0.545

Lystrosaurus_murrayi 0.288 6.003 0.427 0.726 0.466 0.143 2.002 0.175 8.4 0.101 10.358 11.7 0.816 0.316 0.793 0.754 0.478 0.46 0.441 0.843 1.455 0.392 0.605

Shansiodon 0.265 6.064 0.327 0.163 0.538 0.633 1.314 0.13 7.2 0.1 9.78 11.2 1.129 0.286 0.821 0.84 0.575 0.479 ? 0.758 1.363 0.363 0.675

Tetragonias_njalilus 0.378 5.912 0.354 0.201 0.574 0.446 ? 0.125 6.8 0.088 10.009 10.4 1.004 0.205 0.858 0.796 0.447 0.481 0.3 0.675 1.852 0.304 0.596

Vinceria_andina 0.267 6.099 0.352 0.201 0.49 0.466 ? 0.137 7.0 0.153 10.552 11.3 0.983 ? ? ? ? ? ? ? ? ?

Rhinodicynodon_gracile 0.304 6.213 0.253 0.5 0.523 0.435 1.568 0.1 ? ? 9.174 10.1 0.879 0.24 0.875 0.734 0.49 0.354 0.361 ? ? 0.352 0.383

Acratophorus_argentinensis 0.329 ? 0.445 0.205 0.666 0.476 1.872 0.12 6.655 0.094 ? 8.055 1.031 ? 0.716 0.705 0.345 0.468 0.292 0.706 1.206 0.424 0.574

Kannemeyeria_simocephalus 0.421 6.121 0.409 0.289 0.531 0.479 1.461 0.147 9.8 0.074 10.478 12.1 1.147 0.179 0.8 0.686 0.551 0.558 0.338 ? 1.381 0.372 0.411

Kannemeyeria_aganosteus ?

Kannemeyeria_lophorhinus 0.361 6.286 ? 0.663 ? 0.318 2.051 0.149 10.8 0.086 10.432 ? ? 0.077 0.786 0.542 ? ? ? ? ? ? ?

Dolichuranus_primaevus 0.356 6.079 0.392 0.293 0.484 0.4 1.339 0.143 8.7 0.085 10.672 9.7 1.018 0.192 0.756 0.542 ? 0.519 ? ? ? 0.425 ?

Sinokannemeyeria 0.42 6.14 0.478 0.543 0.382 0.175 1.505 0.161 5.9 0.109 10.469 ? 0.918 0.243 0.549 0.385 0.494 0.489 0.556 0.458 1.187 0.408 0.405

Parakannemeyeria 0.455 6.28 0.377 0.359 0.354 0.195 1.468 0.122 7.5 0.102 9.688 12.3 0.92 0.166 0.79 0.515 0.467 0.52 0.478 0.443 1.465 0.411 0.294

Xiyukannemeyeria_brevirostris 0.286 6.203 0.413 0.46 0.433 0.23 ? 0.169 8.5 0.086 10.027 8.9 0.795 0.32 ? 0.668 ? ? ? ? ? ? ?

Rabidosaurus_cristatus 0.464 ? ? 0.268 0.607 ? ? ? ? ? ? ? ? ? ? ? ? ? ? ? ? ? ? ?

Rhadiodromus 0.509 6.144 0.403 0.285 0.574 0.254 ? 0.122 6.9 0.088 10.023 10.8 1.085 ? ? ? ? ? 0.604 ? ? ? ?

Wadiasaurus_indicus 0.423 6.105 0.337 0.539 0.506 0.523 ? 0.218 ? ? ? 10.6 1.052 0.344 0.9 0.81 0.607 0.563 0.45 0.562 1.239 0.417 0.355

Shaanbeikannemeyeria 0.527 6.069 0.513 0.886 0.5 0.414 ? 0.157 7.8 0.176 10.642 11.3 1.432 ? 0.734 ? ? 0.58 ? ? ? 0.416 ?

Rechnisaurus_cristarhynchus 0.51 5.971 0.436 0.154 ? 0.211 ? 0.14 9.9 ? ? ? ? ? ? ? ? ? ? ? ? ? ? ?

Uralokannemeyeria_vjuschkovi 0.49 ? 0.407 0.526 0.454 0.233 ? 0.147 ? 0.091 ? 11.9 1.154 ? ? ? ? ? ? 0.819 1.193 ? ?

Angonisaurus_cruickshanki 0.339 6.301 0.514 0.667 0.572 0.6 1.491 0.19 5.9 0.06 10.206 10.0 1.012 0.143 0.785 0.722 ? 0.524 ? 0.647 2.541 ? ?

Ufudocyclops_mukanelai 0.376 ? 0.468 0.45 0.515 0.332 1.409 0.156 9.31 ? ? 10.9 0.983 ? ? ? ? ? ? ? ? ?

Zambiasaurus_submersus ? ? ? ? ? ? ? ? ? ? ? ? ? ? ? ? ? 0.498 ? ? ? 0.401 ?

Placerias_hesternus ? ? ? ? ? ? ? ? ? ? ? ? ? ? ? ? ? 0.49 0.499 ? ? ? ?

Moghreberia_nmachouensis ?

Pentasaurus_goggai ?

Stahleckeria_potens 0.438 5.992 0.445 0.726 0.491 0.288 ? 0.183 11.1 0.052 10.284 8.7 0.953 0.237 0.856 0.897 0.442 0.53 ? 0.391 2.217 0.434 0.565

Sangusaurus_parringtonii 0.411 6.177 0.461 0.618 ? 0.368 1.129 0.144 ? 0.091 ? 9.2 1.061 ? 0.832 ? ? ? ? 0.592 1.944 0.433 ?

Sangusaurus_sp ?

Eubrachiosaurus_browni ? ? ? ? ? ? ? ? ? ? ? ? ? ? ? ? ? 0.538 ? ? 1.789 ? ?

Ischigualastia_jenseni 0.482 6.139 0.423 0.331 0.479 0.528 1.39 0.151 5.7 0.064 10.023 ? 1.032 ? 0.912 0.841 0.419 0.577 0.561 ? 0.818 0.412 0.526

Jachaleria_candelariensis 0.392 6.078 0.393 0.199 0.379 0.499 1.431 0.161 4.0 0.084 10.269 ? 0.766 ? 0.822 0.766 0.427 ? 0.529 ? 0.808 0.434 0.667

Jachaleria_colorata ?

Dinodontosaurus_brevirostris 0.321 ? 0.388 0.314 0.518 0.354 2.18 0.176 9.106 0.107 ? 9.69 1.01 ? ? ? ? ? ? ? ? ?

Dinodontosaurus_tener 0.398 6.104 0.347 0.24 0.461 0.328 1.414 0.135 7.3 0.074 10.155 10.9 0.926 0.202 0.814 0.653 0.398 0.507 0.423 0.652 1.896 0.31 0.752

& [num]

Biarmosuchus_tener
00000200000000000001000000????000000000000000?2000200000000000010000010010000000000000?01201??0??00?0??0000??0000000000000000??000000000000?0000?100001101?000110000110?00?000??02100??????

Hipposaurus_boonstrai
0000020000000000000010000000????000000000000010200000000000000000010000010110000000000000?01001??0?000?0???000000?000000000000000??00000100000000?10000100011101????0?000010??00?0?0?002100??????

Archaeosyodon_praeventor
000002000000000000001000010 0????0000000100000?2000100000000000001000??0100000010000000?01201??0???0????????????00001100000000??000?????????0?????????????????????????????0??000?0???????????

Titanophoneus_potens 000002000000000010000000000????0000000100100?10000000[02]000000001000000100000010000000?012010000000?001000010000000000000000??000100000000?00000?000000001100110001 2?1?00?000?0???????????

Gorgonops_torvus
000002000000000000000000000????000000001000010200020002000000000100000100000000000000000?012010000000?000000000000000000000000000??00000110000000?000001000100010001101110011?00?000?001100??????

Lycosuchus_vanderrieti
000002000000000000000001000????000200000000000?10201100100000000010000001001000110000000?012010010000100 1?00000000000000000000??01000201000000?000001000100011110???000?????00?000?001100??10??

Glanosuchus_macrops
000002000000000000010000000????000000000000010?10201100100000000010000001001000110000000?012010000000100100000000000000000000000??01000201000000?000001000100011100100001211?00?000?0???????????

Biseridens_qilianicus
000002100000000010010000100????000000100010 0?2000100000000000001001??000000001000000000?00?01??????0?0???000100?00101001000000??000000?1???0??????????????????????????????????000?00210???????

Anomocephalus_africanus
???????0?????00??0?0?100??0??????0???0???00?????????????0??0000?0?01?????????????1???????2?????????????????????1??010??????0???000?0???????????

Tiarajudens_eccentricus

0??????0?0??000010000000100????000??00?0000?????????????00?0000?0?01?????????????011????0??2???00???0001010??????????12?1??0?000?0???????????

Otsheria_netzvetajevi

000002101000000?1001?100?00?????000000000000?2?0010?000000000101010??11??10100001010000?00011???00?000???1?1??0???000?0???????????

Ulemica

000002101010000?1001?000100????000000010000000?200010?000010000101O?000110011102001010010?00011??1000010?10??1?0001010111101000100[0 1]000000100111?????????????????????????????0??000?0???????????

Suminia_getmanovi

000002?0101000001001?100200?????001000000000?210010?0000200001O?01000110O?1102021010010?010110?100?000010100l?0?1000211100000100000000000210?000000000000010000000000010?00?000?0011000?????

Patranomodon_nyaphulii

000?0?10101?00002000?100100?????000000000001001000000100000001000000000001000l0?0110000?01011??0001100?10100100?10?01001000000????00031000010?????????????0110???000?????0??000000110???????

Galeops_whaitsi

000002101010000020O0?100100??????1?000000000???1000?00?0?20000101O?00100001?0010?0?10000?0?0110?1?1?1????????????1000??0100000100?10113100011??001000000100?????????????00??000?0???????????

Galepus_jouberti

?00?02??1????00??0????????0?????????????00?????????????????0?????0???0?01001?0000?????????????1??????1?00010?0?11?00?000?2?1????0?0?0???????????

Galechirus_scholtzi

00??0??010?0?00??000?1001?0??????1??00?????????????????????????0?0???10?0100100??0???????031????1???0000??0?1000011?00?0001211????000?0???????????

Eodicynodon_oelofseni
???????01?10000020001001?0????????0?00000010??001000100201O?200??0??0000111030????012???1310??000???0????0?10?010
11100200001001?01??1??121??????????????????????????????????0??000?002000??????

Eodicynodon_oosthuizeni
000010121010000020002001010000001100000000010010010001002110020101010000011103010010121001310010000100001101 1
000101010020010020010011311112l0?000100000011O?1101000001???100?0000000??0??????

Colobodectes_cluveri
010010121010000020002001010000001100000100010110000000l0?2110020101O??000111103010010121001310010000110O??10??? 0
??000?0020000?????

Lanthanostegus_mohoii
??????????1????0?????200?1?????0???0?0100010101?001000200???0000?0?0??0???1110301?0101211O?310?100?0110????????????? ??0?0?0???????????

Eosimops_newtoni 11101012111000002000021011120001010000100010101100100020021100201110101O[0 1][0 1]11103010010121001310O?000011001?1?1100?1011???4000111000001131?11210?10011?0000010?1101000001????00?000?0021001?????

Diictodon_feliceps 11101012111000002000022??1120001[0 1]1[0 1]000100000101120000O[1 2]00211002011101011111110301001012100121000000112001110110001012???2001111001001131111211?1001100000000?1101000001211 000?00000000000?0010

Robertia_broomiana
11101012111000002000021011120001010000100000101100100020021100201110101000111030100101210012100?000111001?1011 00010111O?20011110O?00113111210?1001?00000000?11???00001211?00?000?0????0??????

Prosictodon_dubei
11101012111000002000021011120001011000100000101120000010?2110020111010100011103010010121001210??00011100111?11 00?1011???20?111100?0?1??1??121??????????????????????????????????000?002000??????

Abajudon_kaayai
100102011?10000120000211110O0??00100000010001010001000100211002010101010001111302001012100121O1?00001100??11??? 0?10112003010202101O0???????2????????????????????????????????????0??000?0?20200?????

Niassodon_mfumukasi
1???22?11?1?0001???0?1101110010101000000000021210020001002010020101010100011113111 0?012110121000000111001111100010110??0400?20200100114?111211????????????????01???1??????0??0?00002100111010

Brachyprosopus_broomi
1011121210110001200002111110010001000010000010110010002002110020101010000011103020010121001211010001120 01?1111000101120020012010010011311112 1??0001??000010????????01??????0??000000000 01????0

Endothiodon_tolani 1001021110120001201002112 00????00[0 1]0000001??0101110101020 02?1??2??0?1101100111130210101210013100000 0?1200??1111000101120030112020010011411112 1?????????? ??????????????????????0??02000???????????

Endothiodon_bathystoma 1001[0 1]2111012000020100111200?????0[1 2]?00100[0 1]1011111101010200211002010111010001111302101012 0?013100000011200 1?1?110001011200301120200100114111121 2?00010?0000100 ?11011?000121100 0?0200002?????????

Pristerodon_mackayi
1100121210100000200002101110010001000010 00?010110010001012110020111010100011103021010121001210010001120011101 1000101120 02?012020010011311112 12?1101000000100?1101?00001211?00?000?000000000000

Emydops
1011101210100000200002001111010101000000000010110010001002010020111010111111103011010121100210000011120010111 10101011[1 2]0040002021010011311112 10?1?010?00000001110???0001211?00?00000?21111????1

Compsodon_helmoedi
1011101210100001201002001111010101000010000021101000003002110020 11?0101110111031110101211002000?01111200111101 01?1???000?00111120???1

Digalodon_rubidgei
1210201210100001200002 2??0110100010000001000101100200030121100201110101111111030110101210012100000111?001?1111 00?1012???40002????100????????????????????????????????????0??000?0111112????2

Thliptosaurus_imperforatus
1????????0?0000??00001???11??1?00100?0001000101?0?20?1???2?10020???01?????????????????1211???????001?1?0?????110??111?
???410??????100?1?11112?????????????????????????????????000?0011?0??????

Rastodon_procurvidens
1???2??210100001200002 2??1110100010000000000101100000010021100201110101110????????0??1210?12100?00??1?00??111100?
201????400??0200100?1?1????1?????????????????????????????0??000?002110??????

Dicynodontoides
1011201210100001200002 2??1110100010000001000201120000010021100201010101000111030110101211002100000111200101111
0002012???4100002101001131111211001011011000 1?1??011001112110011000?002120??????

Kombuisia_frerensis
1010201210100001 2?00012??011010101000000100020102011?1??02?10020?0101?1???111030110 10?21100?1??10011120010110100
?2012???4101002001?011?110121?????????????????????????????0??000?0?311[0 1]?????1

Myosaurus_gracilis
1000211210100001200001 2??1110101012000001000102000200010020100201010101111101031110101211012100100111200111111
0001012???410000210??01131??1210?11011010110?????0??????????00??000?0[0 1]1111201111

Kembawacela_kitchingi
101022121?100001201002 2??1110101010000001 0000?2100200010120100200110101100111031110101211013 1?0??01111000??1110
101112???400020210100113101121 0?????????????1???01??100?????0??00201211212?????2

Cistecephalus_microrhinus 1010201210100001201001 2??111010101000[0 1]101[0
1]000?2100200010120100200110101101111031110101211002 1?00?01112000 1?11100?1112???400020210101113111121 0?11000122100111
1101001101211001100201221212?????

Sauroscaptor_tharavati
1???2??21?100001?000012???110100?1?0?00?10000???0020?0100201002001101011??11103??10?01211?131????01?1?00????1100?1
11????4000?021010??1?1????1?????????????????????????????0??001?1?2121?????2

Cistecephaloides_boonstrai
10002012101000012010012??01101000100000110000?2100200010120100200010101101111103?11010120??0?1????011110?1??1110
0?1112???40002021O1?111?111121?????????????????????????????????0??001?1?1121??????

Kawingasaurus_fossilis
10002012101000012010012??01101000020000010000?21002001???20100200l?0101101111031110101201?0011????011110?0??01100
01012?????00001001111???11121??11000?2200011?11???????1211?01100111231212111l2

Malawian_cistecephalid
1?0?22121?1?0001???0012??1??????0100?000100010210020001002010020011010110011103111010121101?1?0000111100???11101
0??211221?1211112

Daqingshanodon_limbus
12002212101000002000022??11010100200?000100010111000003002l1?02011101011??122030110101210012l0?00??11?????1011?0
?1112???2101301211?01141111?1?????????????????????????????0??000?002120??????

Keyseria_benjamini
120022?21010000?2000022??11010110200000000001011000?0?0021100201110101l??122030?1?10121000210??01?11210111?110
0??????????????????????????2?????????????????????????????????000?002100??????

Rhachiocephalus_magnus
12002212101100002000012??11000100200110001001011200000210211002011101111111220301101012100121000012112001110l1
0001112???2001301001001141111?1??0011[0 1]11010100???????011????1010010?001000??????

Kitchinganomodon_crassus
12002212101100002000012??11000100200110001001011200000211211102011101111011220301101012100131?0?012112011?1011
00?1112???2001?0121??0?1411?121???00???10?010?????????????????0??010?000100??????

Oudenodon_bainii 12002212101100002000012??11010100210[0
1]0100000101110000010121110201110101111122030110101210012100001211200111011000l1112???2001301211001141111212000010010
10100?11011101112110110010?0????0??????

Tropidostoma_dubium
1200221210110000200002101110101002101010000010111000001012111020111010110012203011010121001210?01211200111011
0001111???20013012 11?01141111212?000100101010 0???0???011????000?010?0????0??????

Australobarbarus
1200221210110000200002 10?110101002?0?0100000101110000010121110201110101111122030100101210112 10??01211201111011
00?111120?20013012 11?01141??121??????????????????????????????00?010?0????0??????

Syops_vanhoepeni
1??012?21011000?2000022??110101102001 1?00??020112010101 00??1?????11??01111122030111 1?121?1??1?????2????0??1?010??1
?1????200????????0???11?12??????????????????????????????1??020?0???????????

Odontocyclops_whaitsi
1200221210110000200002 2??110101002001200000021111000002012111020111010111112203011010121001210 0?012112011?1011
00?1112???20013012 1??011411?12120000 1??1010100???0111011?????010000?001100??????

Idelesaurus_tataricus
1200221210110000200002 2??110101002101100000021111000001002111020111010110012203011110121001210000021120 1??1001
00?1112???21013012 11?01141111 21??????????????????????????????0??000?0???????????

Bulbasaurus_phylloxyron 1200221210110000200002 2??1101000[0 1]2[0 1]1000011002011[1 2]01000[1
2]00211102011101011011220301101012100121000012112 0???101100?111????2101?01211??????????1???????????0??????????????????1??0
00?002100??????

Aulacephalodon_bainii 1200221210111000200002 2??11010[0 1]002011200[0 1]100[1 2]001001000[1
2]00211102011101011011220301111012100121000012112[0
1]01110110001112???20013012111011411112121000100101010 0?1101010111211111000 0?0????0??????

Pelanomodon_moschops 1200221210111000200001 2??1101010020112001100210100100020021120201110101111122030111101210[0
1]12100?01211210111011 00??????????????????????????2??????????????????????????????1??000?001100??????

Geikia_locusticeps
1200221210111000200001 2??1101010020112101100211110000 02?0201202011101011111220301111012101121000022112101110 11
00?1112???21013010110011411112 1??00?10??????????????????????1??000?002100??????

Geikia_elginensis
120022?2101110002000012??11010111120??21??100????10000???021120201??01?11111?2030?1??01210??210?10?????????????0?1012???21013012 1?????41??121?????????0101?????????????????????000?001101??????

Elph_borealis
1??02??2101000002010022??1101001000000100000101120000010021100201110 10????12203011010?2100?11?000121120???101100?1112???20?13012111 0???????21?????????????????????????????????0??000?0????0??????

Interpresosaurus_blomi
1200??12101000002010022??1101001?0?000100???10??2?1?????????????????????1???1???30??0??00?0???????????

Katumbia_parringtoni
12002212101?0000??10022??1100001010000100000111120000010021 1?02011?0101111122030110101210102 10??012112111 1?00100?1112???2101301211 10???????21?????????????????????????????0??000?0????0??????

Delectosaurus_arefjevi 12002212101000002100022??1101000011000100000201120101010021100201110101111121030111[12]012101121 10?0121121???1001000???000?0????0??????

Dicynodon_lacerticeps 12002212101000002000022??110100001[01]00110000020112000101002110020111010111112103011110121001210000221121111101100111 12???2101302211111151111 21?????????????????????????00?000?0????0??????

Dicynodon_angielczyki
12002212101000002000022??1101000010001100000201120001010021100201110101111121030111101210112100002211211111011001111 2???2101302011111151111 21?????????????????????????????????????000?002100??????

Daptocephalus_huenei
120022?2101000002110022??1101001011001100000201120101010021100201110101111121030111101210101110101211211111011101???000?012101??????

Daptocephalus_leoniceps
12002212101000002110022??1101001011001100000201120101010021100201110101111121030111101210101110101211211111011101111 2???2101302211111151111 21????????101110????0111????????10?000?001120??????

Dinanomodon_gilli
1200221210100000211012 2??1101000211001100000201120101010021100201110101111121030111101211102 11??01211211111011?011?1?????10?3?121??1?1511?12?????????????????????????????????1??000?0????0??????

Peramodon_amalitzkii
1??0?????0?00000201002???11?10010110001000002011201 0?0100211002011?010????????????????12????21?0?0?2?121?11?0?1???111????210???221111?1511?12?3?100101?????????????????????????1??000?0???????????

Taoheodon_baizhijuni
120022?2101?00002?10022??1101000110001001000 10?1100000100211????111?101???121030111101 20?012110000 2??2?????01010?1112????101?02211?1115?????1?????????????????????????????????0????????1??????

Counillonia_superoculis
120022121010000???00022??1101000??2????????0???????0?0100211002011?0??1111121030 1??10121010211 0?022?120?????01011???00?????????????

Repelinosaurus_robustus
1200221210?10000?100?22??1101001?100?10??10020111000001002110020 1??0??????1????????1012??10?11??022?120?????01??1???00?????????????

Vivaxosaurus_trautscholdi 120022?2101000002010022??1101000111000000000201110101010021100201110101100121030111[12]012101121 10?022112[0 1]?1?10110011112???210130221??1115110121??000??1101110?????????????????0??000?0????0??????

Jimusaria_sinkianensis
1200???2101100002000 02???1102000010000100000101120101010121100201110 10????1210301?11012100?2110102211211 1?10???0?1112???2101302211011151 1?121?????????????????????????????????0??000?0????0??????

Sintocephalus_alticeps
120022?21010000?2000022??1100000001011000000101110 10?010121?0020?1?0??????1210301 1?1012101?210??0?????????????????????????????????????2????????????????????????????????????000?0???????????

Basilodon_woodwardi
120022?2101100002000022??1100000020011100000201110100010121100201110101111122030111101210 1?210??0121121?1?1?1101?1?1?1?????1????221??????1????2????????????????????????????????????000?0????0??????

Turfanodon_bogdaensis
120022?2101100002110122??1101000221001000000201110101010121100201110???11?1210301 1?10121111211??0121121???1011001???000?0????0??????

Turfanodon_jiufengensis
120022121011000021101 22??0101001221011001000201120101010?2110020111010111112103 0?1110121111 21?0101211??0??10?1001111 2???2101302211111151?11213????11?1??0?0????????001??1???0??????22100??????

Gordonia_traquairi
120022?21?10000??000022??1101001?2?0?010?00010112010?010?21100201 1?010?1??1?103??????12101??1???0???12??11???1?0?1112????2?0?30221????1?1??121???001??10?0100???0???????????00?000?0???????????

Euptychognathus_bathyrhynchus
120022?2101101102000022??1101001?0?1?10000001011201010 10?2110020111010111112103 0?1???1210?1210??02211?11??1011 00?1112???2101302211?1???1???21?????????????????????????????1??010?0???????????

Lystrosaurus_hedini
120022121011111020000 22??1101000020011000100101100101010021100201110101111121030111 2?121010411??02211210??1011001111 2???2101302211011151101 21?????1?????????????????????????1??000?001121??????

Lystrosaurus_maccaigi
120022?21011111?2000022??1101001101011 10?10020?10010?0100211002011101?111112103010 12?121010411??02211210??1?1100?1112???2101302 21??11151??1213????????010100?11?11?001121111 0?000?000101??????

Lystrosaurus_curvatus
120022?2101111102000022??1101001021011100100201100101010021100201110101111121030101 2?121011211000221121???1001001111?????10???221101?1511?12???0001??10101?0???1???001????110?0000001100??????

Lystrosaurus_declivis
120022121011111020000 22??1101001021211100100201100101010021100201110101111121030101 2?121011211000221121011100100111112???2101302211011151101213?0??1??1011100?111111011121111 0?0100001100??????

Lystrosaurus_murrayi
1200221210111110200002 2??1101001020211000100201100101010021100201110101111121030101 2?12101121 1?002211211111011
0001112???2101302211011151101 21??000111101110 0?111??101112111 0?010?001100??????

Shansiodon
1200221210110000200002 2??1101001?2?00110100020112011201012010021111 01?????1210301?12?12101??1?0?0221120?111?1100
11112???2001302211 0??0?1??1212?0001??1110111?110???1111211?110000?000101??????

Tetragonias_njalilus 1200221210110000200002 2??110[1
2]00102000100100010112011201012010021111010111112103010 12?12101021101 0?211211110110011112???2101301211011051111212 00
0010011101 00?1101111121211?110000?001101??????

Vinceria_andina
120022?21011000?2000022??1102001020 0?10010001011201120101201002011 0??11111???30??12?12101021 1??022?1?0?111?11??
?1??2????????????????????121????????????????????????????????000?003101??????

Rhinodicynodon_gracile
120022?2101100002000022??1101001021001101000101120112010020100211110 10????121030?112?12101??1?0?022?1?????1?0100
?1112???2101302 21??11??1??121??000100101?100???0111112?????110000?0???????????

Acratophorus_argentinensis
1200221210100000211002 2??1102000031001101101201120 10?010?2010020111010111112103 0?112?1211102110102212 20?1110100
111112???2101?01?1???1?50?112120?0010011101?0???011111??????01000???????0??????

Kannemeyeria_simocephalus
120022?2101000002110022??1102000031001101101201121102010121100201110101111121030111 2?12101011110221220 1??10100
111112???2101302211011151111213000110010101 00?1101110111211111002???00100??????

Kannemeyeria_aganosteus
120022?2101000002110122??1102000031001 10??????????????????????????????111?????????1????????????????????????????????????
??02?????????????

Kannemeyeria_lophorhinus
120022?2101000202110122??1102000031002001101101121102010121102011101?11111210301?12?12101111101022??201??1?000??1112???21013012l??110?010121???00???11?110????0??????????????020?0????1??????

Dolichuranus_primaevus
120022?2101100002110022??1102000030001001100101121102010120100201110101111121030101101210106110?02212200??1?1001?1112???21013012l1?110?11?121??0000??1100101???????012?????110000?002101??????

Sinokannemeyeria
120022?2101000202120022??1102000031O?1001101201120101010120100211110111111121030l??2?12101?211??0221?20?1110100111112???21013012l1???0?11?12120000l0?1110101?110???0111211?110000?0???????????

Parakannemeyeria
120022?2101100202020122??110200003?0110011012011201010101201002111101011111121030l?12?12101011l0?022??2011110100111112???2101?0121???1??11?1213?000100101010O?110111[0 1]111211??10000?0021????????

Xiyukannemeyeria_brevirostris
120????21011002?2020022??110200103?0110011012011201010101?2010021111010111112??301?12?12??10211??022??20?111?000??1112???210???1211??1??11?121???0?1??1110?00?110???0111211?110000?0021????????

Rabidosaurus_cristatus
120?22?2101000002110022??110?000?3?0010011?1201?0?1??010?211??2?1110??????12??30101??121?1?11???0?2????1??1??00?1??????????????????????????????????1?????????????????????000?0???????????

Rhadiodromus120022?21011000020l0022??11020000310[01]10011011111201020l0?20100201110??1111121030?1?1012??1??1?11022?220???10110??000?0???????????

Wadiasaurus_indicus 120022?21010000?21100[12]2??1102000???0010??001??11011??0??120100201?1010????1???30??12?12101??1???022??20???1?10?1?1112???2??130?????????11?121200101?01111101???0111111?????1100?0?000100??????

Shaanbeikannemeyeria
120022?2101100002010022??1102000031001001101101120l0?0101211002111101?111112103011l?012101?211??0221220?????100?
?1112???20?1??121????????1?21???001??1??1100???????011????????020?0????1??????

Rechnisaurus_cristarhynchus
120022?2101100l?2010122??1102000030001001001??1?10102010?2??0?2???????????121030?011012101??1???0221220???????0???
??020?0????0??????

Uralokannemeyeria_vjuschkovi
120022?21?11002?2??0122???102000????01?01101201110l0?010?201?02011101011111???30?????12???1211??022?220???1?100???
??????????????????????????2?2?????????????????0?????????????0?0?0???????????

Angonisaurus_cruickshanki
120022?21?1100002?00112??1101001???00100110000110011101012010020l110??11111???30?1???12101??110?0221120???1?110?1
1112???2101301211011001l?1213??00100?10?10????0111????????111100?00210???????

Ufudocyclops_mukanelai
120?22?2101?00002010?12??1101000?2?0010011000?1101111010220100201110101111121030211l?12111011l?10?211?0???1?1100
?1112????1013?12110??????1?21????????????????????????????????100?002120??????

Zambiasaurus_submersus
120022?21??1???????0012???1?0??????????00???10?1100???010220????2?1????0????????????????????????????????????110????12??
?2??1??????0?????????1?0?111001?01100???0111111?????111??0?0???????????

Placerias_hesternus
120002?21??000202000022??11100000310?10011011010001110102201012011101l?????????????????1????05111002??20?111?101?1
1112???200130???10??1?1??121?00111001?0010????0111111????111111000???????????

Moghreberia_nmachouensis
1?0002?21010002??020022???102000?3?0??0011?12010001110102201201??0?01111121030l1????210???1??0?221?20?????101??1
112????2?013012110????0??121?????????????????????????????1???00?0???????????

Pentasaurus_goggai

??20??????1010??12????200???10?101??????????????????00????101??????????????????111???????????????????

Stahleckeria_potens

120020?2101100002120112??1101000031001011101O?1100101010220100201110101111121030111101211101111102211211 1?10100011112???2101301211011100111213101010011101O1?1101111111211?010100??02100??????

Sangusaurus_parringtonii

120022?2101100000010112??0101000031002011100101110102010220100200110 1?1???121030111 2?121010111102211 21???11100011112????10130121111?100111213????????????????0111111?????0??130?002010??????

Sangusaurus_sp

120022?210110000?010012???10100003?0?201110?10???????010???????0?1?0??1???121030?112?12101??1???3?????????????????

Eubrachiosaurus_browni

??

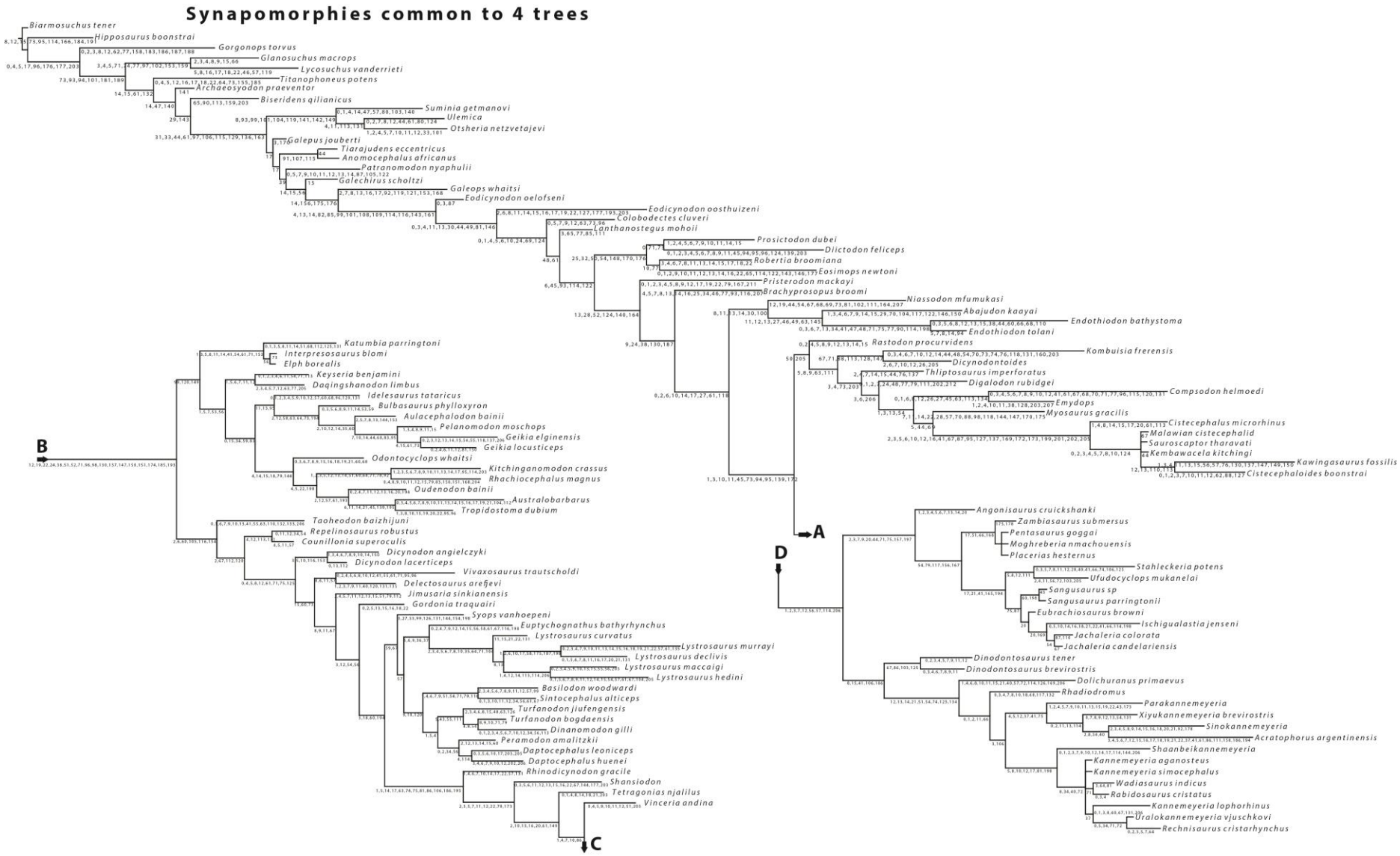
Dinodontosaurus_brevirostris
120022?2101100002010022??1101001031001001000201120112010120100211110101111121030001 1?12101011 1?102211211111010
001??00??????????????

Dinodontosaurus_tener
120022?2101100002010022??1101001031001001000201120112010120100211110101111121030001101210101 11?102211211??10100
011112???2101301211001 0?11?12130000100110010 1?1101110121211?10?000?0021000?????

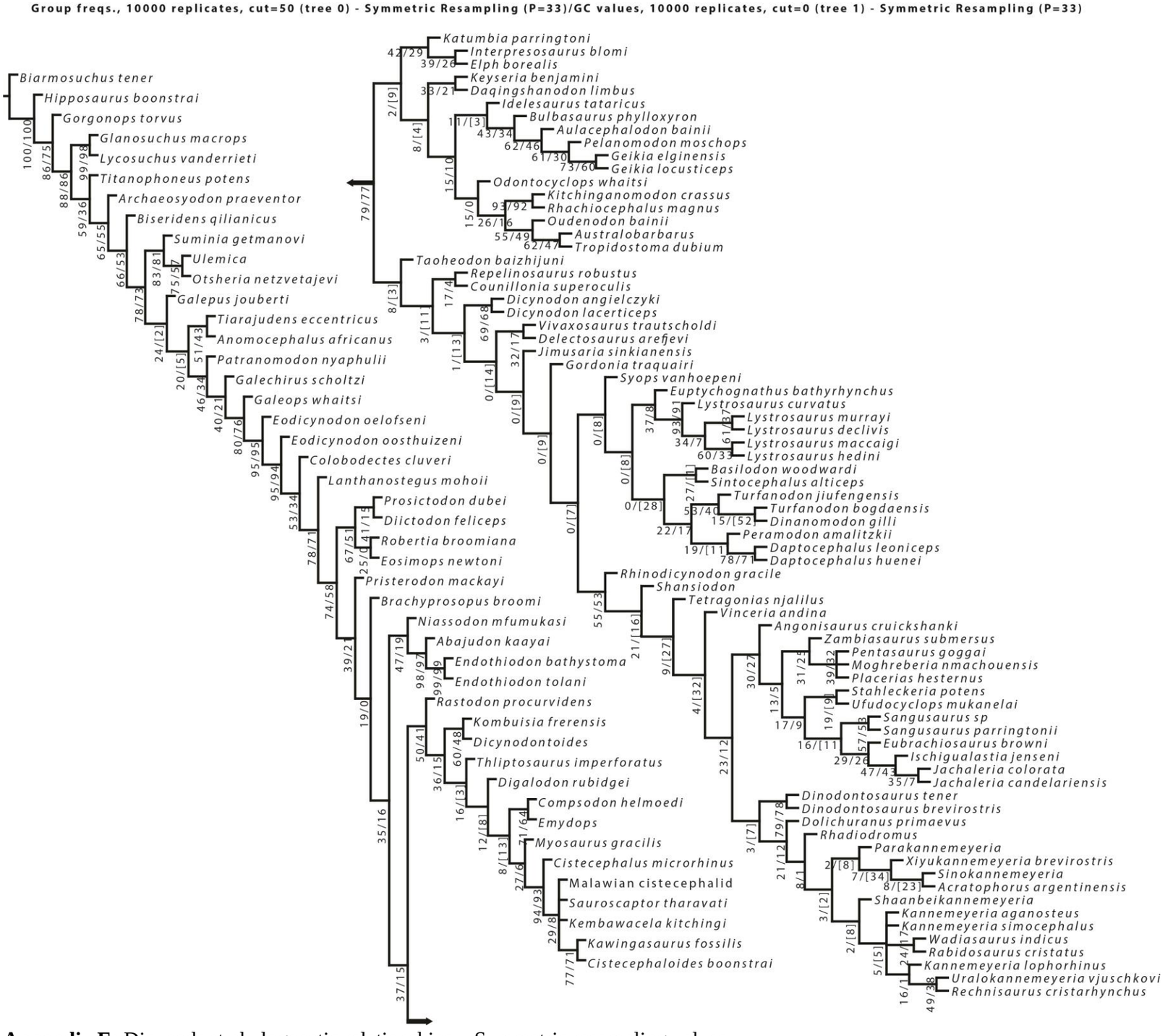
;

proc /;

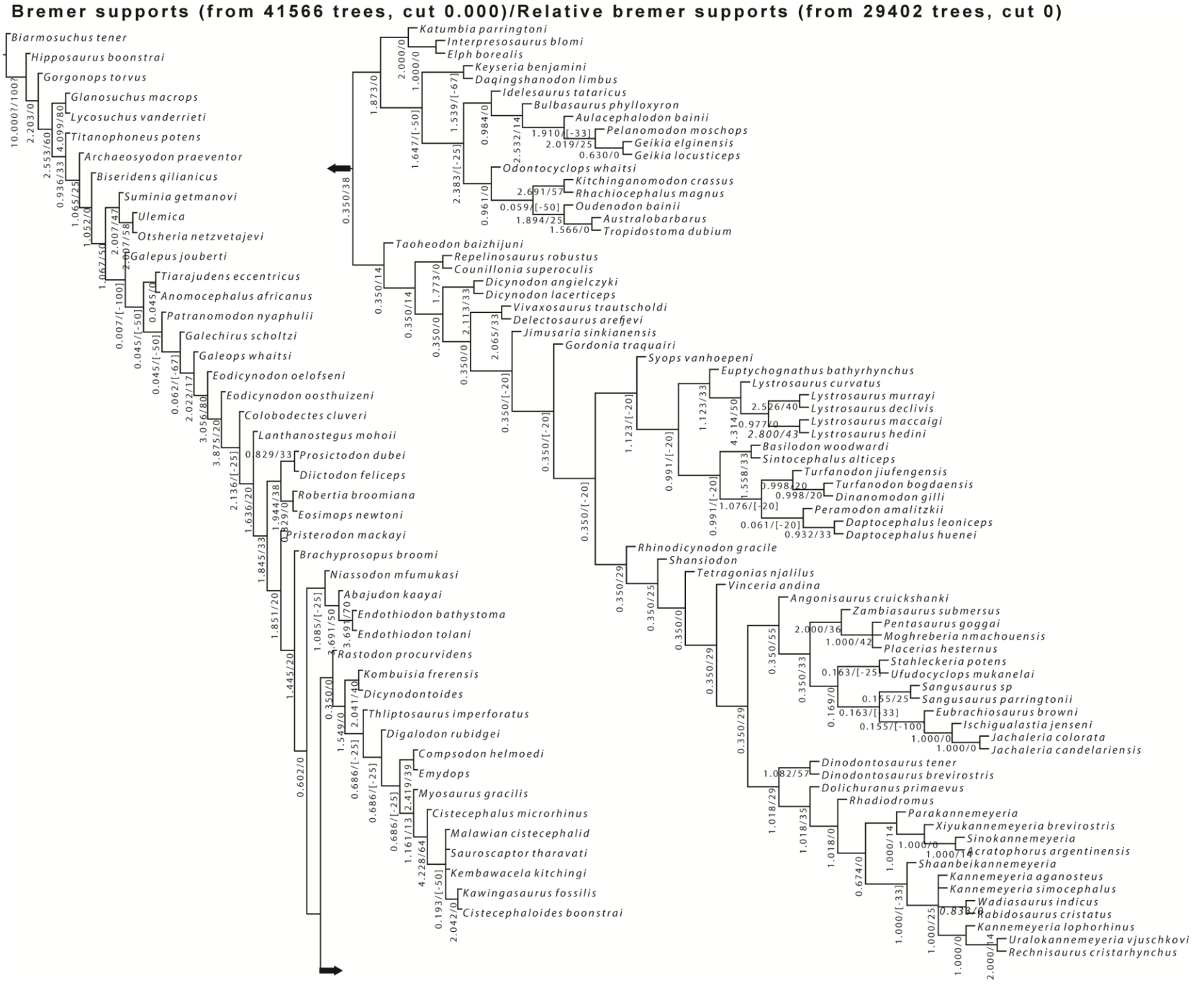
ccode + 57 60 78 139 149 150 165;



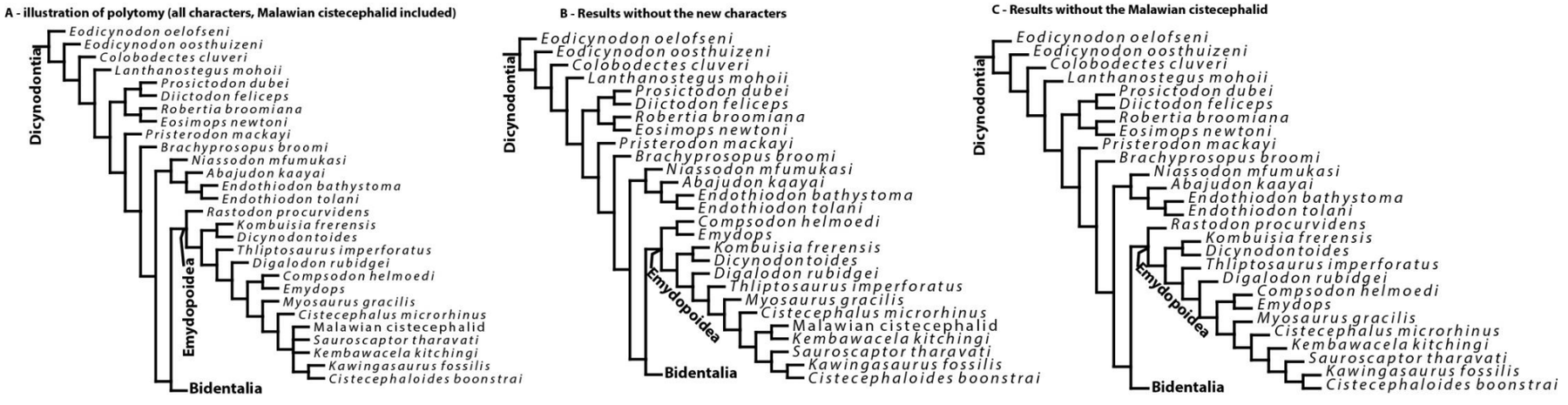
Appendix D: Dicynodont phylogenetic relationships – Synapomorphies common to all four trees. Letters represent the continuity of the trees.



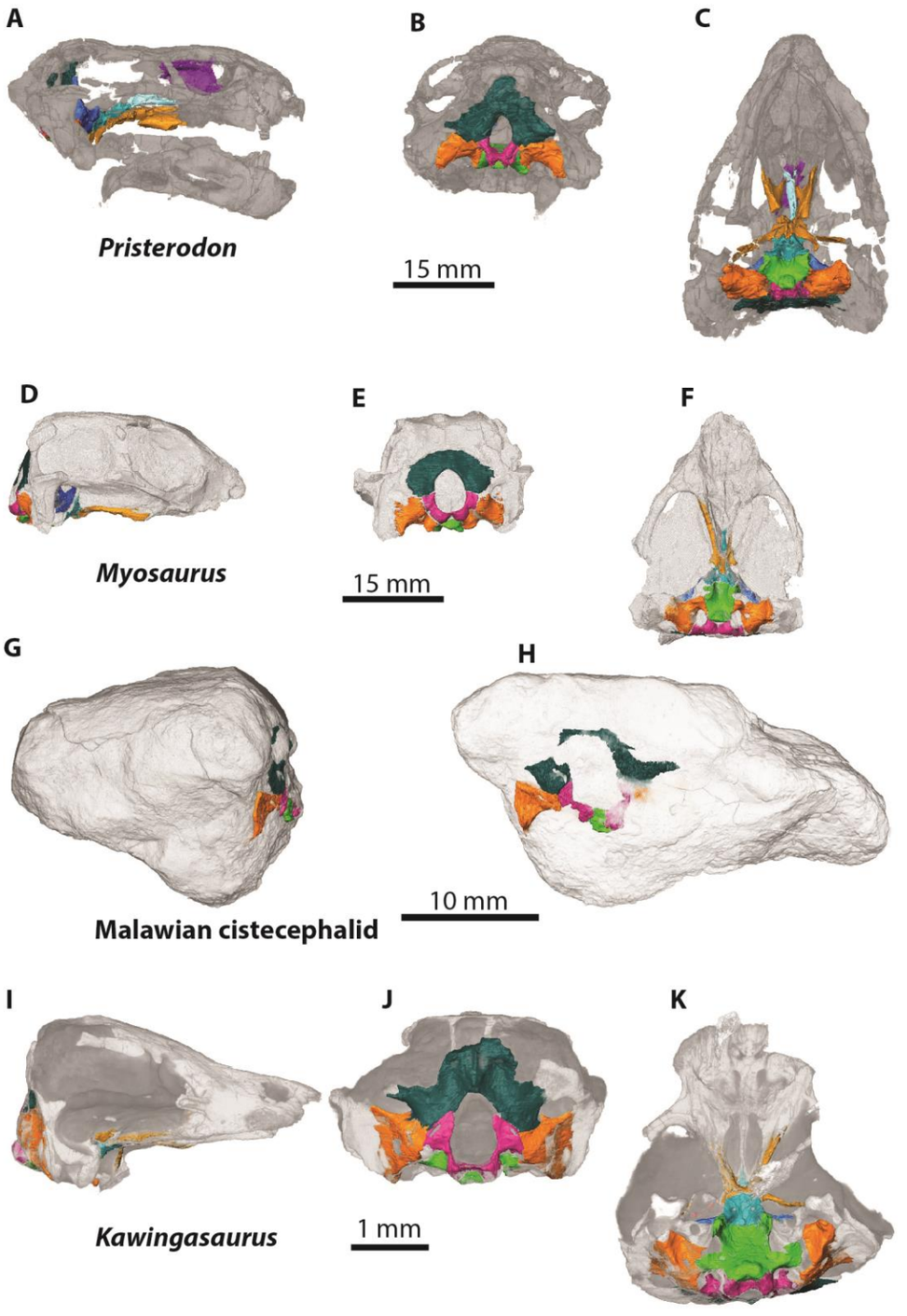
Appendix E: Dicynodont phylogenetic relationships – Symmetric resampling values.



Appendix F: Dicynodont phylogenetic relationships – Bremer support values.



Appendix G: Compared simplified trees illustrating the formation of polytomy among three cistecephalid emydopoids: the Malawian cistecephalid, *Sauroscoptor tharavati* and *Kembawacela*. **(A)** Results with all new characters and the Malawian cistecephalid included; **(B)** Results without the new characters; and **(C)** results without the Malawian cistecephalid.



Appendix H: Illustration of the braincase region within the entire skull. *Pristerodon mackayi* (BP/1/2642) in **(A)** right lateral, **(B)** posterior **(C)** ventral views. *Myosaurus gracilis* (BP/1/2690) in **(D)** right lateral, **(E)** posterior and **(F)** ventral views. The Malawian cistecephalid (PK-16-1) in **(G)** left lateral and **(H)** posterior views. *Kawingasaurus fossilis* (GPIT/RE/9272) in **(I)** right lateral, **(J)**

posterior and **(K)** ventral views. Note that the Malawian cistecephalid specimen is completely covered by matrix such that a good contrast to enable the visibility of the skull was not obtained.